



PEM Fuel Cell System

A practical approach for building, testing
and controlling a self designed PEMFC stack

Magnus HANSETH
Ole Kristian OFTEBRO

Supervisor:
Peter Hugh MIDDLETON

University of Agder
Grimstad, May 19, 2017

Faculty of Engineering and Science
Department of Engineering Sciences



Abstract

Fuel cells are an efficient way to produce electricity, especially if it is combined with heat production. If designed to consume hydrogen, like PEMCF, the only byproduct is water in its purest form H_2O . This would have a great impact in the endeavors for a cleaner environment in densely populated areas. The potential for this technology is widespread, seeing usage from user electronics to onsite power production for commercial buildings.

We believe that this technology will be even more common in the future, and therefore we would like to create a simple, but useful, fuel cell system for educational purpose. An "easily taken apart and understood" approach will be focused for all the components and subsystems. The end product is a small PEMFC stack with a separate control system. This will function as a building platform for testing and improving.

Acknowledgments

We would like to express our gratitude to our supervisor Prof. Peter Hugh Middleton for his support and guidance, as well for his dedication and advocacy for the completion of this project. Also a special thank to you Johan Olav Brakestad, who helped us ordering parts and giving us access to the lab equipment, to Roy Werner Folgerø for making the parts we needed in the workshop, to Trond-Ivar Lynghaug for the electronic guidance, and to Cassandra Pham for proof-reading.

Also a special thanks to friends and families who supported us in these times.

Grimstad

May 19, 2017

Magnus Hanseth and Ole Kristian Oftebro.

Contents

1	Introduction	1
1.0.1	Background	1
1.0.2	Outline of thesis	1
2	Theoretical Background	2
2.1	Basic principles for a hydrogen fuel cell	2
2.1.1	The proton exchange membrane	3
2.1.2	Catalyst	4
2.1.3	PEM fuel cells in series	5
2.2	Fuel cell flow calculations	5
2.2.1	Water management in PEM fuel cells	7
2.3	Modeling the fuel cell	8
2.3.1	Behavior description and behavior explanation	8
2.3.2	Complexity of modeling	8
2.3.3	What are we modeling?	8
2.3.4	Domains of modeling	9
2.4	Cell level modeling with some individual layer modeling imbedded	9
2.4.1	Electrical domain	9
2.4.2	Activation losses	10
2.4.3	Ohmic losses due to membrane and plate	10
2.4.4	Membrane resistivity	13
2.4.5	Concentration losses	14
2.4.6	Double layer capacity	14
2.5	Fluidic domain	14
2.6	Thermal domain	16
2.7	Impedance Spectroscopy	16
2.7.1	Basics of Electrochemical Impedance Spectroscopy	16
2.7.2	Data presentation	18
2.7.3	Equivalent circuit	18
2.8	Arduino	23
2.8.1	Pins of the Arduino	24
2.8.2	Programming Arduino	24
2.9	Power electronic	26
2.9.1	Buck converter	26
2.9.2	Boost converter	27
2.9.3	Buck-Boost converter	27
2.10	Fuel cell comparing	28
3	Method	30
3.1	Work plan	30
3.1.1	Literature study	30
3.2	Initial fuel cell estimation and material choice	30
3.2.1	Cell voltage	31
3.2.2	Cell size	31
3.2.3	Fuel cell material	31

3.2.4	Limitations	32
3.2.5	Previous Concept design	32
3.3	Fuel Cell Modeling	32
3.3.1	Setting up the model	33
3.3.2	Building the model	33
3.3.3	Secondary current distribution	35
3.4	Control system	37
3.4.1	Microcontroller	37
3.4.2	Humidification and dehumidification systems	39
3.4.3	DC-DC Converter	40
3.4.4	Voltage and current sensors	40
4	Design and test review	43
4.1	Two cell setup	43
4.2	testing station	43
4.2.1	Design	43
4.2.2	Design overview	43
4.3	Control system testing	45
4.3.1	Testing Humidification and dehumidification systems	45
4.3.2	Fan control	45
4.3.3	Temperature control	45
4.3.4	LCD screen	46
5	Results and final design	47
5.1	Fuel cell simulation	47
5.1.1	Fuel cell performance	48
5.1.2	EIS measurements	49
5.1.3	Fuel cell comparing	49
5.2	Testing station	49
5.3	Economics	50
6	Discussion	53
6.1	Fuel cell model	53
6.2	Fuel cell stack	53
6.3	testing station	53
6.3.1	Deliverance delays and breakdowns	54
6.4	Future work	54
7	Conclusion	55
	Bibliography	57
	Appendices	58
	Appendix A Nafion Membrane	58
	Appendix B Nafion Resin solution	60
	Appendix C 3D Printer	61
	Appendix D Magic Rubber	65
	Appendix E Fuel Cell Stack Control Circuit A	66
	Appendix F Fuel Cell Stack Control Circuit B	67
	Appendix G Technical drawing: Fuel Cell Plates	68

Appendix H	Technical drawing: Testing station	71
Appendix I	Order schedule	79
Appendix J	Arduino script	80
Appendix K	Comsol DATA	84

List of Figures

2.1	Energy form of the reaction. Illustrates activation energies, reactants and product [1].	2
2.2	Current-voltage characteristic for a typical low temperature, low pressure fuel cell [2]	3
2.3	Lewis structure for Polyethylene (PE) and Tetrafluoroethylene (PTFE) [2]	4
2.4	Lewis structure for the sulphonated side chain[2].	4
2.5	The platinum particles on larger carbon particles [2].	4
2.6	A basic setup of a PEM cell. [3]	5
2.7	The bipolar plates interactions [4].	5
2.8	An overview of different parameters in a bipolar plate, focusing on the anode side. The values are measured in mm.	12
2.9	The oval in the center is known as the Lissajous Figure.. . . .	18
2.10	The Nyquist plot.	19
2.12	A circuit diagram of the Buck converter [5].	26
2.13	A circuit diagram of the Boost converter [5].	27
2.14	A circuit diagram of the Buck-Boost converter [5].	27
3.1	The Serpentine and Parallel patterns from Fuel Cell Systems Explained [2]	31
3.2	The improvements of the bipolar plate.	32
3.3	An overview of the computer model in COMSOL	35
3.4	A simplified schematic of the temperature control setup.	37
3.5	A simplified schematic of the fan control setup.	37
3.6	A simplified schematic of the sensor setup.	38
3.7	A simplified schematic of the LCD setup	39
3.8	Sketch of the humidifier.	39
3.9	Sketch of the dehumidifier	39
3.10	The schematics for a boost converter using LTSpice	41
3.11	The result of the simulation.	41
3.12	The voltage sensors configuration with the safety zener diode.	41
3.13	The current sensing setup.	41
3.14	The circuit board for the boost converter, voltage and current sensors and fan control.	42
4.1	The two cell setup.[6]	43
4.2	Overview of the external design. [6]	44
4.3	Overview of the internal design. [6]	44
4.4	An example of a circuit built up on a breadboard.	45
4.5	Testing the display on the testing rig.	46
4.6	All the electric components placed in the testing station	46
5.1	Modeling results from different cell temperature.	47
5.2	Modeling results from different cell temperature.	48
5.3	Model of the fuel cell stack at 45 deg with full, 2/3 and 1/3 gass supply.	49
5.4	Test results from a two cell setup.	50
5.7	The finance distribution for the total costs.	50

5.5	EIS measurement from a two cell setup.	51
5.6	EIS measurement from a two cell setup.	52
7.1	All the final products placed together as intended.	55

List of Tables

2.1	Physical phenomena in PEMFC (Blunier, 2013).	9
2.2	An overview of different gasses and liquids in the PEMFC.	15
2.3	Circuit elements used in the equivalent circuit.	19
2.4	Specs of both Arduino boards [7].	24
3.1	The work schedule.	30
3.2	Species that are present at each side.	33
3.3	Model parameters in COMSOL. Items marked with a * is parameters changet to fit our cell.[8]	34
5.1	Comparing fuel cell performance.	49
6.1	The actual work schedule.	54

Chapter 1

Introduction

1.0.1 Background

The fuel cell technology is a well known technology, but not widely used. This is mostly due to high cost. From the first discoveries in the early 1800s, extensive research has increased the efficiency and reduced the cost. Lately, fuel cells have seen a renewed interest in areas where large energy storage and long term energy storage, is too inefficient for current battery technologies. Also to combat greenhouse gases and local air pollution, many researchers are now looking for ways to convert countries from using fossil based fuel to using hydrogen based fuel for energy production and transportation. PEM fuel cells, being one of the fuel cell types that have a good efficiency and a low operating temperature, might play an important role in this step.

1.0.2 Outline of thesis

In this thesis, we will continue with performance improvement and implementing a control unit on a self design PEM fuel cell stack. The stack is minted on simplicity and is easily taken apart and understood. The concept idea was conceived in an assignment in the subject “Solar cells and fuel cells” in spring 2016, then the following semester, refined to a working prototype and built in the subject “Energy research project 2” in autumn 2016. The end product should be a fully functional small demo fuel cell stack, with fully customizable control setup. The design allows for any component or variable to easily be changed, and the idea is to sell the product to schools or universities as an educational tool kit or a student project.

The current version has an acceptable voltage, but lack the power output and have no controlling features. Therefore the remaining focus areas are optimization for better performance and control devices for air flows and stable output voltages.

Improvements to test:

- Steel, carbon or titanium plates (Instead of aluminum, to combat corrosion)
- Conductive paste on current collector plates
- Nafion 115 membrane (Thinner membrane)
- Carbon cloth and/or paper (Thinner gas diffusion layer)
- Catalyst with higher platinum content (10% to 50%)
- Higher operating temperature (Up to 80°C)

Features to be implemented:

- Fan /with controller (For sufficient air supply and cooling)
- DC-DC converter (For stable output voltage)
- Standardizing the connections and streamlining the design.

Chapter 2

Theoretical Background

2.1 Basic principles for a hydrogen fuel cell

A fuel cell is a device that converts electrochemical energy into electrical energy in the form of a DC voltage, much like a battery. Unlike a battery, the fuel cell must be fed continuously with the reacting gases. The operating principle of a fuel cell is governed by the basic principles of electrochemistry. These reactions involve electric charges moving between electrodes and the electrolyte. In a fuel cell the two electrodes allow the basic reduction-oxidation process to occur through the external electric circuit and the electrolyte. The negative electrode or the anode is where the oxidation process occurs, which in a PEM fuel cell can be described by the following half-cell reaction equation [1].



The positive electrode or the cathode is where the reduction process occurs, which can be described by



This gives us the overall reaction



For the anode and cathode half reactions to continue simultaneously, the electrons generated at the anode must pass through the external electrical circuit to the cathode, and H^+ ions must pass through the electrolyte. In the PEM fuel cell, pressurized hydrogen gas (H_2) enters on the anode side. When the H_2 molecule comes in contact with the catalyst it splits into two H^+ ions and two electrons. At the cathode, oxygen gas (O_2) enters through the catalyst and form two oxygen atoms, each with a strong negative charge. The negative charge attracts the H^+ ions through the ionic conductor where they recombine with an oxygen atom and two electrons to form a water molecule.

At the anode, hydrogen reacts and releases energy. However, the reaction does not proceed at an unlimited rate, activation energy needs to be supplied to get over the thermodynamic barrier. To increase the kinetics of the reaction we can apply a catalyst to the electrodes, increase the surface area of the electrodes and/or raise the temperature.

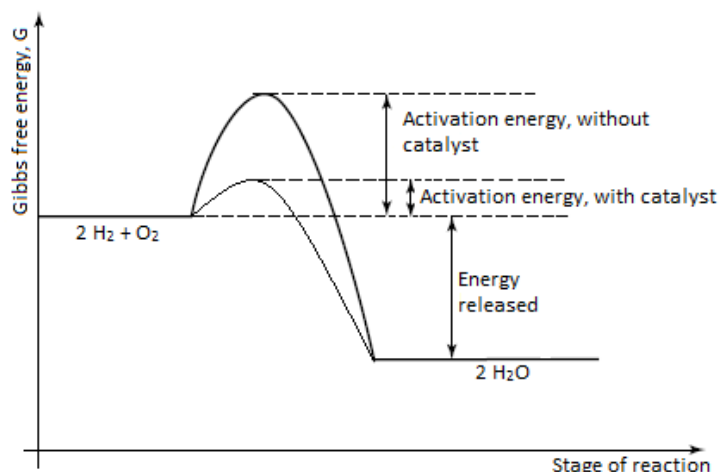


Figure 2.1: Energy form of the reaction. Illustrates activation energies, reactants and product [1].

Gibbs free energy, or the driving force for the overall reaction previously stated, is approximately 474 kJ, which is illustrated in Figure 2.1 by energy released. By using the equation relating G and the cell potential, or EMF (electromotive force), given in equation 2.4 we can calculate the no loss voltage to be 1.23 V for a single cell.

$$\text{Change in Gibbs free energy: } \Delta G^0 = nFE^0 \quad (2.4)$$

where

ΔG^0 = Change in Gibbs free energy under standard conditions [J/mol]

n = Number of electrons involved in reaction [-]

F = Faradays constant [C/mol]

E^0 = EMF under standard conditions [V]

In reality there will be losses, and the voltage will then drop because of that. The main losses are activation losses, fuel crossover and internal currents loss, ohmic losses and mass transport or concentration losses. In Figure 2.2, the characteristic shape of the voltage/current density is shown.

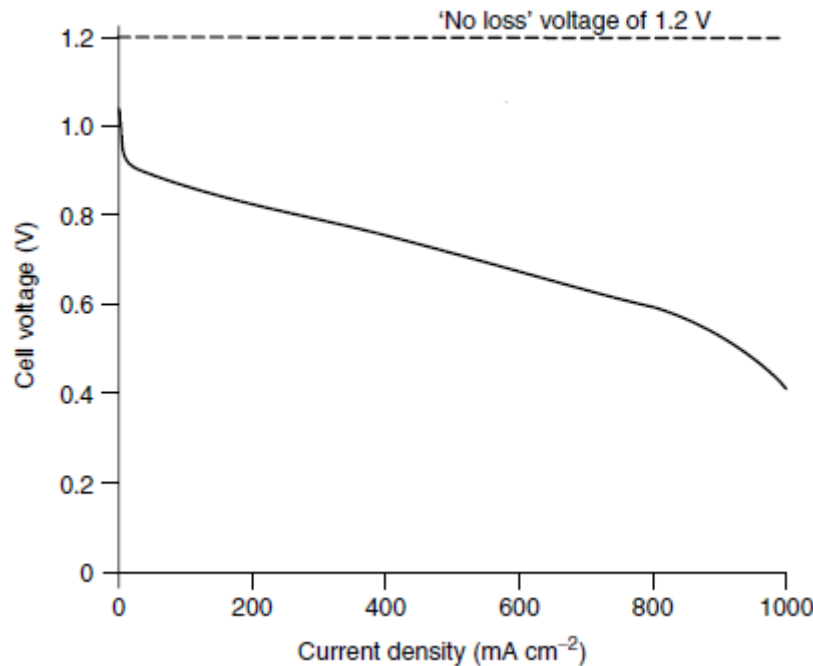


Figure 2.2: Current-voltage characteristic for a typical low temperature, low pressure fuel cell [2]

2.1.1 The proton exchange membrane

The proton exchange membrane, often called by its acronym, PEM, is classified as a solid ion conductive polymer. Although different companies use different methods for producing the membrane, the common practice for the polymer usually starts as Polyethylene (PE). Strings of Polyethylene are then perfluorinated (the process of substituting fluorine for the hydrogen) to tetrafluoroethylene (PTFE). This important step makes the polymer strong, chemically resistant and hydrophobic. The strength allows the membrane to be made very thin, therefore improving the power density. The chemical resistance helps with lowering the degradation, improving the lifetime of the membrane. The hydrophobic property helps with rejecting the product water, preventing flooding. [2]

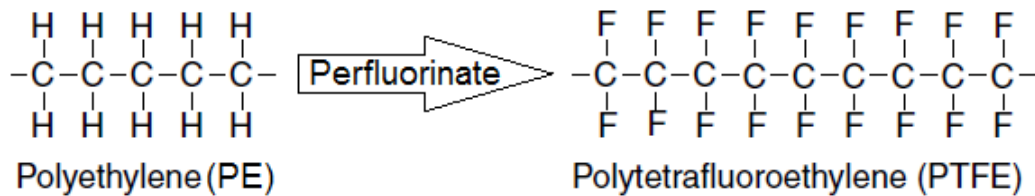


Figure 2.3: Lewis structure for Polyethylene (PE) and Tetrafluoroethylene (PTFE) [2]

The mobile ion in the polymer is an H^+ ion, or often referred to as a proton. For this to happen, a side chain needs to be attached to the PTFE string. A common fabrication practice is the sulphonated side chain method, where the string ends with sulphonic acid (HSO_3), or more correctly, SO_3^- ion. An illustration of this is shown in Figure 2.4. This results in an ionomer structure which creates a strong mutual attraction between the H^+ ions and the SO_3^- ions, and therefore tends to cluster. The final result is a hydrophilic region, which attracts water and is surrounded by hydrophobic regions, which reject water. [2]

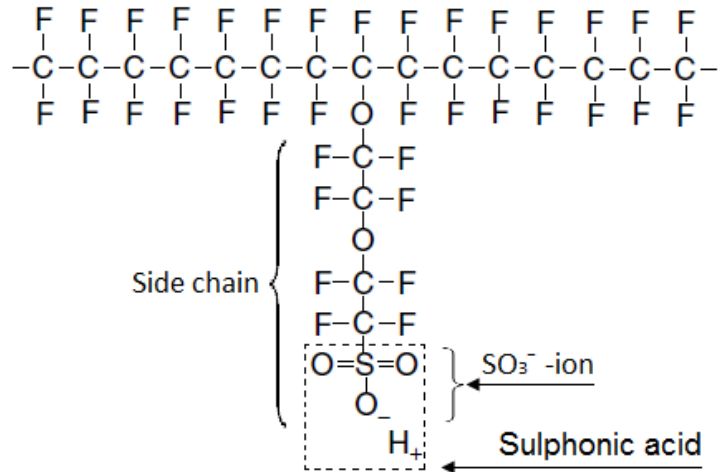


Figure 2.4: Lewis structure for the sulphonated side chain[2].

Because of the hydrophilic regions, large quantities of water can be absorbed. Within these water regions, H^+ ions are weakly attracted to the SO_3^- group and are able to move through the structure. This is however strongly dependent on the water content in the membrane. According to James Larminie and Andrew Dicks in Fuel Cell Systems Explained, a well hydrated membrane requires about 20 water molecules for each SO_3^- side chain, which will give a conductivity of about 0.1 (S/cm). If the water content falls, so does the conductivity.

The movement of H^+ ions creates a diffusion effect, and electrons starts building up (through the load) at the cathode surface. This combined with the applied voltage (Activation overvoltage) and the oxygen supplied at the cathode, makes the H^+ ions attracted to the electrons on the cathode surface and react with the oxygen, thus forming water. [2]

2.1.2 Catalyst

The best catalyst for a PEMFC is platinum. At earlier stages a PEMFC was heavily dependent on larger quantities of platinum, but recently this has been drastically reduced with the method described here. This results in more affordable cells. The platinum is made into very small particles, then attached on bigger carbon based powders i.e. activated charcoal. This can maintain the active area, while reducing the amount of platinum used. The platinum-charcoal solution is applied as a layer between the membrane and a gas diffusion layer. In

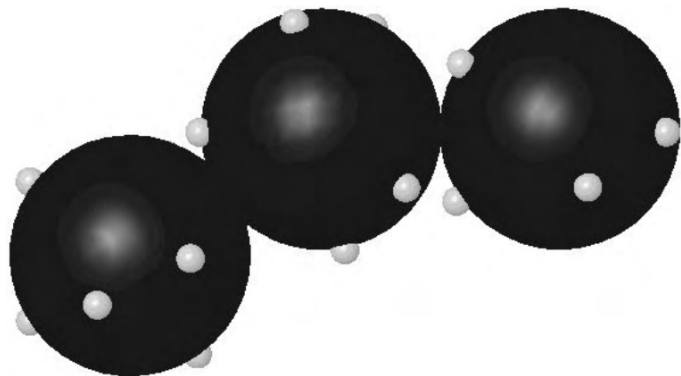


Figure 2.5: The platinum particles on larger carbon particles [2].

Figure 2.5 an illustration of the platinum particles on larger particles is illustrated. The reason to use a catalyst in the first place is to lower the activation energy of the fuel cell, this has been illustrated in Figure 2.1. A three-phase contact between the gas, electrolyte and the electrode catalyst results in better performance of the cell.

2.1.3 PEM fuel cells in series

A basic setup of a PEM cell can be seen in Figure 2.6. A single cell consists of one anode and one cathode collector plate, two electrode layers and proton exchange membrane. The reaction pattern of this cell is described in section 2.1. Normally it is necessary to connect several cells in series to reach the level of power needed. This is commonly done by using bipolar plates [4].

A bipolar plate can be seen in the center of Figure 2.7. The bipolar plate differs from end-plates, because, as shown in Figure 2.7, it works as a connector from one cell to another, operating as an anode current collector in one cell and a cathode current collector in the adjacent cell. In addition to this, the plate is designed in such a way that it carries oxygen at one side and hydrogen at the remaining side [4].

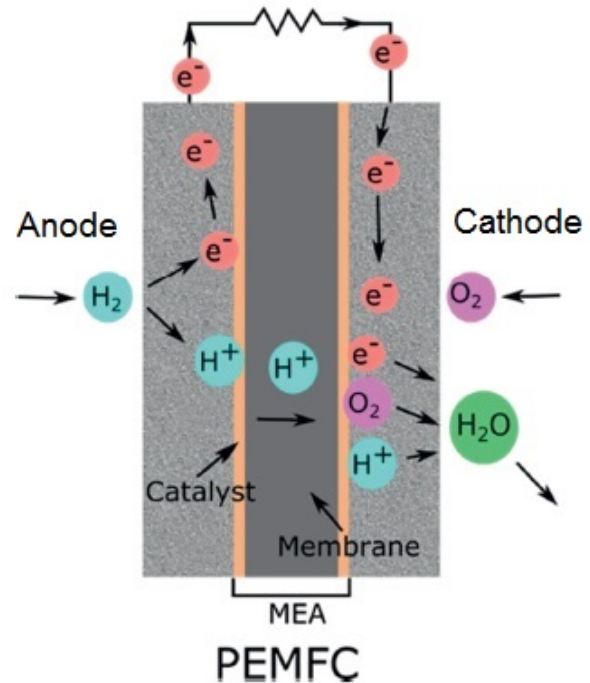


Figure 2.6: A basic setup of a PEM cell. [3]

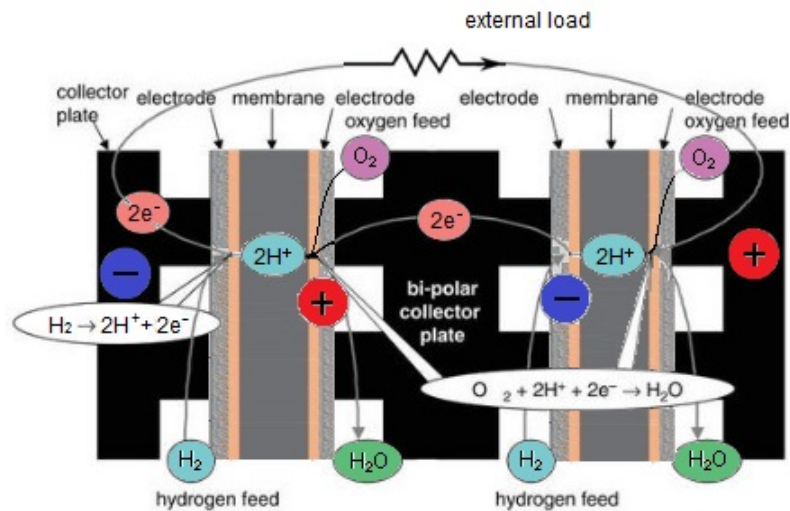


Figure 2.7: The bipolar plates interactions [4]

2.2 Fuel cell flow calculations

Equation 2.5 is used to calculate the fuel cell power. [2]

$$\text{Electrical power: } P_e = V_c \cdot I \cdot n \quad (2.5)$$

where

$$\begin{aligned} P_e &= \text{Electrical power [W]} \\ V_c &= \text{Cell voltage [V]} \\ I &= \text{Current [A]} \\ n &= \text{Number of cells [-]} \end{aligned}$$

Equation 2.3 in Section 2.1 states that for every mole of oxygen converted, four moles of electrons are transferred. Therefore, for a single cell, the oxygen usage is; $O_2\text{usage} = \frac{I}{4 \cdot F} [\text{moles/s}]$. Combining this with Equation 2.5 and changing from $[\text{moles/s}]$ to $[\text{kg/s}]$, we get Equation 2.6.

$$\text{Oxygen usage : } O_2\text{usage} = \frac{32 \cdot 10^{-3} \cdot P_e}{4 \cdot F \cdot V_c} \quad (2.6)$$

where

$$\begin{aligned} O_2\text{usage} &= \text{Oxygen usage [kg/s]} \\ P_e &= \text{Electrical power [W]} \\ V_c &= \text{Cell voltage [V]} \\ F &= \text{Faradays constant [C/mol]} \end{aligned}$$

Since we are not using pure oxygen, but rather oxygen available in the air, it is more practical to find the air usage. Of course, using the exact amount of air for the required oxygen (stoichiometry) is impractical, therefore we use more than required. Assuming a 21% oxygen content in the air, we get Equation 2.7.

$$\text{Air usage : } \text{Air usage} = \frac{28.97 \cdot 10^{-3} \cdot P_e \cdot \lambda}{0.21 \cdot 4 \cdot F \cdot V_c} \quad (2.7)$$

where

$$\begin{aligned} \text{Air usage} &= \text{Air usage [kg/s]} \\ P_e &= \text{Electrical power [W]} \\ \lambda &= \text{Stoichiometry ratio [-]} \\ V_c &= \text{Cell voltage [V]} \\ F &= \text{Faradays constant [C/mol]} \end{aligned}$$

When it comes to the usage of hydrogen, only two moles of electrons are transferred. Deriving in a similar way, we get Equation 2.8.

$$\text{Hydrogen usage : } H_2\text{usage} = \frac{2.02 \cdot 10^{-3} \cdot P_e}{2 \cdot F \cdot V_c} \quad (2.8)$$

where

$$\begin{aligned} H_2\text{usage} &= \text{Hydrogen usage [kg/s]} \\ P_e &= \text{Electrical power [W]} \\ V_c &= \text{Cell voltage [V]} \\ F &= \text{Faradays constant [C/mol]} \end{aligned}$$

2.2.1 Water management in PEM fuel cells

In a PEM fuel cell, there has to be sufficient water in the polymer electrolyte. In order to have optimal function of the fuel cell, there should be enough water content to ensure good proton conductivity, but at the same time there should not be too much water, resulting in blockage of pores in the electrodes of the gas diffusion layer. Ideally, the water formed at the cathode side would be sufficient for hydrating the electrolyte, while the air blown over the same side would dry out any excess water. However, making a design like this could prove difficult [2].

There are several different problems causing drying of cells, both at anode and at cathode side. From the anode point of view there is a problem with the H+ protons "dragging" water molecules with them. This means that even though the cathode side is well hydrated, the anode side could still dry out. Further on there could be difficulties with the air blown over the cathode side drying the cell. This is commonly more present at higher temperatures. These problems with drying can be solved by humidifying the air and the hydrogen blown into the fuel cell [2].

Air humidity blown into a PEM fuel cell is the key to controlling the humidity on the cathode side. In cases with high temperature, this must be closely controlled. The humidity should be above 80% in order to prevent drying, but below 100% to prevent a clutter of liquid water in the electrodes. In order to calculate the humidity of the exit air, Formula 2.9 can be utilized in combination with the saturated vapor pressure [2].

$$\text{water vapor pressure: } P_W = \frac{0.42 \cdot P_{\text{Exit}}}{\lambda + 0.21} \quad (2.9)$$

where

$$\begin{aligned} P_W &= \text{The water vapor pressure at the outlet [kPa]} \\ P_{\text{Exit}} &= \text{The air pressure at the outlet [kPa]} \\ \lambda &= \text{The air stoichiometry [-]} \end{aligned}$$

Formula 2.10 is used to find the relative humidity.

$$\text{Relative humidity: } \phi = \frac{P_W}{P_{\text{Sat}}} \quad (2.10)$$

where

$$\begin{aligned} \phi &= \text{The relative humidity [-]} \\ P_W &= \text{The water vapor pressure at the outlet [kPa]} \\ P_{\text{Sat}} &= \text{The saturated vapor pressure [kPa]} \end{aligned}$$

It is possible to run the fuel cell without extra humidification. If that is the goal, it is all about finding the right conditions, with temperature and air stoichiometry being the determining

factors. From the "Fuel cell systems explained" by J. Larminie and A. Dicks, a conclusion is drawn that extra humidification is necessary in a PEM fuel cell operating above approximately 60°C . Even though it is possible to run PEMFC without extra humidification, it is, in larger cells, very common to apply extra humidity. This is due to the fact that even though the water balance is correct, there will be areas in the cell where humidity will be too low. An example of this is near the inlet [2].

2.3 Modeling the fuel cell

The following theory is based on "Proton Exchange Membrane Fuel Cells Modeling" by Blunier, Benjamin Gao, Fengge Miraoui, Abdellatif. [9], and the references throughout this chapter has been acquired from the same book.

Making a model of the fuel cell provides several great advantages when it comes to optimizing and validating results. A model of a system will never fully describe the realistic system, but a good model will get close. By comparing the model results with actual test results, any significant error could be discovered and dealt with. As fuel cells are relatively costly products, the cost reduction of avoiding buying unnecessary parts or destruction of the cells would be a great advantage in modeling the fuel cell. There is also the advantage of being able to speed up or speed down processes while running a computer model.

2.3.1 Behavior description and behavior explanation

There are two different approaches to the modeling of complex systems, namely behavior description or explanation. Behavior description is used to imitate a given system. By monitoring the behavior of the system at different conditions, one tries to describe the system mathematically. This approach is done without any knowledge of the internal behavior of the given system. The behavior explanation, on the other hand, strives to explain why the system does what it does. This is an approach that requires extensive knowledge about the system and its internal behavior, by decomposing the system to the extent that every process and physical phenomena can be understood.

However, for a fuel cell, a combination of description and explanation approach usually has to be used. While you do wish to use a behavior explanation approach as much as possible, some parameterization or empirical parameter identification is almost always required to describe certain behaviors.

2.3.2 Complexity of modeling

When modeling a fuel cell, the level of difficulty or complexity has to be determined. What level of complexity is necessary to retrieve the necessary information from the cell model?

There are four different space dimensions for fuel cell modeling, namely 0D, 1D, 2D and 3D. As one might think, the complexity increases from 0D to 3D.

- A 0D model has no spatial dimensions. This kind of model would commonly describe variables like voltage of channel pressure. As there are no spatial dimensions in this model, it will not be able to predict distribution of physical quantities.
- A 1D model will be able to describe a physical phenomenon on a single spatial axis. This model is often used to describe electrical, fluid and thermal phenomena along the axis.
- A 2D model utilizes two axes instead of one. This model type gives us the opportunity to study different kinds of channel patterns.
- A 3D model is the most complex model, covering every axes of fuel cell modeling. This is a very detailed modeling approach, able to describe i.g. current density distribution in the electric domain.

2.3.3 What are we modeling?

When making a model, a decision on how much deconstruction of the system is desired, i.e. the system in this project is a fuel cell stack. Depending on what we want out of the model, the

inclusion of layers may vary. A decomposition of the system could be from stack into a single cell, or it could be decomposed into the single layers of one cell.

2.3.4 Domains of modeling

When modeling the fuel cell, there are three different domains, namely electrical, fluid and thermal. Depending on what we would like from the model, one or all of these domains could be modeled. However, the electrical domain is always included.

From table 2.1, a list of the different physical phenomena that can be seen in different layers of the fuel cell has been compiled. The different phenomena have been divided into the different domains of modeling.

Table 2.1: Physical phenomena in PEMFC (Blunier, 2013).

Electrical domain	<ul style="list-style-type: none"> Thermal dynamic voltage Activation losses Ohmic (resistive) losses Non-uniform current density Double layer capacity
Fluidic domain	<ul style="list-style-type: none"> Chanel pressure drop Gas consumption along the channel Channel geometry impact Channel pressure dynamics Biphasic effect of liquid and vapor of water Water condensation/evaporation Gas diffusion in the diffusion layers Diffusion layer flooding Microscopic gas diffusion in catalyst layer Non-uniform water distribution in the membrane Water transport in the membrane Dynamic water content variation in the membrane
Thermal domain	<ul style="list-style-type: none"> Non-isothermal temperature distribution Dynamic temperature variation Conduction between solid materials Forced convection in the channels Heat flux due to convective mass transport Natural convection (or radiation) on external surface Latent heat due to water phase change

2.4 Cell level modeling with some individual layer modeling imbedded

With the setup for the physical phenomena displayed in Table 2.1, a model can be based on the following mathematical suggestions from studying the book and its sources. The electrical domain is described, in-depth, while superficially describing the fluid and thermal domain.

2.4.1 Electrical domain

The thermodynamic voltage of the cell, E_{Cell} , can be expressed by Equation 2.11.

$$\begin{aligned} \textbf{Thermodynamic Voltage: } E_{\text{Cell}} &= 1.229 - 0.85 \cdot 10^{-3}(T_{\text{Cell}} - 298.15) \\ &+ 4.3085 \cdot 10^{-5} \cdot T_{\text{Cell}} \cdot \left(\ln \frac{P_{H_2}}{101325} + \frac{1}{2} \ln \frac{P_{O_2}}{101325} \right) \end{aligned} \quad (2.11)$$

where

$$\begin{aligned} E_{\text{Cell}} &= \text{Thermodynamic Voltage [V]} \\ T_{\text{Cell}} &= \text{Cell temperature [K]} \\ P_{H_2} &= \text{Hydrogen pressure [Pa]} \\ P_{O_2} &= \text{Oxygen pressure [Pa]} \end{aligned}$$

In reality, the cell voltage described above can never be reached, and can be corrected with 0.15 V. [10]

2.4.2 Activation losses

The energy required to initiate the chemical reaction in the cell is called activation energy. This is a loss, as the energy cannot be converted into anything useful.

From [11], the Tafel model has been proposed, describing the activation losses as Equation 2.12.

$$\textbf{Activation losses: } V_{\text{Act}} = \frac{R \cdot T_{\text{Cell}}}{\alpha \cdot n \cdot F} \cdot \ln \frac{i_{\text{Cell}}}{i_0} \quad (2.12)$$

where

$$\begin{aligned} V_{\text{Act}} &= \text{Activation losses [V]} \\ R &= \text{Molar gas constant [C/mol}\cdot\text{K]} (8.314) \\ T_{\text{Cell}} &= \text{Cell temperature [K]} \\ \alpha &= \text{Symmetrical parameter [-]} \\ n &= \text{Number of electrons involved in reaction [-]} \\ F &= \text{Faradays constant [C/mol]} \\ i_{\text{Cell}} &= \text{Cell current [A]} \\ i_0 &= \text{Equilibrium exchange current [A]} \end{aligned}$$

In Equation 2.12, n is the number of electrons in the reaction and α is the symmetrical parameter of the reaction, which has to be identified. i_0 is the equilibrium exchange current (A) and has been empirically calculated by [12], and the resulting equation is shown in Equation 2.13.

$$\textbf{Equilibrium exchange current: } i_0 = 0.9 \cdot A_{\text{Cata}} \cdot \exp \left(3500 \cdot \frac{T_{\text{Cell}} - 343}{343 \cdot T_{\text{Cell}}} \right) \quad (2.13)$$

where

$$\begin{aligned} i_0 &= \text{Equilibrium exchange current [A]} \\ A_{\text{Cata}} &= \text{Effective catalyst surface area [m}^2\text{]} \\ T_{\text{Cell}} &= \text{Cell temperature [K]} \end{aligned}$$

2.4.3 Ohmic losses due to membrane and plate

The voltage drop from Ohmic losses can be described by Equation 2.14.

$$\text{Voltage drop from Ohmic losses: } V_{\text{ohm}} = i_{\text{Cell}} \cdot R_{\text{Cell}} \quad (2.14)$$

where

V_{ohm} = voltage drop from Ohmic losses [V]

i_{Cell} = Cell current [A]

R_{Cell} = Cell current [Ω]

The R_{Cell} resistance is the combined resistance of the plates, gas diffusion layer, catalyst layer and membrane. For this resistance an individual layer model approach has been described [13].

Bipolar plate layer

For the bipolar plates resistance, the resistance is calculated for both the anode and the cathode half of the plate, then summed together.

To calculate the resistance of one half-plate, the plate is divided into two regions, namely the support region and the channel region. The support region is the solid part of the plate, which occurs “behind” the channels. The channel region relate to the part of the plate from the support area to the surface area, covering the channeled part of the plate, resulting in the following formula for resistance in a half plate

$$\text{Resistance in a half plate: } R_{\text{half plate}} = R_{\text{supp}} \cdot R_{\text{ch}} \quad (2.15)$$

where

$R_{\text{half plate}}$ = Resistance in a half plate [Ω]

R_{supp} = Support region resistance [Ω]

R_{ch} = Channel region resistance [Ω]

Furthermore, R_{supp} and R_{ch} are described with Equation 2.16 and 2.17.

$$\text{Support region resistance: } R_{\text{supp}} = \frac{r_{\text{plate}} \cdot \delta_{\text{supp}}}{H_{\text{plate}} \cdot L_{\text{plate}}} \quad (2.16)$$

where

R_{supp} = Support region resistance [Ω]

r_{plate} = Plate resistivity [Ω]

δ_{supp} = Support region thickness [m]

H_{plate} = Total width of the plate [m]

L_{plate} = Total length of the plate [m]

$$\text{Channel region resistance: } R_{\text{ch}} = \frac{r_{\text{plate}} \cdot \delta_{\text{ch}}}{(H_{\text{plate}} - N_{\text{ch}} \cdot H_{\text{ch}}) \cdot L_{\text{plate}}} \quad (2.17)$$

where

$$\begin{aligned} R_{\text{ch}} &= \text{Channel region resistance } [\Omega] \\ r_{\text{plate}} &= \text{Plate resistivity } [\Omega] \\ \delta_{\text{ch}} &= \text{Channel region thickness } [m] \\ H_{\text{plate}} &= \text{Total width of the plate } [m] \\ N_{\text{ch}} &= \text{Number of channels } [-] \\ H_{\text{ch}} &= \text{Width of the channels } [m] \\ L_{\text{plate}} &= \text{Total length of the plate } [m] \end{aligned}$$

Some of these factors have been illustrated for the anode side in Figure 2.8.

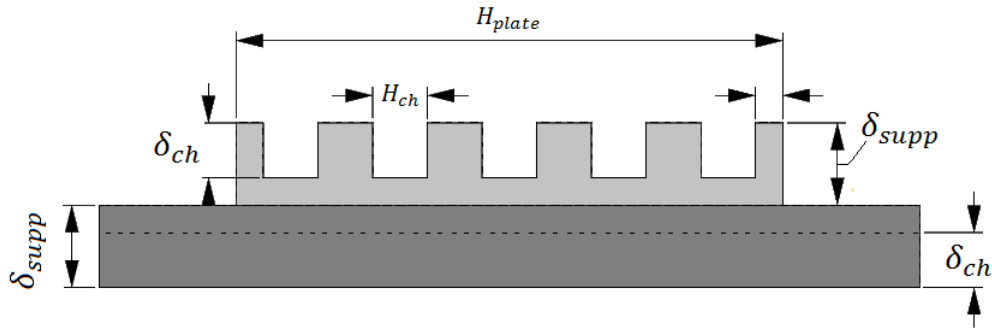


Figure 2.8: An overview of different parameters in a bipolar plate, focusing on the anode side. The values are measured in mm.

Gas diffusion layer

The next part of the electrical domain is the gas diffusion layer (GDL), which, like the bipolar plate, can be represented as an Ohmic resistance. By using Equation 2.18, this resistance can be calculated [14].

$$\text{Gas diffusion layer resistance: } R_{\text{GDL}} = \frac{r_{\text{GDL}}^{\text{eff}}}{8 \cdot N_{\text{ch}} \cdot \delta_{\text{GDL}} \cdot L_{\text{plate}}} \cdot \frac{H_{\text{plate}}}{N_{\text{ch}}} \quad (2.18)$$

where

$$\begin{aligned} R_{\text{GDL}} &= \text{Gas diffusion layer resistance } [\Omega] \\ r_{\text{GDL}}^{\text{eff}} &= \text{Effective resistivity of the Gas diffusion layer } [\Omega] \\ N_{\text{ch}} &= \text{Number of channels } [-] \\ \delta_{\text{GDL}} &= \text{Gas diffusion layer regions thickness } [m] \\ H_{\text{ch}} &= \text{Width of the channels } [m] \\ L_{\text{plate}} &= \text{Total length of the plate } [m] \\ H_{\text{plate}} &= \text{Total width of the plate } [m] \end{aligned}$$

The effective resistivity of the gas diffusion layer, $r_{\text{GDL}}^{\text{eff}}$, can be found by Equation 2.19.

$$\text{Effective resistivity of the Gas diffusion layer: } r_{\text{GDL}}^{\text{eff}} = \frac{r_{\text{GDL}}}{(1 - \varphi_{\text{GDL}})^{\frac{3}{2}}} \quad (2.19)$$

where

$r_{\text{GDL}}^{\text{eff}}$ = Effective resistivity of the Gas diffusion layer $[\Omega]$

r_{GDL} = The normal resistivity of the material $[\Omega]$

φ_{GDL} = The empty fraction of the Gas diffusion layer $[-]$

2.4.4 Membrane resistivity

The resistance of the membrane can be modeled by integrating the local resistivity of the membrane with the thickness of the membrane as limits on the integral. Further dividing this integral with the surface area of the membrane provides the overall resistance. The equation is given in Equation 2.20.

$$\text{Membrane resistivity (Local) : } R_{\text{mem}} = \int_0^{\delta_{\text{mem}}} r_{\text{mem}}(\zeta) \cdot d\zeta \quad (2.20)$$

where

R_{mem} = Membrane resistivity $[\Omega]$

$r_{\text{mem}}(\zeta)$ = Local resistance of the membrane $[\Omega/\text{m}^2]$

δ_{mem} = Membrane thickness $[m]$

To describe the local resistance of the membrane, $r_{\text{textmem}}(\zeta)$, some empirical models have been suggested in ‘‘Proton Exchange Membrane Fuel Cells Modeling’’ [9]. As for which of these will be used is uncertain at this moment, and to calculate the local resistivity of the membrane, the local water content has to be calculated as well.

In addition to this, there are models for calculating global resistance, instead of considering the local resistance of the membrane. An example of this has been suggested [14], and is shown in Equation 2.21.

$$\text{Membrane resistivity (Global) : } R_{\text{mem}} = \frac{\left(\frac{\delta_{\text{mem}}}{A_{\text{mem}}} + \frac{F \cdot K_{\text{hydro}} \cdot c_{h^+} \cdot \Delta P_{A-C}}{\mu_{H_2O} \cdot i} \right)}{\left(\sigma_{\text{mem}} + \frac{F^2 \cdot K_{\text{ec}} \cdot c_{H^+}^2}{\mu_{H_2O}} \right)} \quad (2.21)$$

where

R_{mem} = Membrane resistivity $[\Omega]$

δ_{mem} = Membrane thickness $[m]$

A_{mem} = Membrane surface area $[m^2]$

F = Faradays constant $[\text{C}/\text{mol}]$ (96485.33289)

K_{hydro} = Membrane hydraulic permeability $[m^2]$

c_{h^+} = Charge concentration $[\text{mol}/\text{m}^3]$

ΔP_{A-C} = Pressure difference between anode and cathode side of the membrane $[Pa]$

μ_{H_2O} = Water viscosity of the membrane $[Pa \cdot s]$

i = Current through the cell $[A]$

σ_{mem} = Membrane conductivity(global) $[S/\text{m}]$

K_{ec} = Electrokinetic permeability of the membrane $[m^2]$

This is an easier way to calculate the resistance of the membrane, as values for Nafion type membranes have been calculated empirically, and the only variable would be ΔP_{A-C} , the thickness of the membrane and surface area of the membrane.

2.4.5 Concentration losses

In regards to the gas diffusion layer, there are diffusion from both sides. From the gas channels the gas diffuses towards the catalyst layer, while water diffuses from the catalyst layer towards the gas channels, causing partial pressure gradients of species over the GDL. [15] proposes the following equation to approximate voltage correction for concentration losses:

$$\text{Concentration losses : } V_{\text{conc}} = i \cdot \left(c_2 \cdot \frac{i}{i_{\text{max}}} \right)^{c_3} \quad (2.22)$$

where

$$\begin{aligned} V_{\text{conc}} &= \text{Concentration losses [V]} \\ i &= \text{Current through the cell [A]} \\ i_{\text{max}} &= \text{Max current through the cell [A]} \quad (2.2) \\ c_3 &= \text{Constant [-]} \quad (2) \end{aligned}$$

$$c_2 = \begin{cases} (7.16 \cdot 10^{-4} \cdot T_{\text{cell}} - 0.622) \cdot \left(\frac{P_{O_2}}{0.1173} + P_{\text{sat}} \right) + (-1.45 \cdot 10^{-3} \cdot T_{\text{cell}} - 1.68), & \text{if } \frac{P_{O_2}}{0.1173} + P_{\text{sat}} < 2\text{atm} \\ (8.66 \cdot 10^{-5} \cdot T_{\text{cell}} - 0.068) \cdot \left(\frac{P_{O_2}}{0.1173} + P_{\text{sat}} \right) + (-1.6 \cdot 10^{-4} \cdot T_{\text{cell}} - 0.52), & \text{otherwise} \end{cases} \quad (2.23)$$

2.4.6 Double layer capacity

The double layer effect is “the capacitance of the double layer formed by H^+ or H_3O^+ at the interface of the charged catalyst or carbon particles and polymer electrolyte.” [16], and can be described by Equation 2.24.

$$\text{Capacitance of the double layer : } C_{\text{dl}} = \epsilon_0 \cdot \epsilon_r \cdot \frac{S_{\text{dl}} \cdot \delta_{\text{cata}}}{\delta_{\text{dl}}} \cdot A_{\text{cata}} \quad (2.24)$$

where

$$\begin{aligned} C_{\text{dl}} &= \text{Capacitance of the double layer [F]} \\ \epsilon_0 &= \text{The electric constant [F/m]} \quad (8.854 \cdot 10^{-12}) \\ \epsilon_r &= \text{Static electromagnetic permittivity between electrolytic and electrode phases [F/m]} \\ S_{\text{dl}} &= \text{Effective catalyst surface area [m}^2\text{/m}^3\text{]} \\ \delta_{\text{mem}} &= \text{Electrical double layer thickness [m]} \end{aligned}$$

2.5 Fluidic domain

Modeling the fluidic domain on a cell level enables determination of pressures and flowrates in the cell.

To describe the change in pressure, the following differential equation can be used:

$$\text{Change in pressure: } \frac{dP}{dt} = \frac{dm_g}{dt} \cdot \frac{R \cdot T}{M_g \cdot V} \quad (2.25)$$

where

$$\begin{aligned} \frac{dP}{dt} &= \text{Change in pressure [Pa/s]} \\ \frac{dm_g}{dt} &= \text{Molar mass transfer rates [mol/s]} \\ R &= \text{Molar gas constant [C/mol}\cdot\text{K]} (8.314) \\ T &= \text{Temperature of the gas [K]} \\ M_g &= \text{Molar mass of the gas [g]} \\ V &= \text{Volume of the gas [m}^3\text{]} \end{aligned}$$

In the PEMFC, the gasses and liquids shown in Table 2.2, should be considered

Table 2.2: An overview of different gasses and liquids in the PEMFC.

Cathode	Anode
H_2O - gas	H_2O - gas
H_2O - liquid	H_2 - gas
O_2 - gas	
N_2 - gas	

For these mass flows, the following formulas can be used [17].

$$\text{H}_2\text{- gas: } \frac{dm_{H_2}}{dt} = q_{A,\text{in}} \frac{m_{H_2,\text{in}}}{m_{H_2,\text{in}} + m_{w,g,A,\text{in}}} - \frac{I_{\text{cell}}}{2 \cdot F} \cdot M_{H_2} - (q_{A,\text{Out}} + q_{\text{purge}}) \cdot \frac{m_{H_2}}{m_{H_2} + m_{w,g,A}} \quad (2.26)$$

$$\text{m}_{w,g,A}\text{- gas: } \frac{dm_{w,g,A}}{dt} = q_{A,\text{in}} \frac{m_{w,g,A,\text{in}}}{m_{H_2,\text{in}} + m_{w,g,A,\text{in}}} - \alpha \cdot \frac{I_{\text{cell}}}{2 \cdot F} \cdot M_{H_2} - (q_{A,\text{Out}} + q_{\text{purge}}) \cdot \frac{m_{w,g,A}}{m_{H_2} + m_{w,g,A}} \quad (2.27)$$

$$\text{O}_2\text{- gas: } \frac{dm_{O_2}}{dt} = q_{C,\text{in}} \frac{m_{O_2,\text{in}}}{m_{O_2,\text{in}} + m_{N_2,\text{in}} + m_{w,g,C,\text{in}}} - \frac{I_{\text{cell}}}{4 \cdot F} \cdot M_{O_2} - q_{C,\text{Out}} \cdot \frac{m_{O_2}}{m_{O_2} + m_{N_2} + m_{w,g,C}} \quad (2.28)$$

$$\text{N}_2\text{- gas: } \frac{dm_{N_2}}{dt} = q_{C,\text{in}} \frac{m_{N_2,\text{in}}}{m_{O_2,\text{in}} + m_{N_2,\text{in}} + m_{w,g,C,\text{in}}} - q_{C,\text{Out}} \cdot \frac{m_{N_2}}{m_{O_2} + m_{N_2} + m_{w,g,C}} \quad (2.29)$$

$$\begin{aligned} \text{m}_{w,g,C}\text{- gas: } \frac{dm_{w,g,C}}{dt} &= q_{C,\text{in}} \frac{m_{w,g,C,\text{in}}}{m_{O_2,\text{in}} + m_{N_2,\text{in}} + m_{w,g,C,\text{in}}} - (1 + 2\alpha) \cdot \frac{I_{\text{cell}}}{2 \cdot F} \cdot M_{H_2O} \\ &\quad - q_{C,\text{Out}} \cdot \frac{m_{w,g,C}}{m_{O_2} + m_{N_2} + m_{w,g,C}} - \frac{dm_{w,g \rightarrow l}}{dt} \quad (2.30) \end{aligned}$$

$$m_{w,l,C} \text{- gas: } \frac{dm_{w,l,C}}{dt} = \frac{dm_{w,g \rightarrow l}}{dt} - q_{C,out} \cdot \frac{m_{w,l,C}}{m_{O_2,in} + m_{N_2,in} + m_{w,g,C,in}} \quad (2.31)$$

$$\text{Water transfer coefficient: } \alpha = \frac{q_{mem,H_2O,net}}{q_{mem,H^+,net}} \quad (2.32)$$

2.6 Thermal domain

By modeling the thermal domain, the influence of different heat sources can be determined. A dynamic model can be made and has been described in [18] article as Equation 2.33.

$$\text{Thermal domain: } m_{cell} \cdot C_{p,cell} \cdot \left(\frac{dT_{cell}}{dt} \right) = Q_{theo} - Q_{elec} - Q_{conv} - Q_{lat} - Q_{loss} \quad (2.33)$$

where

m_{cell} = Mass of the cell [g]

$C_{p,cell}$ = The cells thermal capacity [J/g·K·s²]

$\left(\frac{dT_{cell}}{dt} \right)$ = Change in cell temperature [K/s]

Q_{theo} = The theoretically produced power in the electrochemical reaction [W]

Q_{elec} = The electrical power [W]

Q_{conv} = The convective thermal channel flux [W]

Q_{lat} = The latent heat exchange from water phase change [W]

Q_{loss} = The loss [W]

2.7 Impedance Spectroscopy

Impedance spectroscopy allows us to characterize many electrical properties of a material only by measuring with two electronically conducting electrodes. Much of this chapter is inspired by GAMRY Instruments website [19], which have made a very nice explanation for electrochemical impedance spectroscopy.

2.7.1 Basics of Electrochemical Impedance Spectroscopy

Electrochemical Impedance is usually measured by applying voltage to a cell and measuring the response. A sinusoidal voltage is applied to the poles of the cell in question, then measuring the generated AC (alternating current) signal. This usually follows the same frequency, but with a shifted phase angle. In mathematical terms, the following formulas explain the process. [19]

$$\text{The excitation signal: } E_t = E_0 \cdot \sin(\omega t) \quad (2.34)$$

where

E_t = Potential at time t [V]

E_0 = Amplitude of the signal [V]

ω = Radial frequency [rad/s]

t = Time [s]

$$\text{Radial frequency: } \omega = 2\pi f \quad (2.35)$$

where

$$\begin{aligned} \omega &= \text{Radial frequency [rad/s]} \\ f &= \text{Frequency [Hz]} \end{aligned}$$

$$\text{The response signal: } I_t = I_0 \cdot \sin(\omega t + \phi) \quad (2.36)$$

where

$$\begin{aligned} I_t &= \text{Current at time t [A]} \\ I_0 &= \text{Amplitude of the signal [A]} \\ \omega &= \text{Radial frequency [rad/s]} \\ t &= \text{Time [s]} \\ \phi &= \text{Shift in phase [rad]} \end{aligned}$$

Then the impedance of the system is calculated:

$$\text{Impedance of the system: } Z = \frac{E_t}{I_t} = \frac{E_0 \cdot \sin(\omega t)}{I_0 \cdot \sin(\omega t + \phi)} = Z_0 \frac{\sin(\omega t)}{\sin(\omega t + \phi)} \quad (2.37)$$

where

$$\begin{aligned} Z &= \text{Impedance of the system } [\Omega] \\ Z_0 &= \text{Magnitude of the impedance } [\Omega] \\ E_t &= \text{Potential at time t [V]} \\ E_0 &= \text{Amplitude of the signal [V]} \\ I_t &= \text{Current at time t [A]} \\ I_0 &= \text{Amplitude of the signal [A]} \\ \omega &= \text{Radial frequency [rad/s]} \\ t &= \text{Time [s]} \\ \phi &= \text{Shift in phase [rad]} \end{aligned}$$

This is then expressed as magnitude (Z_0), and phase shift (ϕ). Before modern EIS instrumentation became available, the excitation signal and the response signal were displayed on an oscilloscope on the X-axis and the Y-axis, respectively. This created an oval shaped figure known as the “Lissajous Figure”, and was the accepted method for measuring impedance. An example of this is shown in figure 2.9.[19]

It is possible to express the impedance as a complex function using Euler's relationship, by using equation 2.38.[19]

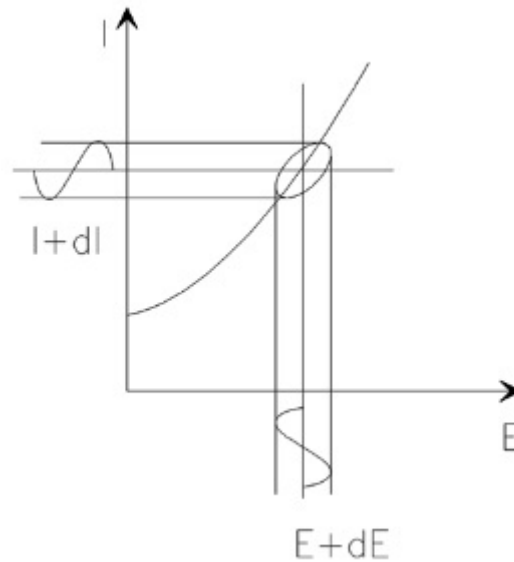


Figure 2.9: The oval in the center is known as the Lissajous Figure..

Impedance as a complex function: $Z_\omega = Z_0 \cdot e^{-j\phi} = Z_0 \cdot (\cos(\phi) + j\sin(\phi))$ (2.38)

where

Z_ω = Magnitude of the impedance [Ω]

Z_0 = Magnitude of the impedance [Ω]

ϕ = Shift in phase [rad]

2.7.2 Data presentation

If the real and imaginary part of (Z_ω) is plotted in the X-axis and the Y-axis respectively, we get the Nyquist plot. The imaginary part is usually plotted as a negative value, for reading in the right upper half quadrant. An example of a simple Nyquist plot is shown in figure 2.10, and it represent an ideal resistor and a capacitor in parallel. One of the drawbacks of this representation is that one cannot see the frequency used at any given data point. We only knowe that high frequency is on the left side, and that the low frequency on the right side. To show the frequency at each data point, one can utilize the popular method called Bode plot. Though in this thesis we will be using the Nyquist plot, as it easily shows the internal resistance, which will be our focus for these measurements.[19]

2.7.3 Equivalent circuit

An equivalent circuit is the representation of a system or process by building up a simple circuit with ideal electrical components. It is best to use as few components as possible, while still mimicking the system's response fairly accurate. [19]

These models can be used for easier understanding and comparing the complex behavior of the electrochemical cell, as well for simpler simulation of the electrical part of a fuel cell.[19]

A basic equivalent circuit of a fuel cell is usually made of a voltage source (E), an activation resistance (R_a) in parallel with the double layer capacitor (Cdl) and, in series, an internal resistance (R_r) (Se fig). Although this is the basic fuel cell representation, not all fuel cells systems can be modeled this way. A bad cell may look quite different in an equivalent circuit representation and may have multiple resistors and capacitors.[19]

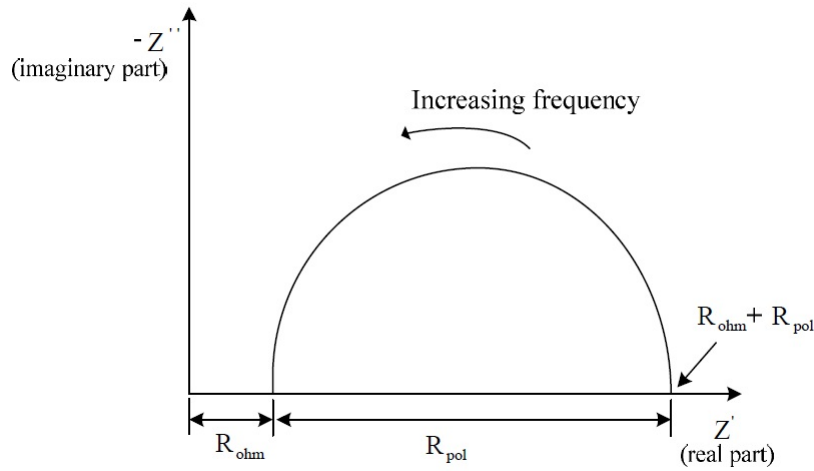


Figure 2.10: The Nyquist plot.

Electrical circuit elements

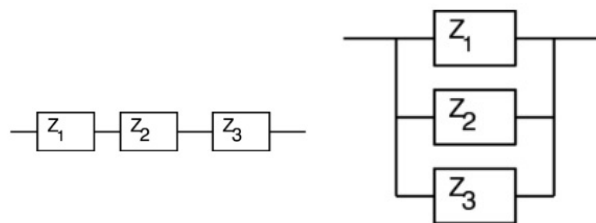
It is useful to have an idea of the elements used in an equivalent circuit. Table 2.3 shows the three common components (Resistor, Inductor and Capacitor) with their current versus voltage relationship and its impedance value. The less known circuit component is the Warburg elements, that represents diffusion process in material with dielectric properties, and the CPE (Constant Phase Element) represent the double layer as an imperfect capacitor or just imperfect dielectric properties.[19]

Table 2.3: Circuit elements used in the equivalent circuit.

Component	Current Vs Voltage	Impedance
Resistor	$E = IR$	$Z = R$
Inductor	$E = L \frac{di}{dt}$	$Z = j\omega L$
Capacitor	$I = C \frac{dE}{dt}$	$Z = \frac{1}{j\omega C}$
W (Infinite Warburg)		$\frac{1}{Y_0} \sqrt{j\omega}$
O (Finite Warburg)		$\frac{1}{Y_0} \tanh(B\sqrt{j\omega})$
CPE (Constant Phase Element)		$\frac{1}{(j\omega)^\alpha Y_0}$

Serial and Parallel combinations

When making an equivalent circuit it is common to use several elements in a network, which include elements in both serial and parallel.



(a) Impedance in series. (b) Impedance in parallel.

Electrolyte resistance

The resistance in an electrochemical cell is often quite significant when measuring the impedance. The resistance depends on several factors like type of ions, ionic concentration and temperature, but here we will focus mostly on the surface area and the length which carries a uniform current. This will be represented as the following formula. [19]

$$\text{Electrolyte resistance: } R = \rho \frac{l}{A} \quad (2.39)$$

where

$$\begin{aligned} R &= \text{Electrolyte resistance } [\Omega] \\ \rho &= \text{Solution resistivity } [\Omega m] \\ l &= \text{Length } [m] \\ A &= \text{Area } [m^2] \end{aligned}$$

Standard chemical will list k values for specific solutions in a datasheet.

Double layer capacitance

A charge will be generated at the interface between the electrode and the electrolyte. This occurs when electrons in the electrode gets attracted to the surface by the H^+ ions in the electrolyte. This phenomenon will behave much like an electrical capacitor, which is given in formula 2.40, but the capacitance value can be estimated to about 20 to 60 μF for every cm^2 . There is, of course, much more to this phenomenon, but that is beyond the scope of this thesis. [19]

$$\text{Capacitance: } C = \epsilon \frac{A}{d} \quad (2.40)$$

where

$$\begin{aligned} C &= \text{Capacitance } [F] \\ \epsilon &= \text{electrical permittivity } [F/m] \\ A &= \text{Surface area } [m^2] \\ d &= \text{Separation of the plates } [m] \end{aligned}$$

Polarization resistance

When a potential is forced away from its open circuit value, current will flow through the reactants that occurs at the electrodes surface. This is often called “polarizing” the electrode, and the amount of current is controlled by the kinetics of the reactants. This phenomenon also happens during corrosion, where the amount of current represent the activity of the corrosion process. It can also be applied to non corrosion cases, which is called mixed potential control. The representation of this is shown in equation 2.41 and 2.42.[19]

$$\text{The measured cell current: } I = I_{\text{corr}} \left(e^{\frac{2.303(E-E_{OC})}{\beta_a}} - e^{\frac{-2.303(E-E_{OC})}{\beta_c}} \right) \quad (2.41)$$

where

$$\begin{aligned} I &= \text{Measured cell current } [A] \\ I_{\text{corr}} &= \text{Corrosion current } [A] \\ E &= \text{Potential of the cell } [V] \\ E_{OC} &= \text{Open circuit potential } [V] \\ \beta_a &= \text{Anodic Beta coefficient } [V/\text{decade}] \\ \beta_c &= \text{Cathodic Beta coefficient } [V/\text{decade}] \end{aligned}$$

$$\text{The corrosion current: } I_{\text{corr}} = \frac{\beta_a \cdot \beta_c}{2.303 \cdot (\beta_a + \beta_c)} \cdot \left(\frac{1}{R_p} \right) \quad (2.42)$$

where

$$\begin{aligned} I_{\text{corr}} &= \text{Corrosion current [A]} \\ \beta_a &= \text{Anodic Beta coefficient [V/decade]} \\ \beta_c &= \text{Cathodic Beta coefficient [V/decade]} \\ R_p &= \text{Polarization resistance } [\Omega] \end{aligned}$$

Charge transfer resistance

Charge transfer resistance is caused by the kinetically controlled electrochemical reaction where substances dissolve into the electrolyte. This reaction has a certain speed depending on the type of reaction, temperature, the potential and the concentration of the reaction products. The relation between the potential and current is shown in Equation 2.43.[19]

$$\text{Electrode current density: } i = i_0 \left(\frac{C_O}{C^{*O}} \exp \left[\frac{\alpha n F \eta}{RT} \right] - \frac{C_R}{C^{*R}} \exp \left[\frac{-(1-\alpha)nF\eta}{RT} \right] \right) \quad (2.43)$$

where

$$\begin{aligned} i &= \text{Electrode current density [A/m}^2\text{]} \\ i_0 &= \text{Exchange current density [A/m}^2\text{]} \\ C_O &= \text{concentration of oxidant at the electrode surface [-]} \\ C^{*O} &= \text{Concentration of oxidant in the bulk [-]} \\ C_R &= \text{Concentration of reductant at the electrode surface [-]} \\ C^{*R} &= \text{Concentration of reductant in the bulk [-]} \\ \alpha &= \text{Charge transfer coefficient [-]} \\ \eta &= \text{Activation overpotential [V]} \\ R &= \text{Molar gas constant [C/mol}\cdot\text{K]} (8.314) \\ T &= \text{Temperature [K]} \\ n &= \text{Number of electrons involved in reaction [-]} \\ F &= \text{Faradays constant [C/mol]} \end{aligned}$$

If the concentration in the bulk is the same as the concentration as the electrode surface, the Equation 2.43 can be simplified to what is called the Butler-Volmert equation. If the over potential is very small and the electrochemical system is at equilibrium, the equation can be simplified even more, as seen in Equation 2.44.[19]

$$\text{Charge transfer resistance: } R_{ct} = \frac{R \cdot T}{n \cdot F \cdot i_0} \quad (2.44)$$

where

$$\begin{aligned} R_{ct} &= \text{Charge transfer resistance } [\Omega] \\ R &= \text{Molar gas constant } [\text{C/mol}\cdot\text{K}] \text{ (8.314)} \\ T &= \text{Temperature } [K] \\ n &= \text{Number of electrons involved in reaction } [-] \\ F &= \text{Faradays constant } [\text{C/mol}] \\ i_0 &= \text{Equilibrium exchange current } [A] \end{aligned}$$

Diffusion

Diffusion will create Warburg impedance, which depends on the frequency of the potential perturbation. Since the diffusing reactants do not have to move very far at high frequencies, the impedance will be small. And at low frequencies, the reactants have to move further to diffuse, thus increasing the impedance. This is only valid for very thick (infinite) diffusion layer, shown with Equation 2.45. For a thin or coated (finite) diffusion layer, one needs to use Equation 2.47. On a Nyquist plot, this will appear as a diagonal line with a slope of 45 deg.[19]

$$\text{Infinite Warburg impedance: } Z_W = \sigma \cdot \omega^{-\frac{1}{2}} \cdot (1 - j) \quad (2.45)$$

where

$$\begin{aligned} Z_W &= \text{Infinite Warburg impedance } [\Omega] \\ \sigma &= \text{Warburg coefficient } [-] \\ \omega &= \text{Radial frequency } [\text{rad/s}] \end{aligned}$$

$$\text{Warburg coefficient: } \sigma = \frac{RT}{n^2 F^2 A \sqrt{2}} \cdot \left(\frac{1}{C^{*O} \sqrt{C_O}} + \frac{1}{C^{*R} \sqrt{C_R}} \right) \quad (2.46)$$

where

$$\begin{aligned} \sigma &= \text{Warburg coefficient } [-] \\ R &= \text{Molar gas constant } [\text{C/mol}\cdot\text{K}] \text{ (8.314)} \\ T &= \text{Temperature } [K] \\ n &= \text{Number of electrons involved in reaction } [-] \\ F &= \text{Faradays constant } [\text{C/mol}] \\ A &= \text{Surface area of the electrode } [m^2] \\ C_O &= \text{concentration of oxidant at the electrode surface } [-] \\ C^{*O} &= \text{Concentration of oxidant in the bulk } [-] \\ C_R &= \text{Concentration of reductant at the electrode surface } [-] \\ C^{*R} &= \text{Concentration of reductant in the bulk } [-] \end{aligned}$$

$$\text{Finite Warburg impedance: } Z_0 = \sigma \cdot \omega^{-\frac{1}{2}} \cdot (1 - j) \cdot \tanh\left(\delta \left(\frac{j\omega}{D}\right)^{-\frac{1}{2}}\right) \quad (2.47)$$

where

$$\begin{aligned} Z_0 &= \text{Finite Warburg impedance } [\Omega] \\ \sigma &= \text{Warburg coefficient } [-] \\ \omega &= \text{Radial frequency } [\text{rad/s}] \\ \delta &= \text{Nernst diffusion layer thickness } [m] \\ D &= \text{diffusion coefficient } [-] \end{aligned}$$

These equations may be written in terms of an admittance parameter, as shown in table 2.3, where Equation 2.48 and 2.49 are used.[19]

$$\text{Admittance parameter: } Y_0 = \frac{1}{\sigma\sqrt{2}} \quad (2.48)$$

where

$$\begin{aligned} Y_0 &= \text{Admittance parameter } [-] \\ \sigma &= \text{Warburg coefficient } [-] \end{aligned}$$

$$\text{Variable B: } B = \frac{\delta}{\sqrt{2}} \quad (2.49)$$

where

$$\begin{aligned} \delta &= \text{Thickness of the diffusion layer } [m] \\ D &= \text{diffusion coefficient } [-] \end{aligned}$$

2.8 Arduino

Parts of the project in this master thesis is based on Arduino. In this sub-chapter an explanation of what an Arduino is, and how the programming language works will be presented. This entire sub-chapter is based on information found on Arduino.cc. [7]

“Arduino is an open-source electronics platform based on easy-to-use hardware and software. Arduino boards are able to read inputs – light on a sensor, a finger on a button, or a Twitter message – and turn it into an output – activating a motor, turning on an LED, publishing something online. You can tell your board what to do by sending a set of instructions to the microcontroller on the board. To do so you use the Arduino programming language (based on Wiring), and the Arduino Software (IDE), based on processing.” [7]

The center-piece or brain of the Arduino is a microcontroller, which is a small computer with one or more central processor units, memory and in- and outputs which can be programmed. This microcontroller is then connected to the different pins on the Arduino board, which vastly decreases the difficulty of connecting cables, and understand where to connect different inputs and outputs to the board, or in other words, the microcontroller.[7]

There are different Arduino boards, but for this project the Arduino Uno or the Arduino Mega 2560 are the most appropriate ones to use. Both boards have digital input/output pins,

analog inputs, a 16 MHz quartz crystal, a USB connection, a power jack. An ICSP header and a reset button. Both boards operate at 5 volts, and can be powered by the USB connection or the power jack. The power supply is recommended to stay between 7-12V, due to stability and overheating issues outside of this span. In addition to this, it must be a DC source of power. [7]

The difference between the Uno and Mega 2560 is the microcontroller, and the differences brought on by the microcontroller. An Arduino Uno is equipped with an ATmega328P microcontroller, while the Mega 2560 has an ATmega2560 microcontroller. This means that the Arduino Mega 2560 has more memory, and more analog and digital pins. The differences between the two boards can be seen in Table 2.4. [7]

Table 2.4: Specs of both Arduino boards [7].

Arduino model	Uno	Mega 2560
Microcontroller	ATmega328P	ATmega2560
Operating voltage	5V	
Input Voltage(recommended)	7-12V	
Input Voltage(limit)	6-20V	
Clock Speed	16 MHz	
Digital I/O Pins	14(6 PWM)	54(15PWM)
Analog Input Pins	6	16
DC Current per I/O Pin	20 mA	
DC Current for 3.3V Pin	50 mA	
Flash memory	32 kB	256 kB
SRAM	2 kB	8 kB
EEPROM	1 kB	4 kB
LED BUILTIN	13	
Length	68.6 mm	101.52 mm
Width	53.4 mm	53.3 mm
Weight	25 g	37 g

2.8.1 Pins of the Arduino

There are both digital and analog pins in the Arduino boards. The analog pins are mainly used as sensor pins, or input pins, which can read 0 to 5 volts. Due to the analog-to-digital converter in the Arduino this span of 0 to 5 volts is converted into integers from 0 to 1023. The digital pins of the Arduino can either be inputs or outputs. As an output, these pins are able to output a HIGH or LOW state, which basically means on or off. In addition to this, some of the digital pins can provide a PWM signal, varying from 0 to 255. PWM is a signal pulsing on and off very fast, with a duty ratio from 0 to 1, enabling i.g. a fan to run at a duty ratio of 0.4, which would mean that it is running at 40% capacity. The PWM is often used on a transistor to control larger units such as motors and fans. As an input, the digital pin receives HIGH or LOW. [7]

2.8.2 Programming Arduino

As pointed out earlier, the Arduino has its own programming language, which is based on Wiring [7]. Some of the functions in this programming language will be explained here.

The first thing you generally do is to include any library necessary to your script. This is done by a `<Library.h>` command. Library

`int` – is used as a way to store numbers. In the Uno and Mega board, this command stores a 16-bit value, which means a range of plus/minus 32 767. As example of this could be the following, which in this case enables the variable `voltage1` to store the value of analog pin seven:

```
int voltage1= A7;
```

`pinMode()` – This command defines a pin as either an input or output. The example below shows how a digital clicker is connected to the digital pin 1, as an input:

```
pinMode(digitalClicker1,INPUT);
```

`begin()` – in order to communicate with a computer this command is to set the rate of transmission of data. Example or a transfer rate of 9600bps:

```
Serial.begin(9600);
```

`analogRead()` – This command is used to read the values from an analog pin. The Arduino maps input voltages on analog pins from 0 to 5 volts, to integer values between 0 and 1023. The example provided below allows the Arduino to read the potpot analog pin and store it in the variable `sensorValue`:

```
sensorValue=analogRead(potpot);
```

`analogWrite()` – This is used to write a PWM wave to a pin. Using `analogWrite` will send a square wave signal to the specified pin, at the specified duty cycle. The example below sends an PWM signal to output 3, or `mosfetControl` as it is called in the script. The PWM signal used is the one stored in the variable `outputValue`:

```
analogWrite(mosfetControl,outputValue);
```

`digitalread()` – This is used in the same manner as the `analogRead`. To read a digital input pin the Arduino must be told to do so. This reads the clicker connected to a digital pin:

```
digitalRead(digitalClicker1);
```

`digitalWrite()` – To output a HIGH or LOW signal to a digital pin, this function must be used. The following is used to turn off a relay which controls a heating element:

```
digitalWrite(heater, LOW);
```

`map()` – This is used to remap one value from the original value span to a new value span. The example presented below converts the value of the variable `sensorValue`, which holds the potpot analog pin, which is 0 to 1023, to the value span of a PWM signal on the Arduino, 0 to 255:

```
outputValue=map(sensorValue,0 ,1023 ,0 ,255);
```

`delay()` – This command pauses the program for as long as you would like. The length of the pause is given in milliseconds. In this example the program pauses for ten milliseconds:

```
delay(10);
```

`setup()` – This function is used to initialize. In the void `setup()` one sets up pin modes, variables etc. An example of the void `setup()` for controlling a fan with a potentiometer is shown below:

```
Void setup() {  
  Serial.Begin(9600);  
  pinMode(currentSensor,INPUT);  
  pinMode(mosfetControl,OUTPUT);  
  pinMode(potpot,INPUT);
```

}

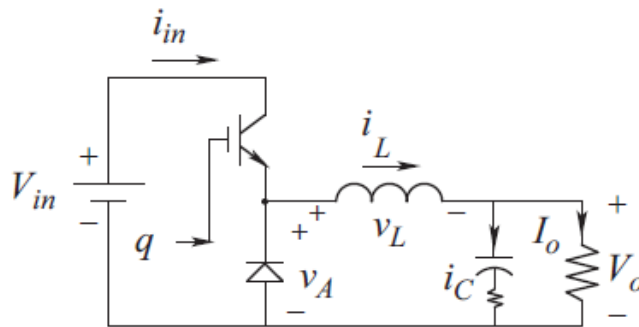
In addition to these very commonly used commands, there are commands activated by the libraries connected. These can be libraries and commands for i.g. LCD screens.

2.9 Power electronic

DC-DC converters are used to manipulate DC voltages and currents from one level to another. They can be used to regulate steady state input to a steady state output, or they can regulate varying DC sources to i.g. a steady state voltage output. The three covered converters in this section is the Buck converter, the Boost converter and the Buck-Boost converter. A brief explanation will be provided on each of them.

2.9.1 Buck converter

A Buck converter can change the output voltage to be lower than the input voltage. This can be done by changing the on-off switching cycle, for each time period. This ratio is also called the duty ratio. When turning the transistor on the current in the transistor increases, and when the transistor is turned off, the current in the inductors freewheels through the diode. [20]



Assuming that ideal components is used, the duty ratio can be calculated by using the input as output voltages, as shown in Equation 2.50[20].

Figure 2.12: A circuit diagram of the Buck converter [5].

$$\text{Ratio between output and input voltage: } V_0 = D \cdot V_{\text{inn}} \quad (2.50)$$

where

$$\begin{aligned} V_0 &= \text{output voltage [V]} \\ V_{\text{inn}} &= \text{input voltage [V]} \\ D &= \text{Duty ratio [-]} \end{aligned}$$

If the inductor runs out of energy, meaning it can no longer provide current through the circuit, the converter will go into what is called discontinuous conduction mode(DCM). Here it can no longer provide the energy required for the load, and it increases the stress throughout the device. This is undesirable, and to avoid this an appropriate inductor value should be calculated to ensure continuous conduction mode (CCM). An approach for calculating this is to find the critical inductor value, where the device is in between the borders of CCM and DCM, then choose a component larger than this (usually three times larger). The critical value for the inductor can be determined by using equation 2.51[20].

$$\text{Critical inductor value : } L_{\text{crit}} = \frac{R(1 - D)}{(2 \cdot f_s)} \quad (2.51)$$

where

$$\begin{aligned} L_{\text{crit}} &= \text{output voltage [H]} \\ R &= \text{Equivalent load resistance [\Omega]} \\ D &= \text{Duty ratio [-]} \\ F_s &= \text{Switching frequency [Hz]} \end{aligned}$$

2.9.2 Boost converter

A boost converter can change the output voltage to be higher than the input voltage. When turning the transistor on, the diode is isolating the output. The input ramps up the current/energy in the inductor. When the transistor is off, the inductor outputs the stored energy, meaning that energy from both the inductor and the input is directed towards V_{out} . [20].

Assuming that ideal components are used, the duty ratio can be calculated by using the input and output voltages, as shown in Equation 2.54 [20].

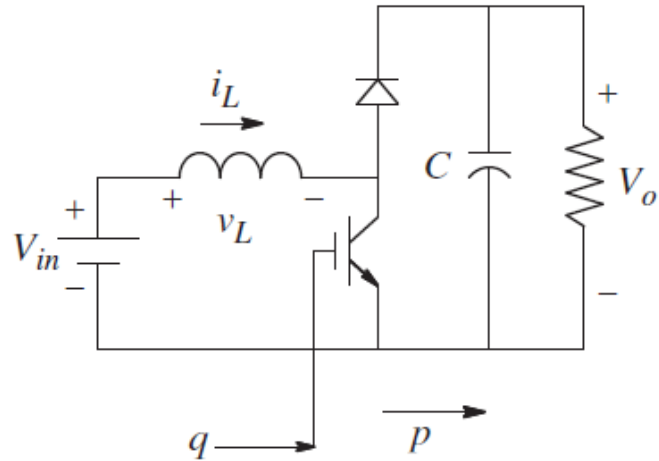


Figure 2.13: A circuit diagram of the Boost converter [5].

$$\text{Ratio between output and input voltage : } \frac{V_o}{V_{in}} = \frac{D}{(1-D)} \quad (2.52)$$

where

V_o = output voltage [V]

V_{in} = input voltage [V]

D = Duty ratio [-]

The critical value for the inductor can be determined by equation 2.55[20].

$$\text{Critical inductor value : } L_{crit} = \frac{R \cdot D(1-D)^2}{(2 \cdot f_s)} \quad (2.53)$$

where

L_{crit} = output voltage [H]

R = Equivalent load resistance [Ω]

D = Duty ratio [-]

f_s = Switching frequency [Hz]

2.9.3 Buck-Boost converter

A Buck-Boost converter (shown in figure 2.14.) can change the output voltage (V_o) to be greater or lower than the input voltage (V_{in}). This can be done by changing the on-off switching cycle (q), for each time-period (TS). This ratio is also called the duty ratio (D). When turning the transistor on, the inductor will experience the same voltage as the source (V_{in}) and “charge up”. At a certain point the transistor turns off and the inductor will release its energy through the load and the diode.[20]

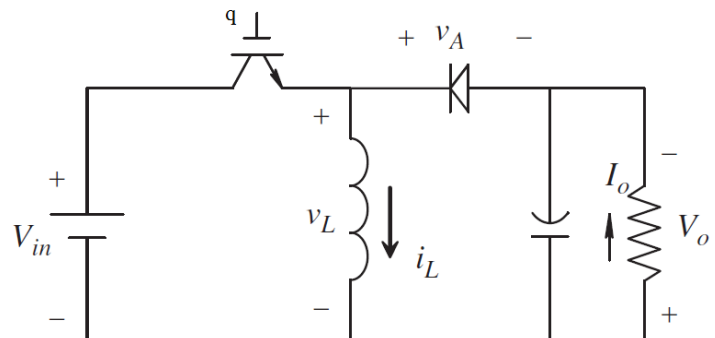


Figure 2.14: A circuit diagram of the Buck-Boost converter [5].

Assuming that ideal components are used, the duty ratio can be calculated by using the input and output voltages, as shown in Equation 2.54.

$$\text{Ratio between output and input voltage : } \frac{V_0}{V_{\text{inn}}} = \frac{D}{(1-D)} \quad (2.54)$$

where

$$\begin{aligned} V_0 &= \text{output voltage [V]} \\ V_{\text{inn}} &= \text{input voltage [V]} \\ D &= \text{Duty ratio [-]} \end{aligned}$$

The critical value for the inductor can be determined by using Equation 2.55[20].

$$\text{Critical inductor value : } L_{\text{crit}} = \frac{R(1-D)^2}{(2 \cdot f_s)} \quad (2.55)$$

where

$$\begin{aligned} L_{\text{crit}} &= \text{output voltage [H]} \\ R &= \text{Equivalent load resistance } [\Omega] \\ D &= \text{Duty ratio [-]} \\ f_s &= \text{Switching frequency [Hz]} \end{aligned}$$

2.10 Fuel cell comparing

When comparing a fuel cell with other cells and power sources, certain standard values need to be calculated. The most common units are Current density (Equation 2.56), Power density (Equation 2.57) and Specific power (Equation 2.58) [2].

$$\text{Current Density: } I_{\text{Density}} = \frac{I}{A} \quad (2.56)$$

where

$$\begin{aligned} I_{\text{Density}} &= \text{Current density [mA/cm}^2] \\ I &= \text{Cell current output [mA]} \\ A &= \text{Cell area [cm}^2] \end{aligned}$$

$$\text{Power Density: } P_{\text{Density}} = \frac{P}{V} \quad (2.57)$$

where

$$\begin{aligned} P_{\text{Density}} &= \text{Power density [kW/m}^3] \\ P &= \text{Fuel cell power output [kW]} \\ V &= \text{Fuel cell volume [m}^3] \end{aligned}$$

$$\text{Specific Power: } P_{\text{Specific}} = \frac{P}{M} \quad (2.58)$$

where

$$P_{\text{Specific}} = \text{Specific Power [kW/kg]}$$

$$P = \text{Fuel cell power output [kW]}$$

$$M = \text{Fuel cell Mass [kg]}$$

Chapter 3

Method

This chapter will provide an overview of what thoughts and initial calculations we chose for our raw foundation in the design choices. In addition, a review to the limitations and a description of the design from our previous project has been included.

3.1 Work plan

This thesis will be divided into two parts. The first part will cover the fuel cell stack and the process for better performance and construction. The other part will cover all the control systems for the fuel cell and the test station is developed for the stack and others like it.

As described in chapter 1, the goal for this project is to make a functioning cell with a voltage output of 5 voltage DC. This was chosen because it is a common voltage for user electronics, like mobile phones and other USB devices.

Table 3.1: The work schedule.

Tasks	Estimated time consumption
Start presentation	1 Week
Ordering parts	1 Week
Modeling and calculation	5 Weeks
Parts arriving	
Preparation / Test assembly	2 Weeks
Testing	4 Weeks
Report writing	4 Weeks
Finalizing project	1 Week
Total	18 Weeks

3.1.1 Literature study

There has been some extensive work on the theory of modeling. Our thought being that a working model, yielding results close to the actual fuel cell, will help us understand the effect of different operating conditions.

The literature study has provided us with a deeper knowledge of the theory behind fuel cell, and PEMFC in particular.

3.2 Initial fuel cell estimation and material choice

As previously mentioned, the goal for this project is to be able to deliver an output voltage of 5 volts. This can be accomplished by connecting multiple cells in series, interconnected with bipolar plates. Interconnecting with bipolar plates is by far the most common practice, as it is a space-saving solution (since the plate stacks comprises almost 80% of the fuel cell stack volume [2]), in comparison with having one anode and one cathode endplate for each individual cell.

Before embarking on the design, some calculation is needed to find out key values. Then after, one can start making the design based on these findings.

3.2.1 Cell voltage

From Equation 2.4 in Chapter 2.1, we know that the no loss voltage is 1.23 Volt. As described in Chapter 2, the voltage quickly drops, due to different losses. An I-V curve of a typical low temperature, low pressure fuel cell has been illustrated in Figure 2.2. From this figure, an output voltage of approximately 0.7 Volt would give the maximum output power per ideal cell. With this voltage level for each cell, a stack of 7-8 cells should be sufficient to achieve the desired output voltage and provide optimal power output. For this project, seven stacks were chosen. Should the need for adjusting this number of cells arise, there will be no problems in doing so. After knowing the number of cells necessary to achieve the desired current, the next step was to choose the proper size for the cell.

3.2.2 Cell size

Having both the voltage and number of cells calculated, the next focus is the cell sizing. The fuel cell power output is mostly proportional to the area, though the usual standard for experimental cells is 5 by 5 centimeters [21]. Another important feature of the fuel cell stack design is the reactant gasses properties, or rather the state they are in. Hydrogen gas is stored in pressurized canisters to minimize the space required. This makes the pressure drop throughout the cell a small problem, since the gas comes out in high pressure, and needs to be reduced anyway. However, the oxygen comes from the air at ambient pressure, and may need a fan to push it through. This requires power to run, and is something one would want to minimize, therefore the pressure drop on this side should also be minimized.

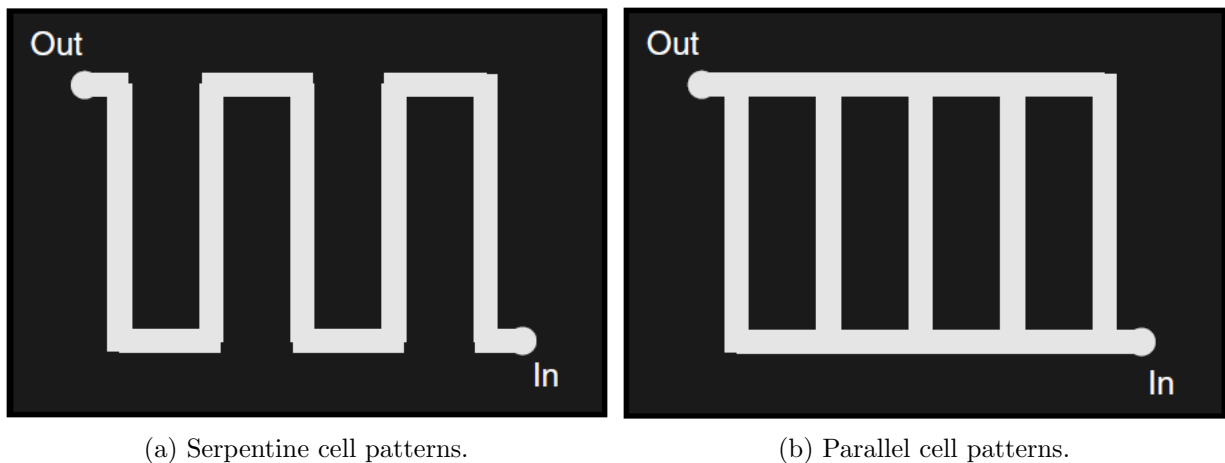


Figure 3.1: The Serpentine and Parallel patterns from Fuel Cell Systems Explained [2]

Utilizing this information, we decided on a design where the channel on the anode side (hydrogen gas side) is maximized in length, meaning, a single long channel in a serpentine pattern, illustrated in Figure 3.1a. The cathode side (air side), has many straight and short parallel channels, illustrated in Figure 3.1b. To still be able to use the standard experimental size material, the aimed area will be halved to a a 2.5 by 5 centimeters cell size.

3.2.3 Fuel cell material

The material used in the fuel cell is a quite important topic. Having multiple cells in the stack means that bipolar plates will be used. This is by far the most common in stacks, though there are alternatives. The material requirements for bipolar plates is good electrical conduction, good heat conductivity, good gas permeability, corrosion resistant, reasonable stiffness and low cost. If it is to be commercially manufactured it would also need to be lightweight, slim and easy to manufacture. Achieving all the requirements are quite difficult [22].

Often used materials are graphite plates or metals plates (like stainless steel, titanium and aluminum) usually with coatings [22]. To improve the lifetime the material, we changed from aluminum to stainless steel. This increases the weight and lower the electrical conductivity, but is more corrosion resistant in a fuel cell environment and it is easier to mill out smaller traces

while maintaining good strength. We also want to use carbon graphite plate, which has the best corrosion resistant properties.

The housing is to be printed using a 3D printer utilizing a dense type of plastic (to avoid hydrogen gas from leaking through the material) with wax support. All technical drawings was made in Rhinoceros 5 and needed to be converted to CAD (.IGS and .STP) files for 3D printing. The 3D printer used was a ProJet 3510 SD. The plastic material was a VisiJet M3 Navy, with melt-away wax as Support [23]. More information on the printer and the plastic used is in Appendix C.

3.2.4 Limitations

As this project is a rather practical project, limitations are connected to the available equipment, production time and funding. As there are some limitations to the CNC machine available, we have made the bipolar plate design relatively simple. We change the 2 mm channel width for the aluminum plate to 1mm for the stainless steel plate. Production time for this is estimated 2 to 4 weeks.

As for funding we are limited to only a few plates, as it is very expensive to administrate and prepare the process. After this, it is fairly cheap to repeat the process, but not in the scale for this project.

For printing the plastic parts we have reached limitations with accuracy and plastic material for the 3D printer available for students, but the 3D printer used by Roy has the required accuracy and material properties.

3.2.5 Previous Concept design

When designing a fuel cell, one should try to make the design with at least one or more advantages of other fuel cells or other energy sources. One of these advantages is the power density and/or specific power. It is preferable to generate as much power as possible with the material and volume chosen. Therefore the design is made as small as possible while still be within the limitations. Another advantage when building small is the reduced cost of material per unit.

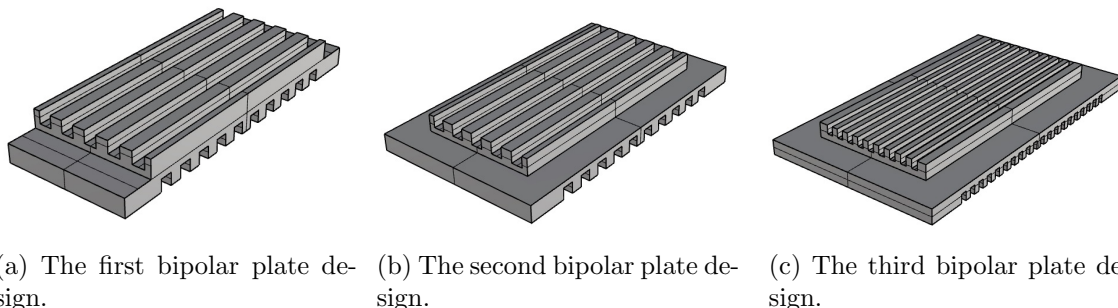


Figure 3.2: The improvements of the bipolar plate.

Combining the cell voltage (Section 3.2.1), cell size (Section 3.2.2), material properties (Section 3.2.3) and limitations (Section 3.2.4), a concept was developed. The design idea were to make a metal plate with simple grooves to be fitted in a complex plastic manifold section. The plates where to be made at a local workshop, and would need to be as basic and easy to make as possible. While the plastic parts where to be made by a 3D printer, and only limited to the accuracy of the printer itself, and the material it uses.

In total there need to be three different metal parts and the associated plastic cover parts. That is the anode side, the interconnecting bipolar plate and the cathode side. There is also the need for a end plates on each side. This would only serve as a reinforcements for the compressing the stack, and no gasses need to cover this part.

3.3 Fuel Cell Modeling

The following chapter aims to describe the process of modeling the fuel cell. The theoretical part of this chapter is based on the theoretical background chapter, in combination with the help

section in the chosen modeling program. [8]

The computer modeling of the fuel cell was done in ComSol Multiphysics, after recommendation from the project supervisor, Prof. Middleton. ComSol Multiphysics is a “general-purpose software platform, based on advanced numerical methods, for modeling and simulating physics-based problems” [8]

3.3.1 Setting up the model

ComSol offers two different way to start a project. Either starting with a blank model, or start by using their Model Wizard to set initial parameters and physics. By choosing the Model Wizard you get the advantage of defining the space dimension and physics, right at the beginning. For this project a 3-dimensional modeling was chosen.[8]

For this model, there is a need to cover the transport of gases and liquids in the GDL, and electrodes. In addition to this the physics in regards to the electrolyte must be considered as well.[8]

To cover the gases and liquids in the channels, GDL and electrodes, the physics section “Reacting Flow in Porous Media” is chosen. This covers the flow and chemical composition of gas or liquid moving through porous materials such as the GDL and electrodes. This is done by utilizing Brinkman equations, Navies-Stokes equations and continuity equations.[8]

This physics section is added both for the anode and cathode side of the cell, specifying which species is present at each side. This is shown in table 3.2.[8]

Table 3.2: Species that are present at each side.

Cathode species	Anode species
O_2	H_2
H_2O	H_2O
N_2	

Further on the Secondary current distribution physics is added to the model. This section considers the transport of ions in the electrolyte as well as current conduction in electrodes. This section, as opposed to the Primary Current Distribution section, considers activation overpotentials. By using Butler-Volmer and Tafel equations the relationship between charge transfer and overpotential solved.[8]

In addition to choosing the two physics sections, the following parameters where added to the model, and can be seen in Table 3.3[8].

3.3.2 Building the model

The next step is to make the computer drawing(CAD) of the cell. The model will be of one single cell, with a cathode and an anode plate, with the GDL, electrode and electrolyte between them.

Initially the anode channels were created. There are ten channels, which was added one at a time. By adding squares to the model and placing them with 1mm between them. Once this was done, the GDL layer was added underneath the channels, followed by the electrode, membrane, electrode, GDL and the cathode channels. The difference from the cathode and anode channels being that the cathode channels are rotated 90 degrees in regards to the anode channels, with the length of the channels decreasing and the number of channels increasing. The visual result of this part can be seen in figure 3.3.

Once the model was built, the work of defining the different sections of the fuel cell had to be done. Defining the following sections was done:

- Anode Channels

Table 3.3: Model parameters in COMSOL. Items marked with a * is parameters changet to fit our cell.[8]

Name	Expression	Value	Description
L^*	$0.042[m]$	$0.042m$	Cell length
H_{ch}^*	$1.5e^{-3}[m]$	$0.0015m$	Channel height
H_{gdl}^*	$360e^{-6}[m]$	$3.6E - 4m$	GDL height
$H_{electrode}$	$50e^{-6}[m]$	$5E - 5m$	Porous electrode thickness
$H_{membrane}^*$	$127e^{-6}[m]$	$1.27E - 4m$	Membrane thickness
W_{gdl}	$20e^{-3}[m]$	$0.02m$	Gass diffusion layer width
W_{ch}	$1e^{-3}[m]$	$0.001m$	Channel width
W_{rib}	$1e^{-3}[m]$	$0.001m$	Rib width
ϵ_{gdl}	0.4	0.4	GDL porosity
κ_{gdl}	$64.9e^{-12}[m^2]$	$6.49E - 11m^2$	GDL permeability
σ_{gdl}	$315[S/m]$	$315S/m$	GDL electric conductivity
w_{H_2in}	0.743	0.743	Inlet H_2 mass fraction (Anode)
w_{H_2Oin}	0.023	0.023	Inlet H_2O mass fraction (Cathode)
w_{O_2in}	0.228	0.228	Inlet O_2 mass fraction (Cathode)
$U_{inAnode}$	$0.2[m/s]$	$0.2m/s$	Anode inlet flow velocity)
$U_{inCathode}$	$0.5[m/s]$	$0.5m/s$	Cathode inlet flow velocity)
μ_{Anode}	$1.19e^{-5}[Pa \cdot s]$	$1.19E - 5Pa \cdot s]$	Anode viscosity
$\mu_{Cathode}$	$2.46e^{-5}[Pa \cdot s]$	$2.46E - 5Pa \cdot s]$	Cathode viscosity
M_{H_2}	$0.002[kg/mol]$	$0.002kg/mol$	Hydrogen molar mass
M_{N_2}	$0.028[kg/mol]$	$0.028kg/mol$	Nitrogen molar mass
M_{H_2O}	$0.018[kg/mol]$	$0.018kg/mol$	Water molar mass
M_{O_2}	$0.032[kg/mol]$	$0.032kg/mol$	Oxygen molar mass
$D_{H_2-H_2O}$	$9.15e^{-5}^*$ $(T/307.1[K])^{1.75}[m^2/s]$	$1.8076E - 4m^2/s$	$H_2 - H_2O$ Binary diffusion coefficient
$D_{N_2-H_2O}$	$2.56e^{-5}^*$ $(T/307.15[K])^{1.75}[m^2/s]$	$5.0559E - 5m^2/s$	$N_2 - H_2O$ Binary diffusion coefficient
$D_{O_2-N_2}$	$2.2e^{-5}^*$ $(T/293.2[K])^{1.75}[m^2/s]$	$4.7131E - 5m^2/s$	$O_2 - N_2$ Binary diffusion coefficient
$D_{O_2-H_2O}$	$2.82e^{-5}^*$ $(T/308.1[K])^{1.75}[m^2/s]$	$5.5394E - 5m^2/s$	$O_2 - H_2O$ Binary diffusion coefficient
$T * F$	$25 + 273.15[K]$	$298.15K$	Cell temperature
P_{ref}	$101e^3[Pa]$	$1.01E5PaK$	Reference pressure
V_{cell}	0.9	0.9	Cell voltage
c_{O_2ref}	$40.88[mol/m^3]$	$40.88mol/m^3$	Oxygen reference conscentration
c_{H_2ref}	$40.88[mol/m^3]$	$40.88mol/m^3$	Hydrogen reference conscentration
ϵ_l	0.3	0.3	Electrolyte phase volume fraction
ϵ_{cl}	$1 - \epsilon_l - \epsilon_{gdl}$	0.3	Open volume fraction for gas diffusion in porous electrodes
κ_{cl}	$\kappa_{gdl}/5$	$2.36E - 12m^2$	Permeability (porous electrode)
σ_m	$10.0[S/m]$	$10.00S/m$	Membrane conductivity

- Anode GDL
- Membrane
- Cathode Electrode
- Cathode GDL
- Cathode Channels
- Anode inlets and outlets

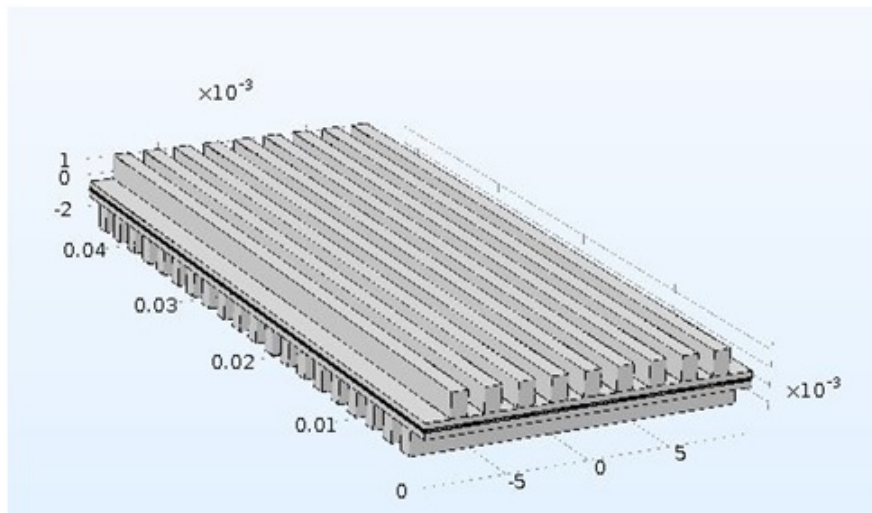


Figure 3.3: An overview of the computer model in COMSOL

- Cathode inlets and outlets
- Anode Compartment
- Cathode Compartment

The reason for defining these sections are to easily refer to the right parts of the cell when we couple it up to the physics sections.

3.3.3 Secondary current distribution

In this section, we set up the model for current distribution. The active parts of the fuel cell for this section of physics is the Anode electrode, Cathode electrode, gas diffusion layers on both sides and the electrolyte. All of the mentioned sections are added to the domain selection of the secondary current distribution physics.

Porous Electrode Reaction

Initially there are added two porous electrode nodes. One for the cathode electrode and one for the anode electrode. Both nodes are used to set up charge balances for the pore electrolyte in the porous electrodes in question, and the electrodes themselves. Further one there is added a sub-node called porous electrode reaction to “define the charge transfer reactions between the electrolyte and the electrode phases within the porous electrode.” (ComSol)[8]. One of the differences between the two porous electrode nodes are that the cathode porous electrode node has an equilibrium potential of 1.15, while the anode is at zero.

Electrode

The next step is to define the GDL. As there is no electrochemical process in the GDL, an electrode node is sufficient to model the current conduction. As there are no differences between the GDL on each side of the membrane, only one electrode node is necessary to define both. [8]

Ground, Potential and initial values

The last thing to do is defining ground, potential and the initial values of the cell. Electric ground is defined at the top of the anode GDL, while the electric potential is defined at the top of the anode GDL. Lastly the initial voltage in the cathode GDL and electrode is set to V_{cell} . [8]

Additional nodes

In addition to the nodes added by us, there are some nodes present by default in the Secondary Current Distribution physics, namely Insulation 1, Initial Values 1 and Electrolyte 1. [8]

In these nodes, the relevant domains are added by default. As the domains of the manually added nodes are defined, these domains are then taken out of account in the predefined nodes.

An example of this would be the insulation node, which covers the outer walls of the domains. Initially all walls are covered, but as the electric ground and electric potential is defined at the outer top wall of the GDLs, these two surfaces are automatically removed in the insulation node. [8]

As to what these different nodes do, it will be described briefly. The insulation node is a boundary which describes the faces/walls of the cell which is not faced toward a conductor. The electrolyte node simply defines the electrolyte domain. The last predefined node is the Initial Values 1 node. This node defines the initial potential. Since the Initial Values 2 node already defines the initial potential in the cathode half of the cell, this node sets the initial value of the anode side of the cell, including the membrane. The potential here is set to zero. [8]

Reacting Flow in Porous Media

In this section, we set up the mass transport in the anode mass flow section, meaning the gas channels, gas diffusion layer and electrode. The first step is choosing the anode compartment as the domain for the current physics. In addition to this a Maxwell-Stefan diffusion model is chosen. [8]

Porous Matrix Properties

To define a porous domain, and the properties of this domain, two Porous Matrix Properties nodes are added. One for the GDL and one for the electrode. In both nodes, the Porosity and Permeability for the domain in question is supplied. In these domains, the porous media flow is solved by Brinkman equations, while in the remaining are solved with Navier-Stokes equations. [8]

Porous Electrode Coupling

By adding this node, the anode electrode is coupled to the Secondary Current distribution physics, which will help the system explain the gas disappearing because of electrochemical reactions. [8]

Inflow, outflow, inlet and outlet

Inflow, outflow, inlet and outlet The next part is about setting up our inlet and outlet conditions. This is done by adding nodes for inflow and outflow, specifying the inflow mass fraction of the specified species. And adding an Inlet and outlet node. In these nodes, the input average velocity is specified, as well as the output pressure. [8]

Additional nodes

The default nodes in Reacting Flow in Porous Media, are the following nodes: Transport Properties 1, No Flux 1, Wall 1 and Initial Values 1. These nodes domains work like described in the Secondary Current Distribution subchapter.

The transport Properties node is used to define the fluid properties. As well as defining the Maxwell-Stefan diffusivity matrix. In fluid properties, the Fluid Material, viscosity and density is described, as well as the molar mass. Further on the No flux node describes which surfaces of the anode department without any flux. The wall node includes a boundary condition, which in our case is a No Slip condition, meaning there is no movement of fluid at the wall. The Initial Values 1 provides initial values for mass fractions. The initial values can either be initial conditions, or an initial guess of initial values. [8]

Reacting Flow in Porous Media 2

In this physics section the fluid flow and mass transport for the cathode is set up. This setup is very like the anode setup. There is of course different species present at this side of the fuel cell. The same nodes are added and adjusted here as in the anode section. [8]

Mesh

After adding the desired physics, a mesh must be created before simulating the system. Creating a mesh for the current model, turned out to be a critical point of the model. ComSol creates a mesh for your geometry by default, but this is often so detailed that the simulating reaches

critically long simulation times. To reduce the time of simulation, it is necessary to create the mesh manually. Creating a mesh in ComSol proved to be extremely difficult. The guide previously mentioned, has the advantage of simple design. By following the meshing sequence described here, we were able to create a mesh for a PEMFC with one single channel, but any additional geometry resulted in several errors from the program. Initially the geometry of the cell was as shown in figure 3.3, however, we were unable to solve the problem. To overcome this, a decision was made to rotate the cathode channels in such a manner that they align with the anode channels. This does mean that the quality of the simulations decreases. Even by doing this a significant amount of time was used to achieve a working meshing sequence.[8]

After successfully creating a mesh, the next step is to define the steps of simulation. This is defined in the node called Study 1. In our case the system is initially set to a 0.9V potential, and then solved for secondary current distribution, and reacting flow in porous media on both sides individually. Once this is complete, the system is simulated with varying voltage from 0.9V down to 0.1V to get an IV-plot. A measurement is made for every 0.05V through the span of the simulated potential of the cell. This simulation is repeated several times, with varying temperatures and gas flow, to understand how the cell works under different conditions. [8]

3.4 Control system

3.4.1 Microcontroller

To control the fan speed, heat of the air blown into the cell, measuring the parameters of a cell, and displaying these in a LCD screen an Arduino is used. The possible areas of use for an Arduino is enormous. Cost-wise the Arduino excels compared to other comparable products like MyRio. In addition to this the Arduino programming language, which is based on Wiring, is easy to learn, and there are an enormous number of tutorials for different projects available.

Pressure control

At this point the pressure control has not yet been resolved. The ideas are to either apply a valve controlled by the Arduino and a motor, or use valves controlled by a system designed by bachelor students. The second solution would require a rather big additional valve unit, which would be placed outside of the test rig.

Controlling the heating element

To control the temperature of the air blown into the cell a heating element is added to the rig, in front of the fan. This results in the fan “pulling” air over the heating element and into the cell. To control the temperature, a heat sensor is put into the airstream. By feeding this into the Arduino, the Arduino can either turn on or off the heating element depending on if the temperature is below or above a preset temperature. Controlling the heat of the system will provide an opportunity to test fuel cells at different temperatures to understand how temperature affects the performance of the cell. To illustrate the designed setup, figure 3.4 has been added.

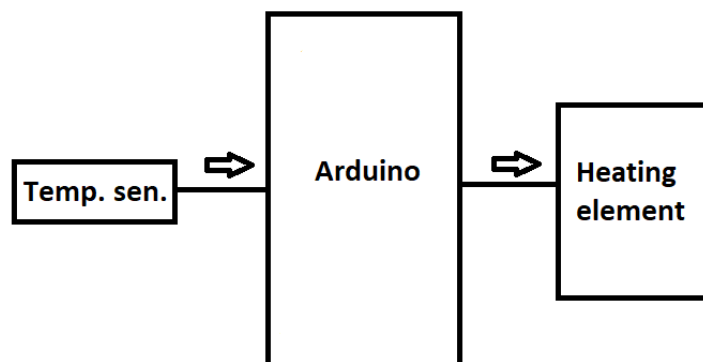
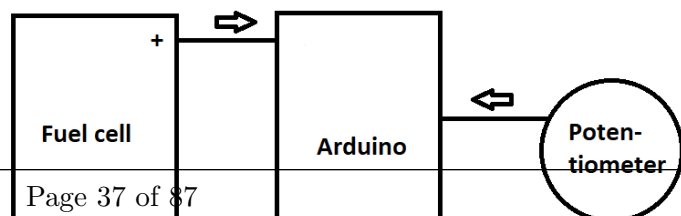


Figure 3.4: A simplified schematic of the temperature control setup.

Controlling the fan

The idea for controlling the speed of the fan is to have a two-option control. Either speed is controlled manually by turning a potentiometer, or



the fan speed is proportional to the current of the fuel cell. By having the first option of manually controlling the air flow, it is possible to test and understand how the air blown over the cathode side of the cell affects the performance of the cell. By using both the potentiometer connected to the Arduino, and the current sensor we designed, it is possible to control a transistor by PWM signal. This transistor is connected to the fan, and will control the flow of power, thus controlling the speed of the fan. An overview of this design is shown in figure 3.5.

IR-Sensors

As the humidification and dehumidification systems has been designed, and are going to be implemented, the water level of these systems should be monitored. To do this an infrared sensor is going to be measuring across the transparent plastic pipe, placed outside the system to be able to visually check the water level of both tanks. This infrared sensor will give different voltages to the Arduino, depending on what gas or liquid is present between the emitter and sensor. The idea is to have a maximum and minimum sensor on the humidification tank, and a maximum level sensor on the dehumidifier tank. A simple layout of this system can be seen in figure 3.6.

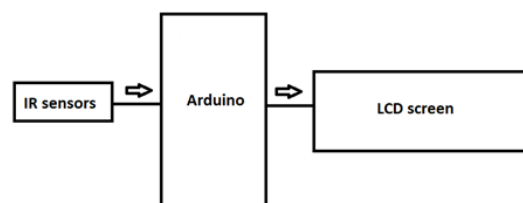


Figure 3.6: A simplified schematic of the sensor setup.

LCD screen and keypad

As the test rig is designed to work without an external computer, adding a screen to the system is needed to read the different values of the cell, i.e. voltage, current, power, fan speed and temperature. However, this quite a lot of information, and cannot all be displayed at once. The LCD screen used in this project is a 16x2 screen, which can roughly display four different values in real-time. To be able show more than these four, a keypad is added. This keypad consists of four digital buttons, which again is used to switch between different screens. The information which must be displayed are the following:

- Current passing through the cell
- Voltage of the entire stack
- Voltage of each cell in the stack
- Total power produced
- Temperature of the air blown into the cell
- Fan speed
- Pressure

By using all the connected units, like the fuel cell, keypad, potentiometer, temperature sensor and transistor, we can provide the LCD screen with the information needed. A simple version of this design can be seen in figure 3.7.

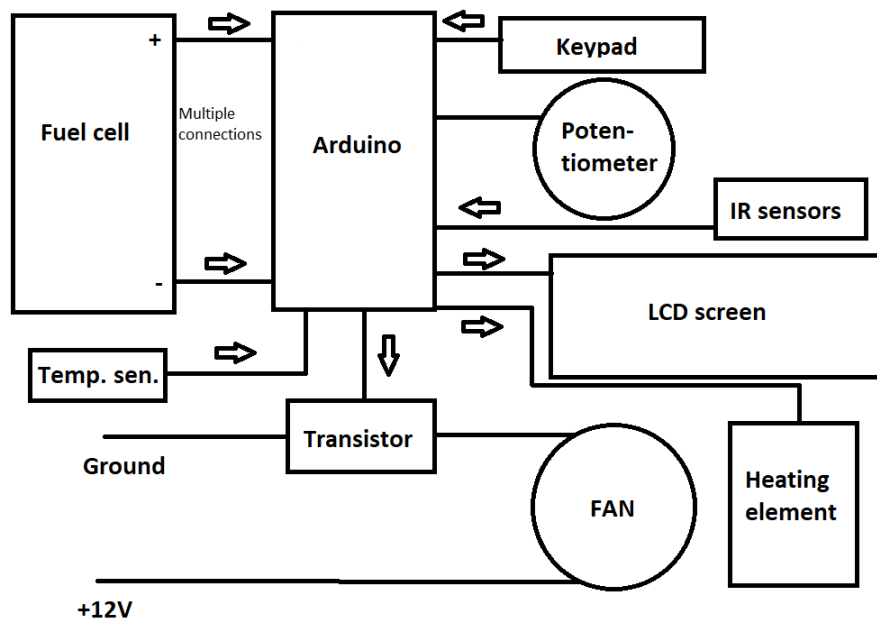


Figure 3.7: A simplified schematic of the LCD setup

3.4.2 Humidification and dehumidification systems

As a part of the test rig design, a humidifier and dehumidifier has been designed for the anode gas supply. The idea behind this is to run the hydrogen through a bubbler, to humidify the hydrogen. This will help prevent the anode side from drying out due to water molecules being dragged through the membrane by protons, as mentioned in section 2.2.1. In addition to this we would like to prevent the system to be overly humidified by using the dehumidifier.

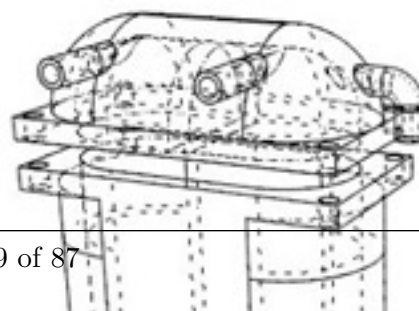
From figure 3.8 a sketch of the humidifier is shown. The idea for the two vertical pipes on the right side is to have a transparent pipe, showing the water level of the humidifier.

The bottom horizontal single pipe is there to connect to the dehumidifier. The two horizontal outward-facing pipes are designed to be used as an inlet and outlet. By filling the humidifier with water, the inlet H₂ is forced to travel through the opening at the bottom center wall, where the outlet and the inlet section are connected, and water vapor will be dragged with the hydrogen gas. This process only increases the humidity of the gas at about 2 to 4% in room temperature. To increase this, one needs to increase the water temperature, but this will not be implemented until the rest of the systems are functioning. [21]

The dehumidifier will work towards removing excess water in the hydrogen exiting the fuel cell. As mentioned previously, the humidifier and dehumidifier will be connected, meaning that in addition to collecting excess water the dehumidifier will



Figure 3.8: Sketch of the humidifier.



work as a water storage for the humidifier. A sketch of the dehumidifier can be seen in figure 3.9. As it can be seen here the wall in the center of the design is stopped removed in the bottom of the unit, leaving the center wall only in the lid. The idea behind this design is to get the hydrogen with excess water to pass this wall, and in doing this some of the water vapor will collect at this wall, and then fall towards the bottom of the unit. The vertical pipes at the left side will work as in the humidifier, and the horizontal lines pointing outwards will be the inlet and outlet of the system.

3.4.3 DC-DC Converter

Initially we wanted to have a steady voltage output from the fuel cell at 5V. This was to power the microcontroller as well as an external load, which utilizes 5V. Since the fuel cell output voltage will vary, from max voltage (7V for our cell) at no load, to almost zero voltage when heavily load (almost short circuited), we need to utilize power electronics to maintain the voltage at a steady value regardless of load variation.

Since our input voltage is varying at a higher and lower value than our aimed output, we will need a buck-boost converter. There are numerous of DC-DC converters on the market, so we intended to use one that suited our need. Though this turned out to be more difficult than intended. None of the converters we manage to find was in the voltage specter we needed.

This setback led us to change the DC-DC converter from Buck-Boost to a Boost converter. The boost converter will convert any voltage below 10V and boost it up to 12 volts. This range of voltage gap is much more common for boost converters. 12 volts is also a common voltage for many equipment, and the Arduino also have a built in voltage regulator which allows for 12V supply.

Since we still did not find pre made modules for our power requirement, we needed to make our own version. The LTC 1872 makes it possibility to change the external components to adjust the power requirements. Using the simulation program called LTSpice we tested a boost converter that operates from 9.8V to 2.5V and boost to a steady 12V. This setup utilizes a DC-DC controller from Linear Technology with external components. The schematics is from Linear Technology's datasheet for the LTC 1872 Constant Frequency, Current mode, Step-up, DC-DC Controller. External components are chosen to allow the DC-DC converter to handle a load up to 20W.

3.4.4 Voltage and current sensors

We can use the Arduino's analog input, to directly measure the voltage at about 0.005 V/Bit. Since the maximum voltage into the Arduino is 5V, we need to make sure that the voltage never goes above this value. This can easily be done with a zener diode. The zener diode works like a regular diode, but at a certain voltage, the barrier breaks down, and it can start conduct electricity. This will protect the Arduino for harmful voltages, as it will redirect the current flow to ground. A 1K resistor is also placed in series, for avoiding short circuit, and thus reducing the load on the zener diode. This will slightly interfere with the input values, and some calibration is needed to achieve accurate readings.

At input voltages above 4.5V, a voltage divider is needed to reduce the voltage within the 5 volts range to the Arduino. Dividing the voltage in two should suffice. And to reduce the current flow, two 10K resistors is put in series, as shown in the figure 3.12b.

For measuring the current, a precision current sense resistor from Ohmite is used in series

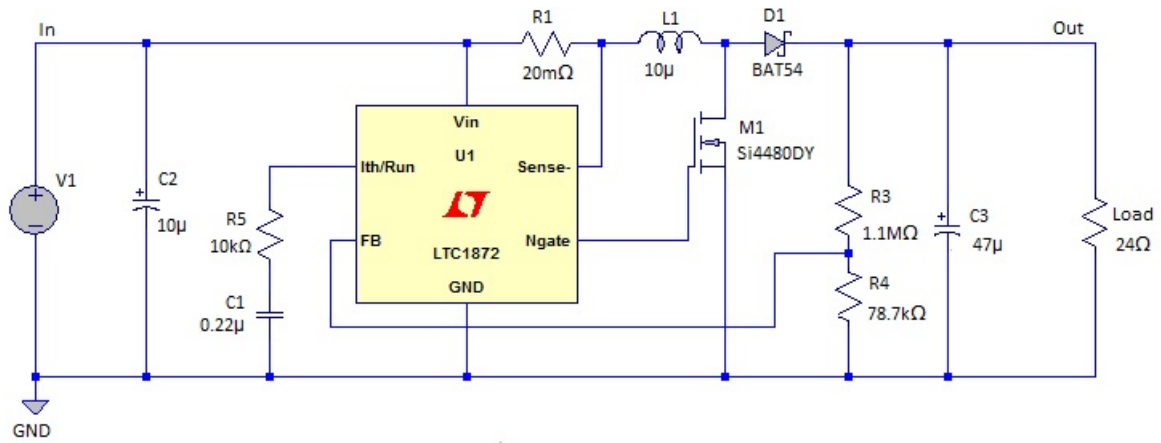


Figure 3.10: The schematics for a boost converter using LTSpice

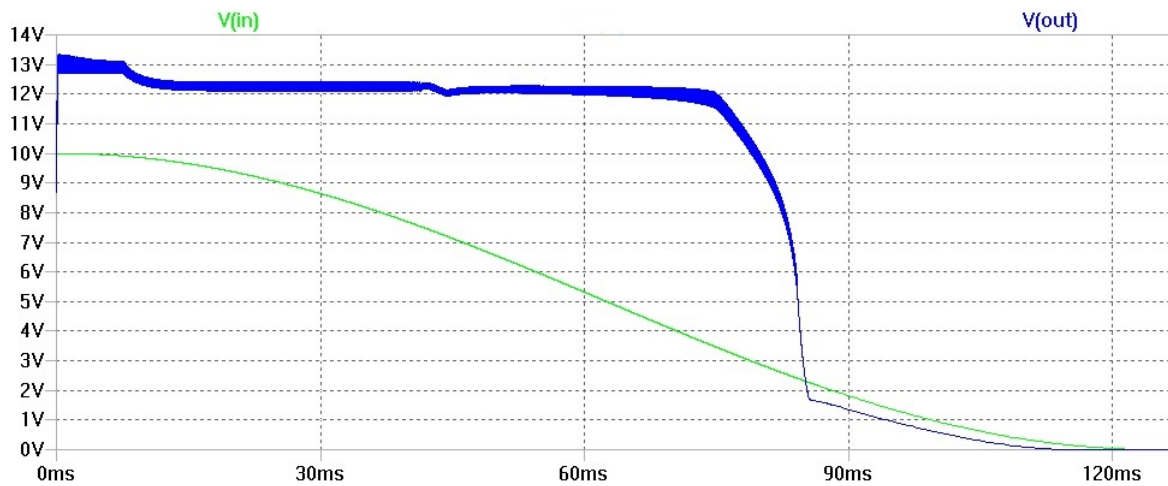
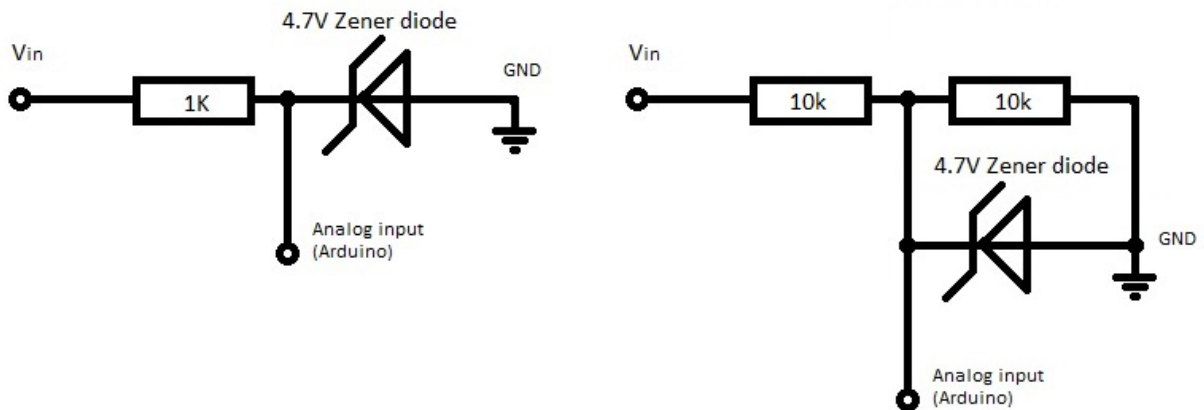


Figure 3.11: The result of the simulation.



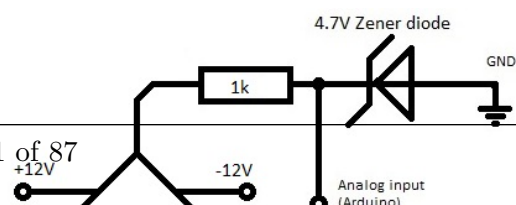
(a) Voltage sensors for 0 to 4.5 volts.

(b) Voltage sensors for 4.5 to 9 volts.

Figure 3.12: The voltage sensors configuration with the safety zener diode.

with the load. This resistor has a very low and precise value, and is capable of managing the full power of the fuel cell. Following Ohms law, the resistor will then cause a small voltage drop dependent on the current which flows trough. This voltage drop can be detected, but need to be amplified for the Arduino to register the value in a useful range.

By using the LT1101 Instrumentation Amplifier from Linear



Technology, one can amplify the voltage difference from 10 to 100 times. To sense even the low currents, we put two amplifiers in series for a total amplification of 1000 times. Since the supply voltage for the amplifiers is ± 12 volts, the amplifiers could deliver dangerously high voltage at the output, which would harm the Arduino. This can be avoided using the same setup of resistor and zener diode, as for the voltage sensor setups.

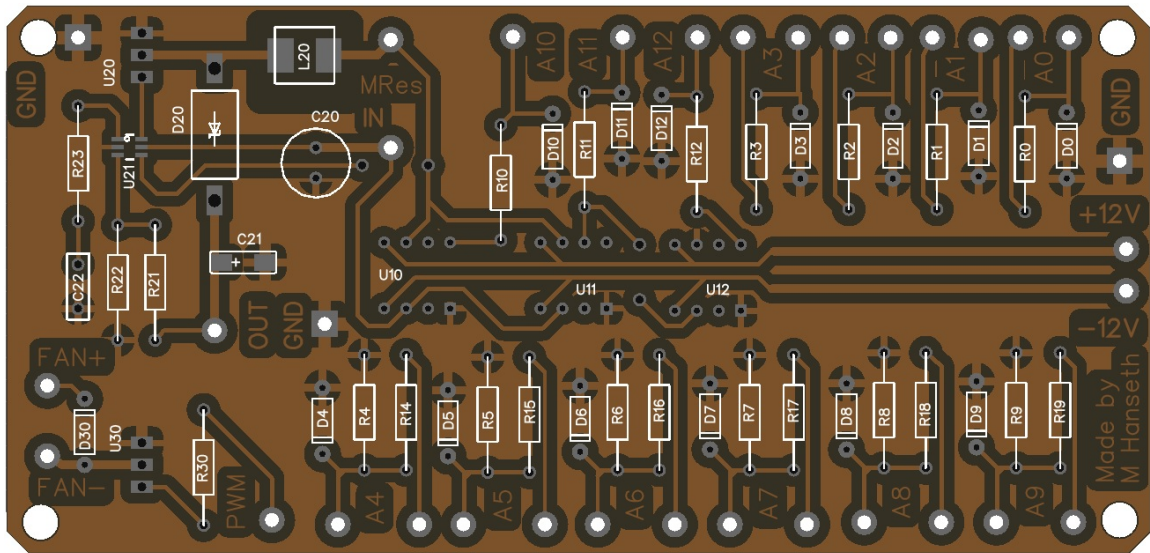


Figure 3.14: The circuit board for the boost converter, voltage and current sensors and fan control.

Electronics schematic

To achieve the described system, extensive work on the electronic layout of this system has been done. Initially the idea was to use an Arduino UNO. This board has 14 digital input/output pins with six of them being able to provide PWM outputs. In addition to this it has 6 analog inputs.

The circuit drawing for Arduino UNO is shown in Appendix E.[24]

To simplify the system, a decision to use the Arduino board called Mega was taken. This is a bigger board connection wise, and the “multiswitches” are now redundant. Removing these from the circuit decreases the possibility of the design not working, and simplifies the coding related to enabling the Arduino to control switching in these units.

The circuit drawing for Arduino Mega is shown in Appendix F.[24]

Chapter 4

Design and test review

4.1 Two cell setup

Testing two cells utilizes all the components necessary for building a fuel cell stack. The bipolar section is added in order to stack several cells together. This is also referred as the repeating section, as it can stack to the desired voltage level is reached. Our desired voltage is 5 volts, and as mention earlier, we should need at least 7 cells. But for testing purposes, two cells would represent the system without making it too difficult to assemble the stack each time. The entire setup is shown in figure 4.1.

4.2 testing station

For the second goal of the thesis work, a way to control the conditions in which the PEMFC runs at must be made. The idea is to design and create a test rig for fuel cells, with customizable control. This means that different units must be controlled and programmed to achieve the flexibility in control which we strive for.

4.2.1 Design

The idea of the design is to create a rig that can be used to test different kind of low temperature fuel cells. There will be a limit to the size of fuel cells tested on this rig, but this unit will not be designed uniquely to the fuel cell in this project.

4.2.2 Design overview

In figure 4.3 an overview of the internal layout is presented. In the upper left corner, an Arduino has been placed. Below the Arduino card there are two tanks located, which are linked to the humidification of the hydrogen blown into the cell, and the dehumidification of any excess water at the outlet side of the cell. At the right side of the Arduino, a square box can be seen. This is the power supply of the test rig. As the test rig is a rig designed to control the different external parameters of the fuel cell, to test the cell at different conditions, a decision to externally supply power was taken. Below this square box, a fan a heat element has been placed. This is to control both the airflow into the cell and the temperature of the cell.

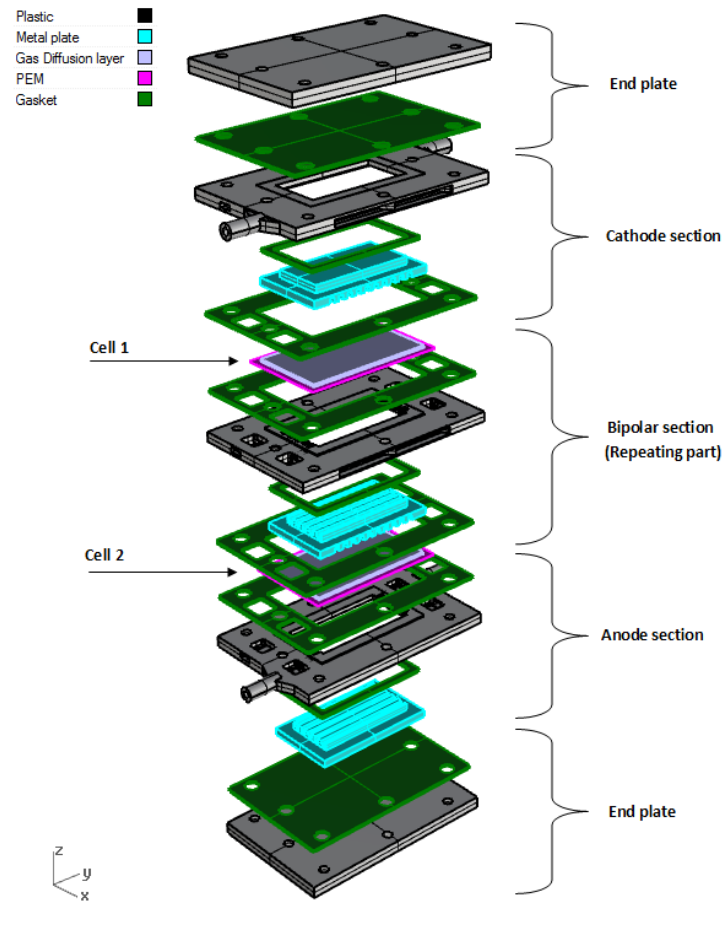


Figure 4.1: The two cell setup.[6]

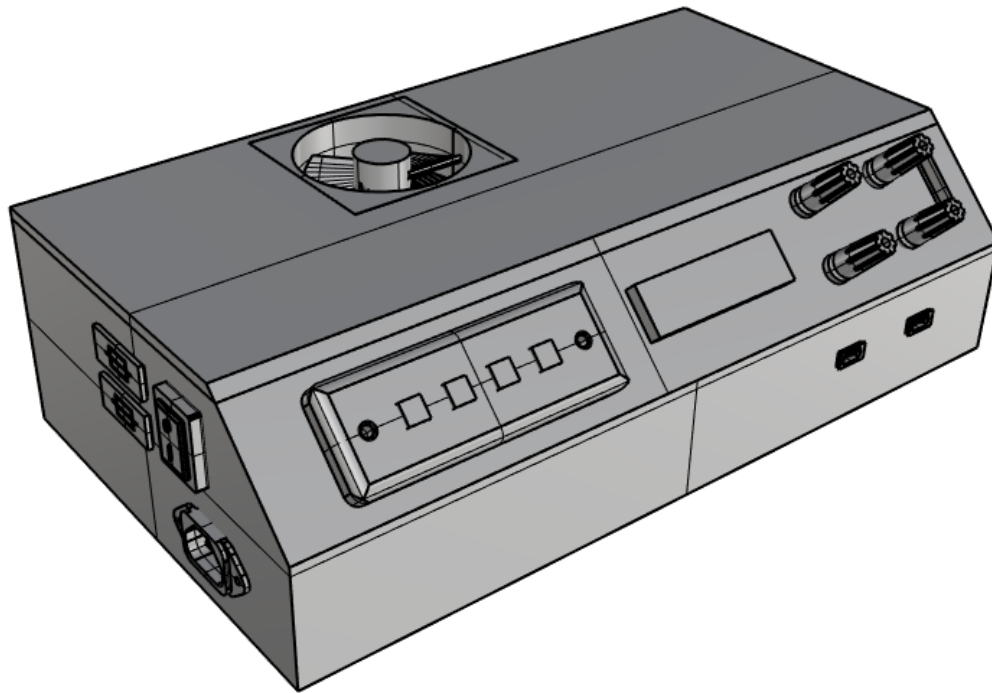


Figure 4.2: Overview of the external design. [6]

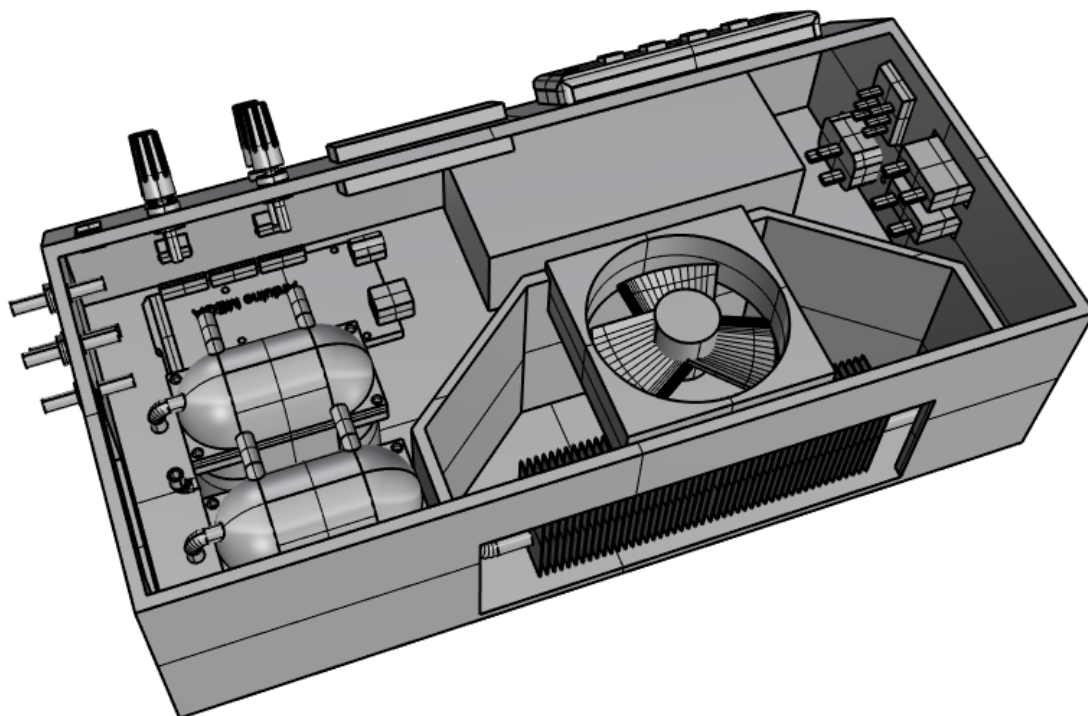


Figure 4.3: Overview of the internal design. [6]

In figure 4.2 the external design of the test rig is presented. In the front side at the lower right corner, two USB outlets is located. One outlet is to use the fuel cell power to charge i.e. a battery. Charging a battery requires a stable output, so in addition to the USB connection a boost converter is to be designed and implemented. The second outlet is to connect the Arduino to a computer (Connecting the test rig to a computer will be explained further later). Above these USB outlets four power connections is located. Two for connecting the fuel cell to the rig, and two for connecting the system to an external load. To the left of these power connections,

a LCD screen is placed. The Idea behind this screen is to provide real-time readings of the different parameters of the fuel cell, i.e. voltage, current and power. To the left of this LCD screen a keypad consisting of four buttons can be seen. As there are several different parameters to be shown in the screen, the keypad is there to enable the screen to display different values, depending on what buttons has been pressed. To the left of this keypad, on the short end of the rig, the power supply connection, and relays are located.

4.3 Control system testing

By testing each of the scripts made to control and measure the different aspects of the test rig, one can verify or falsify the scripts for the Arduino and/or the circuit design. In addition to this there is a safety aspect of testing each system by itself before pairing it up with the entire system, in regards to overheating and fire hazards. The corresponding circuits were built up on a breadboard and connected to an Arduino on each script.

4.3.1 Testing Humidification and dehumidification systems

To measure the water level of the humidifier and dehumidifier, infrared sensors are used. One of the insecurities of this is if the IR-sensor can pick up the difference from a plastic pipe filled with gas, and a plastic pipe filled with water. Initially the system was tested without and resistance between the 5V source, and the first leg of the emitter. During the test of this setup, the IR-sensor overheated and fried. Further on some initial calculations were done on the current passed through the emitter side of the sensor.

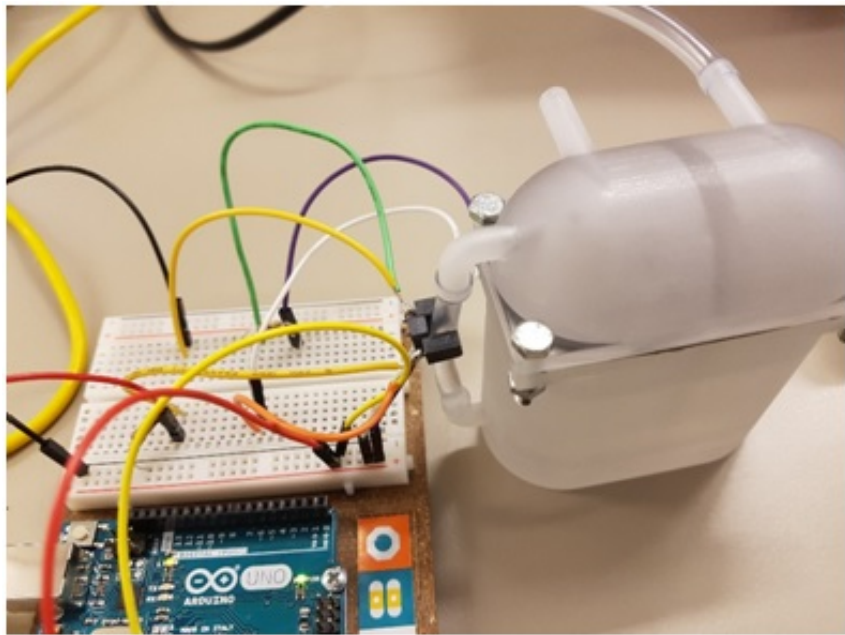


Figure 4.4: An example of a circuit built up on a breadboard.

By doing this, it was clear that a resistance of at least 190 Ohm had to be inserted to the circuit. The second test was done with a 220 Ohm yielding a positive result, clearly giving different values for pipe with and without water.

4.3.2 Fan control

Testing of the fan control was done as described in the method chapter, and yielded positive results. For the individual test, it was only tested with potentiometer control, as there are no fuel stack connected to provide the current source. By turning the potentiometer, we were able to change the speed of the fan, ranging from maximum fan speed to a full stop.

4.3.3 Temperature control

To test the temperature, control the heater was connected to an 230V AC outlet via a relay, which again was connected to the Arduino. In addition, the thermostat was connected to the Arduino. By using 25 degrees Celsius as a reference temperature, we could turn the heater on by touching the thermostat, and when the thermostat cooled down below 25 degrees, the heater turned off again.

4.3.4 LCD screen

The LCD screen was tested once mounted in the test rig. The screen was connected, and the complete script with all sub control systems was uploaded to the Arduino. Due to lack of time the subsystems were not yet connected, but the LCD screen received information from the Arduino, as can be seen in figure

Arduino results Initially there was made a script for each function in the system. After successfully testing these scripts, they were all integrated into one bigger script, which was to be up-

loaded to the Arduino. This script can be seen in Appendix J. As described previously, all the individual Arduino has been tested, and has yielded positive results. Since the test rig was not completely installed, each system has not been test simultaneously, but the main script was uploaded and we could communicate with the LCD screen and the keypad. We firmly believe that the script would work as intended if the test box was completely installed.



Figure 4.5: Testing the display on the testing rig.

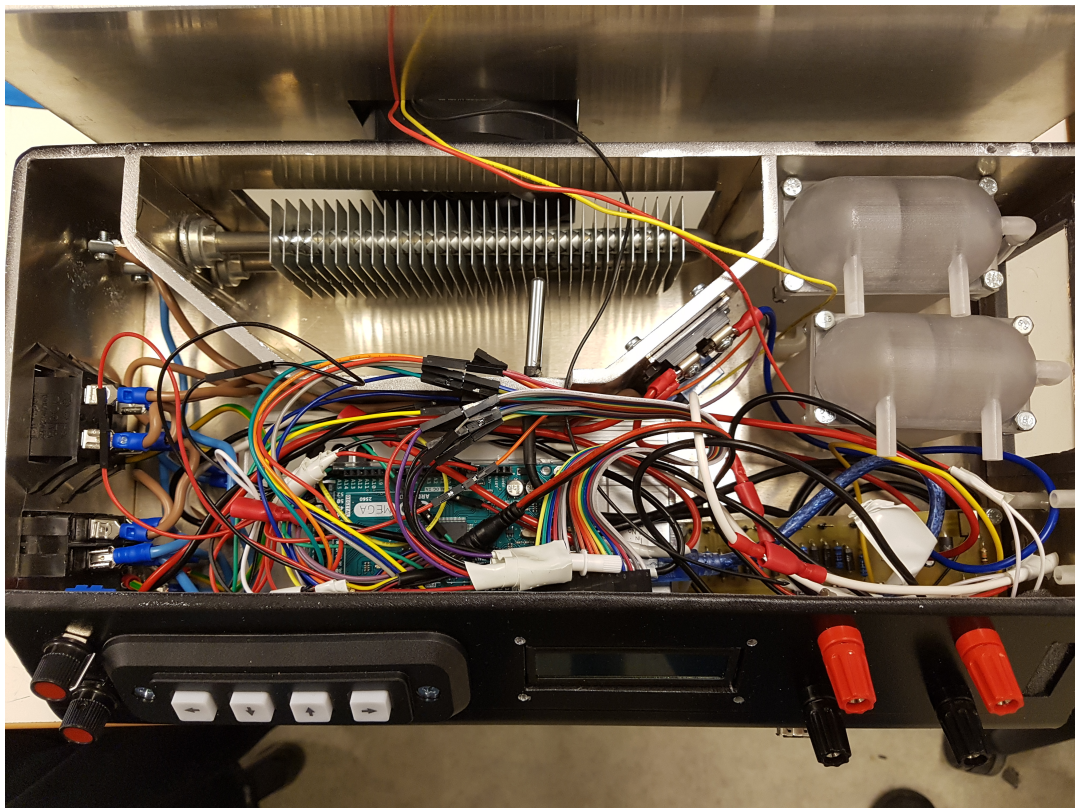


Figure 4.6: All the electric components placed in the testing station

Chapter 5

Results and final design

After several tweaks and tests, the final design is presented here.

5.1 Fuel cell simulation

The simulation results in form of an I-V curve can be seen in figure 5.1. The Lower temperature PEM is simulated and 25°C , while the higher temp PEM is simulated at 65°C . Both curves follow the same trend, with minor differences. Close to OC, at 0.9 volt, the low temperature cell produces just below 9.5% more power compared to the high temperature cell. This difference decreases steadily until the potential drops below 0.25V. At this point the high temperature cell produces more power than the low temperature cell. The difference close to short circuit is however smaller than the difference close to open circuit. At 0.1 volt, which is where the simulation ends, the difference between a high and low temperature cell is at 0.4%, in favor of the high temperature cell. As mentioned earlier the cell has been simulated at 25,35,45,55 and 65°C , the remaining simulation data can be seen in appendix K.

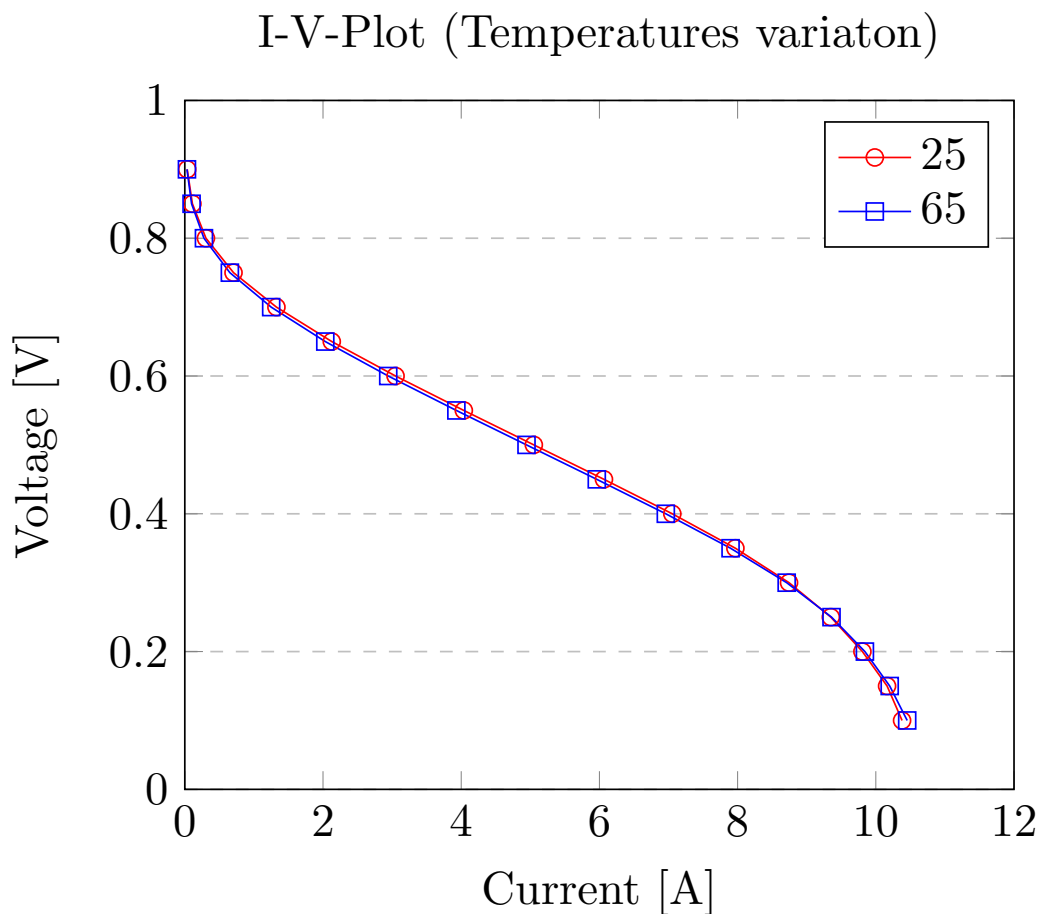


Figure 5.1: Modeling results from different cell temperature.

In figure 5.2, the power output of the stack has been plotted. To get this graph, the power output of a single cell simulated from 0.9-0.1 volt has been multiplied with seven. This provides the power output of the intended fuel cell stack. At peak power(0.4V), with the low temperature

cell, the stack produces 19.7W. The stack with the high temperature cell peaks at the same voltage, producing 19.5W.

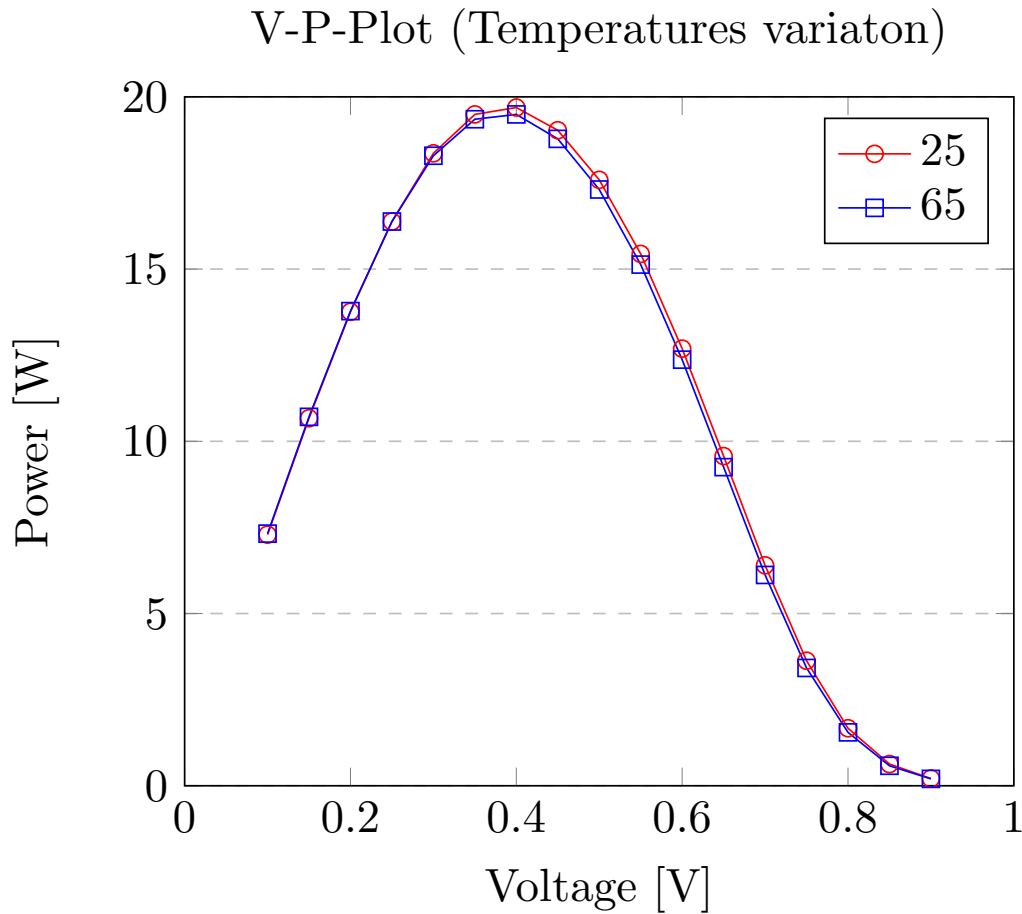


Figure 5.2: Modeling results from different cell temperature.

To show the effect of gas starvation, the system was simulated at 45 degrees, with a gas supply of $0.2\text{m}^3/\text{s}$ and $0.5\text{m}^3/\text{s}$ at anode side and the cathode side, respectively. Further on the simulation was repeated with a gas reduction of 0.66% and 0.33 %. The result is shown in figure 5.3.

5.1.1 Fuel cell performance

To prove that the redesigned fuel cell is still viable, a test was done. The only membrane, GDL and catalyst available was the Nafion 115, Nickel foam GDL and 5% platina on activated charcoal. Since this is not the setup which the new cell is designed for, two extra gaskets where used in each cell. This is because the combination of fuel cell materials is thicker than the ones ordered, and to try to overcome difficulties with leakages this was implemented. To validate that the additional gaskets where enough to prevent gas leakage, a submersion test was completed before testing the cell. The test showed that the setup had some gas leakages, but we felt confident that we could still perform a test on the stack.

The stack consisted of two cells, and was connected to a decade box and a multimeter to measure the potential at variable loads. During the testing, we noticed that the voltage was very dependent on pressure. The gas output was connected to a tube, which again was submerged in water to monitor the gas flow. At one point the tube was pulled out of the water, reducing the pressure in the system, and the voltage rose significantly. We expect that this is because we have the mentioned gas leakages due to the two extra gaskets. At higher pressures the leakage increases, reducing the voltage of the stack. To overcome this, we let the outlet gas in the cell into an exhaust pipe, without being submerged in water. In addition to this we connected our fan to a 9V battery, and blew air over the cathode, to supply air and to blow as much leakage hydrogen as possible away. This gave the I-V curve presented in figure 5.4.

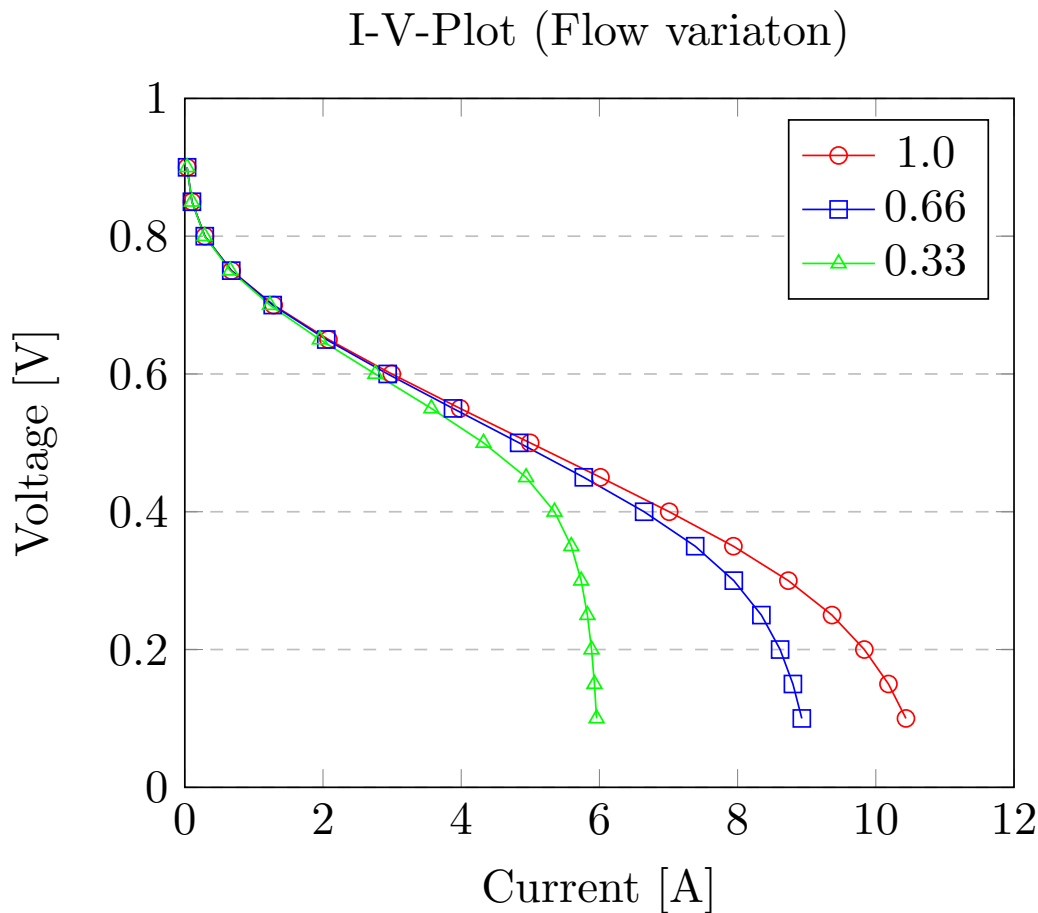


Figure 5.3: Model of the fuel cell stac at 45 deg with full, 2/3 and 1/3 gass supply.

5.1.2 EIS measurements

The results for m the EIS measurement is somewhat difficult to interpret due to lots off disturbance and inconsistent measuring, but we can see that the internal resistance is somewhere between 3 and 4 ohm and a infinite Warburg impedance with this characteristically 45 degree slope.

5.1.3 Fuel cell comparing

For comparison, we have applied the equations in chapter 2.10 on the simulation model and our actual fuel cell stack (V7). The gap in the values is partially caused by using different MEA. This is because our model was made for the ordered material, and not for our old design MEA.

Table 5.1: Comparing fuel cell performance.

Units	Model value	Actual value
Current density	0.837	7.74E-3
Power density	29.22	0.22
Specific power	77649	584

5.2 Testing station

Initially there was made a script for each function in the system. After successfully testing these scripts, they were all integrated into one bigger script, which was to be uploaded to the Arduino. This script can be seen in Appendix J. As described in section 4.3 , all the individual Arduino has been tested, and has yielded positive results. Since the test rig was not completely installed, each system has not been test simultaneously, but the main script was uploaded and we could communicate with the LCD screen and the keypad. We firmly believe that the script would

I-V-Plot (two cell setup)

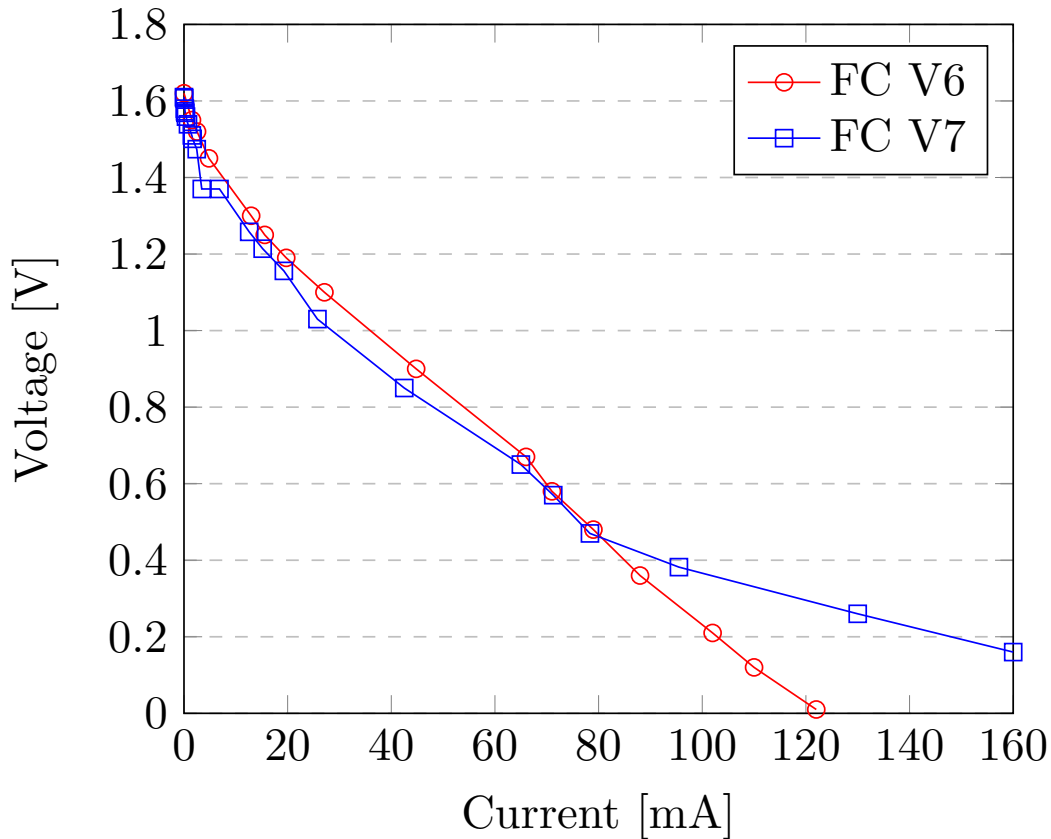


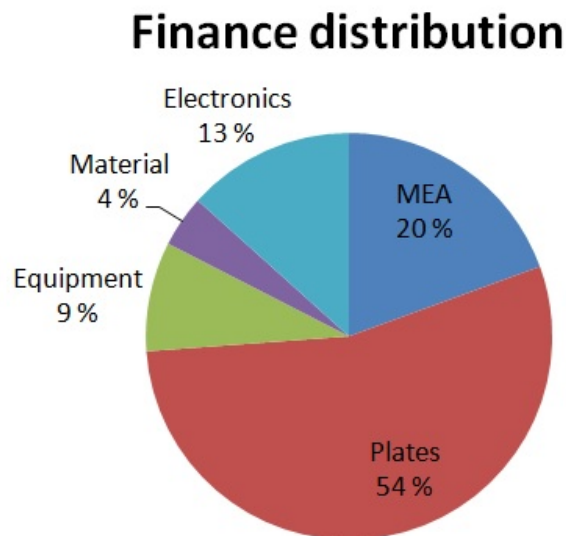
Figure 5.4: Test results from a two cell setup.

work as intended if the test box was completely installed.

5.3 Economics

Fuel cells is usually quite expensive, therefore we have focused on using as few material as possible with minimum waste material. Even with this focus, we still needed to reduce the cost, resulting of a single MEA type. Though this premade MEA is with 60% platinum content and should give good results. A pie chart is shown I figure 5.7 which shows the finance distribution for the total costs.

One can clearly see that the plates are our most expensive area. This is mostly because we used an external manufacturer to produce a few custom units. In a large scale production, this would be significantly reduced. Then we have our



fuel cell material, which was a custom built MEA. This is usually considered the most expensive part, due to the presence of precious metals. Though, still quite expensive, this has been reduced with the technological advances, as mention in section 2.1.2. The electronics section is

Figure 5.7: The finance distribution for the total costs.

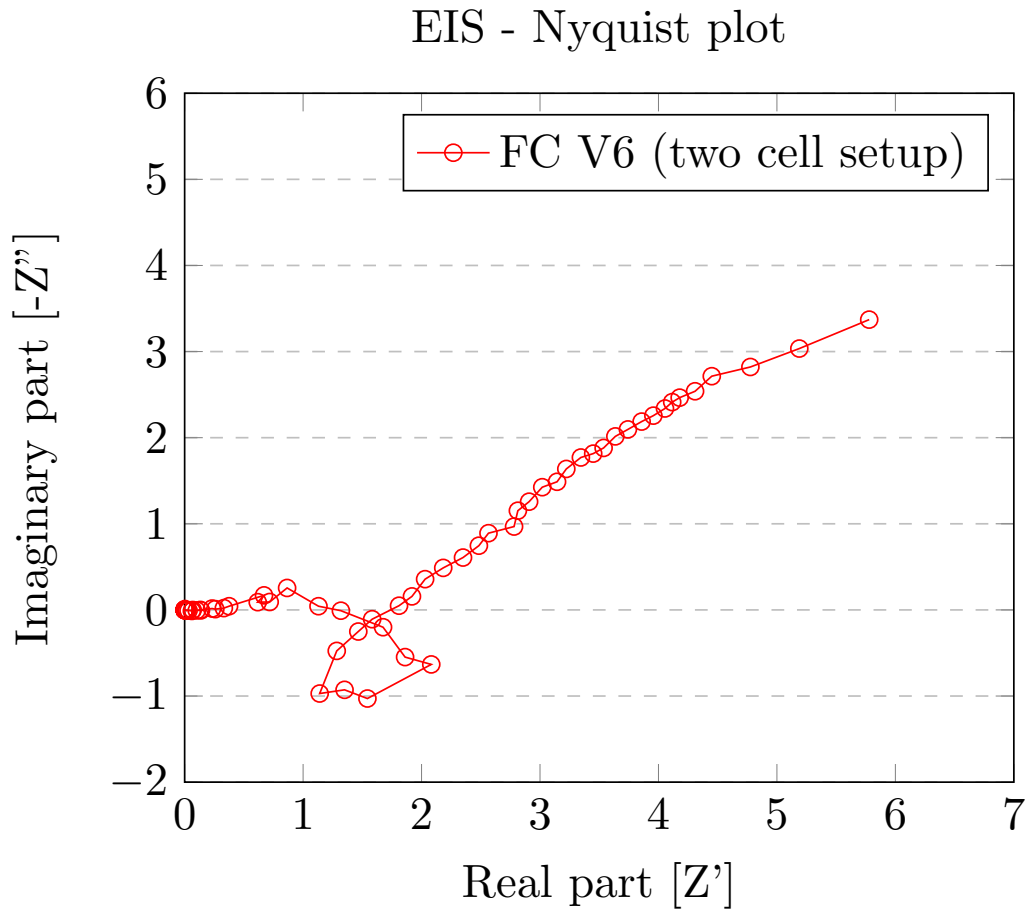


Figure 5.5: EIS measurement from a two cell setup.

quite large in our case since we have a standalone testing unit, which can test any fuel cells up to 20W power output, and not just managing itself. The material post and equipment post is mostly fitting items and safety equipment necessary for assembly the fuel cell stack. Interestingly though, the overall cost is for this project is surprisingly similar to other fuel cell systems in general.

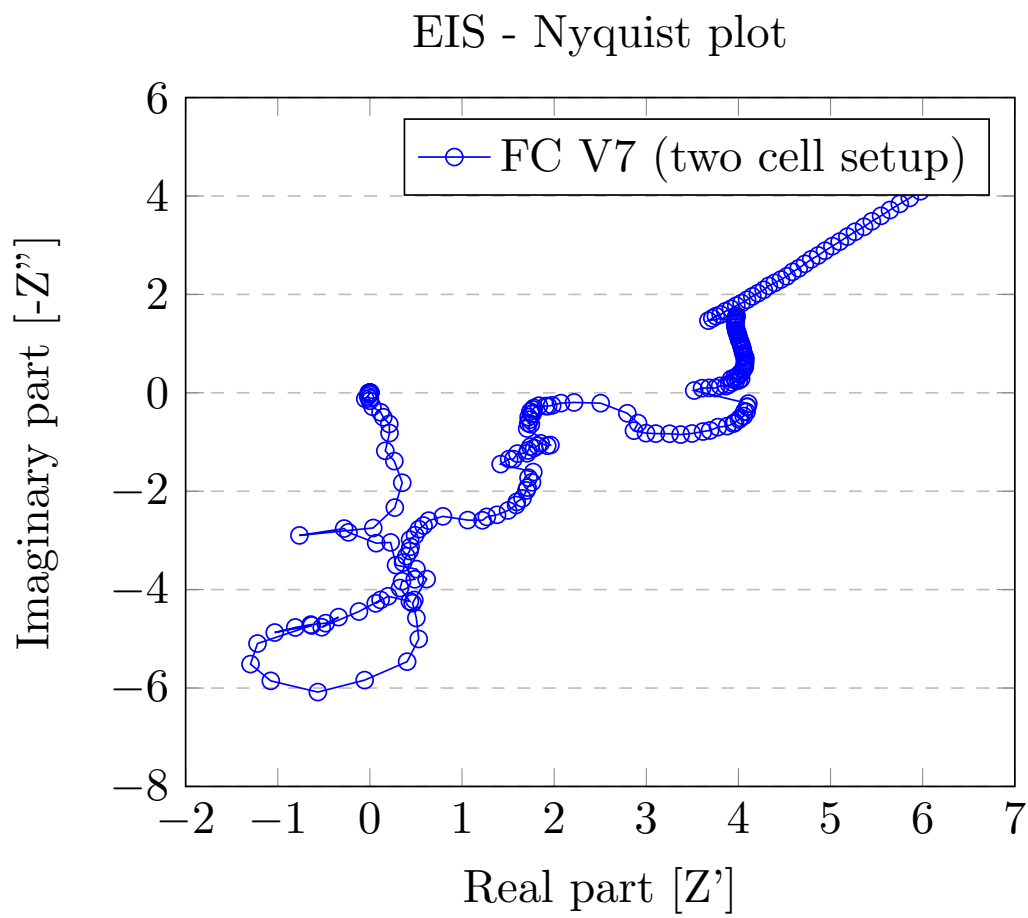


Figure 5.6: EIS measurement from a two cell setup.

Chapter 6

Discussion

In this chapter we highlight problem areas and difficulties that we faced.

It is important to outline that this is a practical project, and that the product was designed to fulfill a need in the laboratory. The thesis introduces the reader to most of the major aspects of fuel cell systems without going too specific in each area. The complete fuel cell system utilizes several different skills in engineering. Therefore we encourage the reader to make improvements as they see fit, at the same time learning about the remaining system.

6.1 Fuel cell model

The model used in this project was initially intended to be a way of comparing our cell design to a modeled version. Since we did not get all the material needed in time, we used the model as an ideal value for our design aims for.

By simulating different temperatures and gas flows we feel that we have covered parts of what we wanted to inspect, even if it is done in the form of a model simulation. Though we have used the parameters available to us, through datasheets from the suppliers, there is still parameters which needs a thorough investigation to get closer to what we would get in reality. The fact that we were unable to get the model running with the cathode channels rotated 90 degrees, is also unfortunate in regards to achieving a correct gas distribution in the GDL and electrode. However, as the current model is not used to compare to a real cell, the model serves its purpose as a method to show the performance and performance change of a PEM fuel cell under different temperatures and flows. Achieving a maximum power of 19.7W proves that our initial calculations on size and number of cells is valid.

6.2 Fuel cell stack

The test of a two-cell stack shown in the result chapter proves that our concept still works. There are difficulties with gas leakages, but we expect this to decrease vastly when using the intended MEA. Additionally, the steel plates used for this test has proved to work, as the test is one of the best test we have performed with the current MEA. We have managed to get a better result, with the same MEA, and a fuel cell design that decreases the overall size with 38.7%.

6.3 testing station

The testing station was never fully assembled, due to late arrival of critical parts. However, we have been able to fit all components inside, and the remaining work is finalizing and a thorough test run for all the situations. We have been working continuously trough this project on improving the schematics for the test rig, and vast quantities of time has been used on trying our best to design a well-functioning, safe system. However, there are some known flaws that could be improved. Initially the idea was for the fuel cell to run the fan, but as the test rig developed we decided to run the fan from the testing station. This means that the fan could be bigger, enabling testing at a wider range of air flows. It can also be used on small cells which is not powerful enough to drive the load, making it possible to test small single cells. Another function which could be implemented in regards to the fan, is reading the feedback wire to get the RPM information, thus knowing how much air is pushed through the cell. Additionally, the temperature sensor used to control the heater, is placed in the testing station. Ideally there

should be a sensor inside the fuel cell to measure the actual temperature of the fuel cell, not only the air blow into it, resulting in a more precise temperature reading.

6.3.1 Deliverance delays and breakdowns

During this thesis, several of the ordering and deliverance was delayed for different reasons. Our ordering process was delayed by 4 weeks due to extra calculation of new systems, and then delayed two weeks extra for cost reduction. The internal ordering process took 6 to 7 weeks before order confirmation from the suppliers was given. Most of the suppliers operate at about 2 to 4 weeks delivering time, but also here we were met with delays due to out of stock, breakdown of critical machines and lower priority due to order backlog. This naturally increased deliverance time with an uncertain degree. Any one of the delays would be a minor inconvenience, but all together made the practical part on this thesis unachievable. A more specific schedule of the material deliverance is shown in Appendix I. This forced the thesis in a more theoretical direction, which was not the intended strategy, but a necessity due to the unfortunate events. The actual time consumption looks more like in table 6.1.

Table 6.1: The actual work schedule.

Tasks	Estimated time consumption	Actual time consumption
Start presentation	1 Week	1 Week
Ordering parts	1 Week	5 Weeks
Modeling and calculation	5 Weeks	8 Weeks
Parts arriving		
Preparation / Test assembly	2 Week	1 Week
Testing	4 Weeks	1 Week
Report writing	4 Weeks	2 Weeks
Finalizing project	1 Week	0 Weeks
Total	18 Weeks	18 Weeks

6.4 Future work

For future studies and work on the fuel cell stack design and the testing station, we have the summarized the logical next steps.

- Improve the ComSol model, more specifically getting the mesh to work with the first design and calculate or estimate the remaining parameters.
- Test the fuel cell with new materials, which will arrive soon
- Connect the test rig electronics using the electronic schematic A in appendix E, and test it.

Chapter 7

Conclusion

It is safe to say that the re-design has not had a negative effect on the performance of the cell. Even though we have not been able to test the new design with the intended MEA, we firmly believe that significant improvements in performance would be seen if the testing was performed. To conclude the fuel cell design, we have been able to reduce the overall size by 38.7%, we have solved the problem with uneven pressure distribution during assembly of the cell, and we have tested the cell with a different plate metal (Stainless steel) successfully and the 115 membrane has been tested. In our opinion the re-design of the fuel cell system has been a success, even though we have not been able to perform the tests we would like to do. The design is still minted on the simplicity which we strive for, and we hope and believe that the PEM stack we have created will decrease the threshold for understand how a PEM fuel cell works, and increase the lab activity, in combination with our test rig.

The test rig is, in our opinion, a neat, sturdy rig. Except for the boost converter and the op-amps we have been able to test every single system successfully, and we're very confident that the system will work properly once fully and correctly assembled.

Even though we have not been able to do the tests we would like with our fuel cell, we have presented modeling results under varying conditions. The model works, and can easily be manipulated in terms of simulating under different gas flows, materials used, and temperature differences.

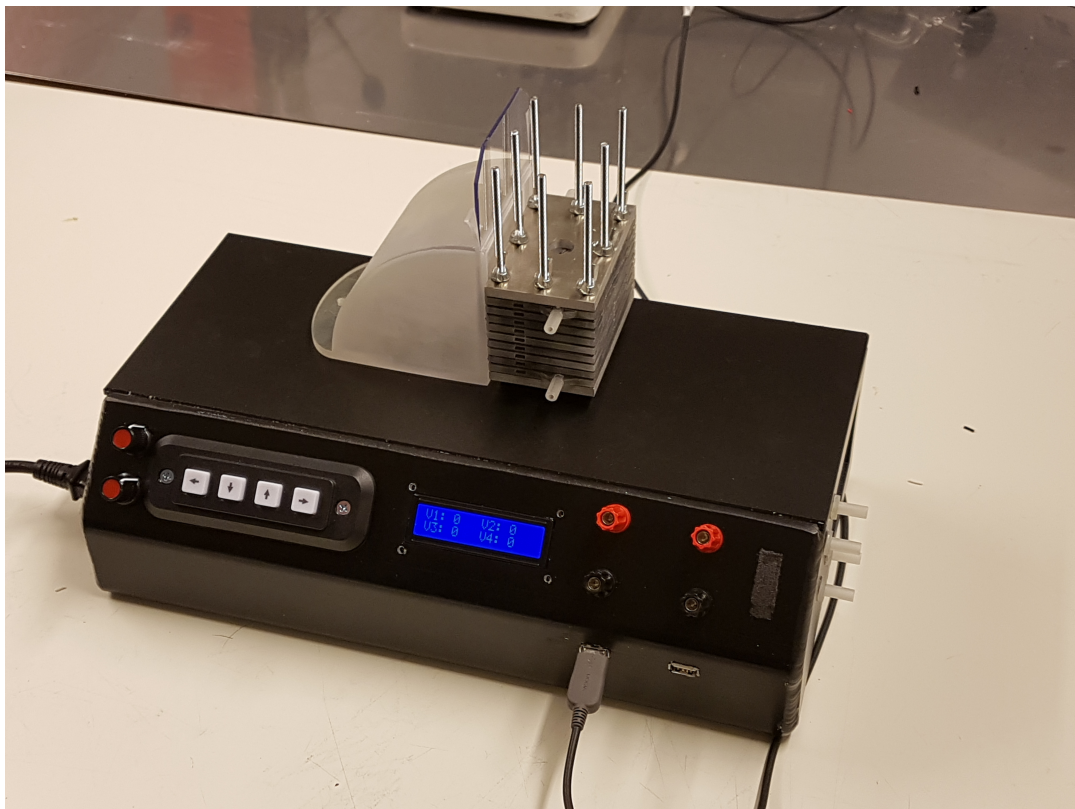


Figure 7.1: All the final products placed together as intended.

Bibliography

- [1] D. Haugen and E. Jernquist, “DC-DC Converter Design Using a PEM Fuel Cell As Voltage Source,” University of Agder, Grimstad, Norway, project report, Nov. 2015.
- [2] J. Larminie and A. Dicks, *Fuel cell systems explained*. Chichester, West Sussex: J. Wiley, 2003.
- [3] S. Lædre, “Bipolar Plates for PEM Systems,” Thesis for the Degree of Philosophiae Doctor, Jun. 2016.
- [4] F. Barbir, *PEM fuel cells: theory and practice*, 2nd ed. Amsterdam ; Boston: Elsevier/Academic Press, 2013.
- [5] N. Mohan, *Power electronics: a first course*. Hoboken, N.J: Wiley, 2012, oCLC: ocn726822530.
- [6] “Rhinceros.” [Online]. Available: <http://www.rhino3d.com/>
- [7] “Arduino - Home.” [Online]. Available: <https://www.arduino.cc/>
- [8] “COMSOL Multiphysics® Modeling Software.” [Online]. Available: <https://www.comsol.com/>
- [9] F. Gao, B. Blunier, and A. Miraoui, Eds., *Proton exchange membrane fuel cells modeling*. London : Hoboken, NJ: ISTE ; Wiley, 2012.
- [10] C. Bao, M. Ouyang, and B. Yi, “Modeling and control of air stream and hydrogen flow with recirculation in a PEM fuel cell system—I. Control-oriented modeling,” *International Journal of Hydrogen Energy*, vol. 31, no. 13, pp. 1879–1896, Oct. 2006. [Online]. Available: <http://linkinghub.elsevier.com/retrieve/pii/S0360319906001194>
- [11] G. Maggio, V. Recupero, and L. Pino, “Modeling polymer electrolyte fuel cells: an innovative approach,” *Journal of Power Sources*, vol. 101, no. 2, pp. 275–286, Oct. 2001. [Online]. Available: <http://linkinghub.elsevier.com/retrieve/pii/S0378775301007583>
- [12] M. De Francesco and E. Arato, “Start-up analysis for automotive PEM fuel cell systems,” *Journal of Power Sources*, vol. 108, no. 1-2, pp. 41–52, Jun. 2002. [Online]. Available: <http://linkinghub.elsevier.com/retrieve/pii/S0378775302000034>
- [13] F. Grasser and A. Rufer, “A Fully Analytical PEM Fuel Cell System Model for Control Applications,” *IEEE Transactions on Industry Applications*, vol. 43, no. 6, pp. 1499–1506, 2007. [Online]. Available: <http://ieeexplore.ieee.org/document/4384992/>
- [14] J. Baschuk and X. Li, “Modelling of polymer electrolyte membrane fuel cells with variable degrees of water flooding,” *Journal of Power Sources*, vol. 86, no. 1-2, pp. 181–196, Mar. 2000. [Online]. Available: <http://linkinghub.elsevier.com/retrieve/pii/S0378775399004267>
- [15] J. T. Pukrushpan, H. Peng, and A. G. Stefanopoulou, “Control-Oriented Modeling and Analysis for Automotive Fuel Cell Systems,” *Journal of Dynamic Systems, Measurement, and Control*, vol. 126, no. 1, p. 14, 2004. [Online]. Available: <http://DynamicSystems.asmedigitalcollection.asme.org/article.aspx?articleid=1410183>
- [16] M. Eikerling and A. Kornyshev, “Electrochemical impedance of the cathode catalyst layer in polymer electrolyte fuel cells,” *Journal of Electroanalytical Chemistry*, vol. 475, no. 2, pp. 107–123, Oct. 1999. [Online]. Available: <http://linkinghub.elsevier.com/retrieve/pii/S0022072899003356>

- [17] C. Wang, M. Nehrir, and S. Shaw, "Dynamic Models and Model Validation for PEM Fuel Cells Using Electrical Circuits," *IEEE Transactions on Energy Conversion*, vol. 20, no. 2, pp. 442–451, Jun. 2005. [Online]. Available: <http://ieeexplore.ieee.org/document/1432859/>
- [18] X. Xue, J. Tang, A. Smirnova, R. England, and N. Sannes, "System level lumped-parameter dynamic modeling of PEM fuel cell," *Journal of Power Sources*, vol. 133, no. 2, pp. 188–204, Jun. 2004. [Online]. Available: <http://linkinghub.elsevier.com/retrieve/pii/S0378775304002782>
- [19] "Basics of EIS: Electrochemical Research-Impedance." [Online]. Available: <https://www.gamry.com/application-notes/EIS/basics-of-electrochemical-impedance-spectroscopy/>
- [20] N. Mohan, T. M. Undeland, and W. P. Robbins, *Power electronics: converters, applications, and design*, 3rd ed. Hoboken, NJ: John Wiley & Sons, 2003.
- [21] P. H. Middleton, "Privat communication," Apr. 2016.
- [22] EG&G Technical Service, U.S. Department of Energy, United States, Office of Fossil Energy, and National Energy Technology Laboratory (U.S.), *Fuel cell handbook*, 2016, oCLC: 957455519.
- [23] "ProJet® 3510 SD | 3d Systems." [Online]. Available: <http://www.3dsystems.com/3d-printers/professional/projet-3500-sd>
- [24] "EasyEDA - Online PCB design & circuit simulator." [Online]. Available: <https://easyeda.com/>

Appendix A

Nafion Membrane



www.fuelcellstore.com
sales@fuelcellstore.com
(979) 735-1925

Properties of Nafion® PFSA Membrane

A. Thickness and Basis Weight Properties¹

Membrane Type	Typical Thickness (microns)	Basis Weight (g/m ²)
N-115	127	250
N-117	183	360
N-1110	254	500

B. Physical and Other Properties²

Property	Typical Value	Test Method
Physical Properties		
Tensile Modulus, MPa (kpsi)		
50% RH, 23 °C	249 (36)	ASTM D 882
water soaked, 23 °C	114 (16)	ASTM D 882
water soaked, 100 °C	64 (9.4)	ASTM D 882
Tensile Strength, maximum, MPa (kpsi)		
50% RH, 23 °C	43 (6.2) in MD, 32 (4.6) in TD	ASTM D 882
water soaked, 23 °C	34 (4.9) in MD, 26 (3.8) in TD	ASTM D 882
water soaked, 100 °C	25 (3.6) in MD, 24 (3.5) in TD	ASTM D 882
Elongation at Break, %		
50% RH, 23 °C	225 in MD, 310 in TD	ASTM D 882
water soaked, 23 °C	200 in MD, 275 in TD	ASTM D 882
water soaked, 100 °C	180 in MD, 240 in TD	ASTM D 882
Tear Resistance - Initial, g/mm		
50% RH, 23 °C	6000 in MD, TD	ASTM D 1004
water soaked, 23 °C	3500 in MD, TD	ASTM D 1004
water soaked, 100 °C	3000 in MD, TD	ASTM D 1004
Tear Resistance ³ - Propagating, g/mm		
50% RH, 23 °C	>100 in MD, >150 in TD	ASTM D 1922
water soaked, 23 °C	92 in MD, 104 in TD	ASTM D 1922
water soaked, 100 °C	74 in MD, 85 in TD	ASTM D 1922
Specific Gravity	1.98	—
Other Properties		
Conductivity, S/cm	0.10 min	see footnote ⁴
Available Acid Capacity, meq/g	0.90 min	see footnote ⁵
Total Acid Capacity, meq/g	0.95 to 1.01	see footnote ⁵

¹ Measurements taken with membrane conditioned to 23 °C, 50% relative humidity (RH).

² Physical Properties measured for N-115. Where specified, MD - machine direction, TD - transverse direction. Conditioning state of membrane given. Measurements taken at 23 °C, 50% RH.

³ Tear resistance (g/mm) of dry membrane increases with thickness. Values given measured using 50 micron membrane.

⁴ Conductivity measurement as described by Zawodzinski, et.al, *J. Phys. Chem.*, 95 (15), 6040 (1991). Membrane conditioned in 100 °C water for 1 hour. Measurement cell submersed in 25 °C D.I. water during experiment. Membrane impedance (real) taken at zero imaginary impedance.

⁵ A base titration procedure measures the equivalents of sulfonic acid in the polymer, and uses the measurement to calculate the acid capacity or equivalent weight of the membrane.

Properties of Nafion[®] PFSA Membrane

C. Hydrolytic Properties²

Property	Typical Value	Test Method
Hydrolytic Properties		
Water content, % water ⁶	5	ASTM D 570
Water uptake, % water ⁷	38	ASTM D 570
Thickness change, % increase		
from 50% RH, 23 °C to water soaked, 23 °C	10	ASTM D 756
from 50% RH, 23 °C to water soaked, 100 °C	14	ASTM D 756
Linear expansion, % increase ⁸		
from 50% RH, 23 °C to water soaked, 23 °C	10	ASTM D 756
from 50% RH, 23 °C to water soaked, 100 °C	15	ASTM D 756

Recommended Roll Storage Conditions

Unopened roll packages of Nafion[®] PFSA membrane should be stored in the original shipping box, out of direct sunlight, and in a climate-controlled environment, maintained at 10 to 30°C, and 30 to 70% relative humidity. Before opening the package, pre-condition the membrane roll to the processing area temperature for 24 hours.

Once opened and exposed to the environment, the membrane will equilibrate to the ambient relative humidity, and change in dimensions accordingly. Membrane order dimensions are specified and measured at 23°C and 50% Relative Humidity.

Handling Practices

Ventilation should be provided for safe handling and processing of Nafion[®] PFSA membrane. The amount of local exhaust necessary for processing Nafion[®] PFSA membrane at elevated temperatures will depend on the combined factors of membrane quantity, temperature, and exposure time.

Scrap Disposal

Preferred disposal options are (1) recycling and (2) landfill. Incinerate only if incinerator is capable of scrubbing-out hydrogen fluoride and other acidic combustion products. Treatment, storage, transportation, and disposal must be in accordance with applicable federal, state/provincial and local regulations.

Safe Handling and Use of Nafion[®] PFSA Membranes

The following information should be reviewed before handling and processing Nafion[®] PFSA Membranes:

- DuPont Material Safety Data Sheet for Nafion[®] PFSA Membranes N-115, N-117 and N-1110
- Nafion[®] Technical Information "Safe Handling and Use"
- "Guide to Safe Handling of Fluoropolymer Resins", Fourth Edition, November 2005, Published by the Fluoropolymers Division of the Society of the Plastics Industry, Inc.

⁶ Water content of membrane conditioned to 23 °C, 50% relative humidity (RH), compared to dry weight basis.

⁷ Water uptake from dry membrane to water soaked at 100 °C for 1 hour (dry weight basis).

⁸ Typical MD and TD values. MD expansion is slightly less than TD.

Appendix B

Nafion Resin solution

SIGMA-ALDRICH[®]

sigma-aldrich.com

3050 Spruce Street, Saint Louis, MO 63103, USA

Website: www.sigmaaldrich.com

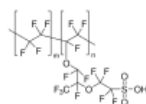
Email USA: techserv@sial.com

Outside USA: eurtechserv@sial.com

Product Specification

Product Name:
Nafion[®] perfluorinated membrane - Nafion[®] 115, thickness 0.005 in.

Product Number: **541346**
CAS Number: 31175-20-9
MDL: MFCD00132790



TEST	Specification
Appearance (Color)	Colorless
Appearance (Form)	Conforms
Sheets	
Miscellaneous Supplier Data	Pass
Visual Quality	
Miscellaneous Supplier Data	Pass
Complete Hydrolysis	
Size	
Thickness: Mils	
Miscellaneous Assay	0.130 - 0.190
Weight Caliper: g/sq. in	
Miscellaneous Assay	
Expansion MD	
Miscellaneous Assay	
Expansion TD	
Vendor Information	Conforms
Nafion is a registered trademark of The Chemours Company FC, LLC	

Specification: PRD.0.ZQ5.10000067260

Sigma-Aldrich warrants, that at the time of the quality release or subsequent retest date this product conformed to the information contained in this publication. The current Specification sheet may be available at Sigma-Aldrich.com. For further inquiries, please contact Technical Service. Purchaser must determine the suitability of the product for its particular use. See reverse side of invoice or packing slip for additional terms and conditions of sale.

Appendix C

3D Printer

ProJet® 3500 SD & HD

Professional 3D Printers



Easily create high-definition, precise plastic functional prototypes and end-use parts

The ProJet® 3500 series of plastic 3D printers are ideal for creating durable, high-definition functional prototypes, rapid tooling such as injection molds and casting patterns, and end-use parts right in your office. This versatile range of workhorse printers is easy to use, with fast print times and easy post-processing. Parts made on ProJet 3500s are beautifully precise, with sharp edges and true-to-CAD fidelity. Efficient material use, low-maintenance operation and a five-year print head warranty means you can print with confidence and keep costs down.

Using 3D Systems' MultiJet Printing (MJP) technology and VisiJet® M3 performance engineered materials, ProJet 3500s print in hard ABS-like plastics in a variety of colors, tensile strengths and other properties to match your application—including clear and biocompatible parts. You can even print sacrificial patterns in precision-castable plastics



www.3dsystems.com

MANUFACTURINGTHE FUTURE

Productive, high-capacity ProJet® 3500 professional printers



The widest applications range: concept models, verification models, pre-production, digital manufacturing

Easy connectivity and high productivity with high resolution and accuracy

ProJet 3510 SD

The affordable ProJet 3510 SD prints high-quality, durable plastic parts for engineering and mechanical design applications, including functional testing, form and fit verification, rapid prototyping, design communication, rapid tooling and more. This office-friendly 3D printer delivers exceptional parts on demand.

AFFORDABILITY • QUALITY • EASE-OF-USE

ProJet 3510 HDPlus

The ProJet 3510 HDPlus offers the flexibility to choose between three resolution modes to print concept models, verification prototypes and patterns for pre-production and digital manufacturing. Just connect to the printer to create extremely fine-featured plastic parts with greater output.

RESOLUTION *Plus* • PARTS SIZE *Plus* • FLEXIBILITY *Plus*

ProJet 3510 HD

The ProJet 3510 HD prints precision, durable plastic parts ideal for functional testing, design communication, rapid manufacturing, rapid tooling and more. With a choice in materials and selectable print resolutions, this office-friendly, easy-to-use 3D printer is packed with features that help you maximize your return on investment (ROI).

HIGH DEFINITION • PRECISION • PRODUCTIVITY

ProJet 3500 HDMax

The high-capacity ProJet 3500 HDMax offers greater productivity, especially with the high-speed printing mode, and larger high-definition prints for the production of functional plastic parts. Users also benefit from increased throughput, part size, feature detail and quality only possible with ProJet printers.

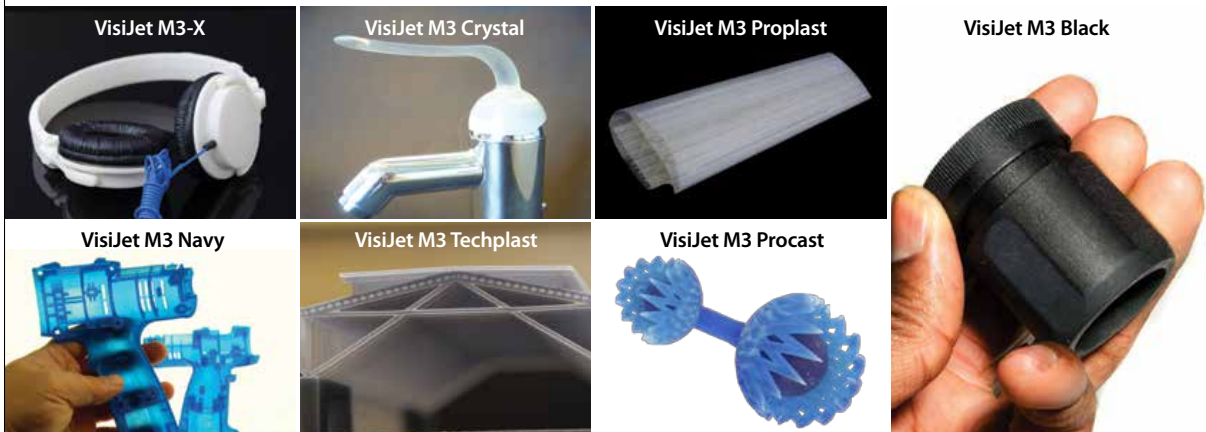
Max THROUGHPUT • *Max* DEFINITION • *Max* VOLUME

VisiJet® M3 Materials for ProJet SD & HD Printers

The VisiJet line of plastic materials offers numerous capabilities to meet a variety of commercial applications. 3D Systems' ProJet 3500 3D printers use VisiJet M3 materials to build accurate, high-definition models and prototypes for proof of concept, functional testing, master patterns for moldmaking, and direct investment casting. Vertical markets for the ProJet 3500 line include transportation, energy, consumer products, recreation, healthcare and education. Toughness, high temperature resistance, durability, stability, watertightness, biocompatibility and castability are a few of the key attributes you will find within the VisiJet M3 materials line. Parts can be drilled, glued, painted, plated, etc. Support material offers easy, non-hazardous post-processing and preserves delicate features.

Properties	Condition	VisiJet M3-X	VisiJet M3 Black	VisiJet M3 Crystal	VisiJet M3 Proplast	VisiJet M3 Navy	VisiJet M3 Techplast	VisiJet M3 Procast	VisiJet® S300
Composition		UV Curable Plastic							Wax Support Material
Color		White	Black	Natural	Natural	Blue	Gray	Dark Blue	White
Bottle Quantity		2 kg	2 kg	2 kg	2 kg	2 kg	2 kg	2 kg	2 kg
Density @ 80 °C (liquid)	ASTM D4164	1.04 g/cm ³	1.02 g/cm ³	1.02 g/cm ³	1.02 g/cm ³	1.02 g/cm ³	1.02 g/cm ³	1.02 g/cm ³	N/A
Tensile Strength	ASTM D638	49 MPa	35.2 MPa	42.4 MPa	26.2 MPa	20.5 MPa	22.1 MPa	32 MPa	N/A
Tensile Modulus	ASTM D638	2168 MPa	1594 MPa	1463 MPa	1108 MPa	735 MPa	866 MPa	1724 MPa	N/A
Elongation at Break	ASTM D638	8.3 %	19.7 %	6.83 %	8.97 %	8 %	6.1 %	12.3 %	N/A
Flexural Strength	ASTM D790	65 MPa	44.5 MPa	49 MPa	26.6 MPa	28.1 MPa	28.1 MPa	45 MPa	N/A
Heat Distortion Temperature @ 0.45MPa	ASTM D648	88 °C	57 °C	56 °C	46 °C	46 °C	46 °C	N/A	N/A
Ash Content		N/A	N/A	N/A	0.01 %	0.01 %	0.01 %	0.01 %	N/A
Melting Point		N/A	N/A	N/A	N/A	N/A	N/A	N/A	60 °C
Softening Point		N/A	N/A	N/A	N/A	N/A	N/A	N/A	40 °C
USP Class VI Certified*		No	No	Yes	No	No	No	No	N/A
ProJet Compatibility		SD, HD	SD, HD	SD, HD	SD, HD	SD, HD	SD, HD	HD	SD, HD
Description		ABS-like Plastic	High strength & flexibility plastic	Tough Plastic, Translucent	Plastic, Natural	Plastic, Blue	Plastic, Gray	Castable Plastic	Non-toxic wax material for hands-free melt-away supports

DISCLAIMER: It is the responsibility of each customer to determine that its use of any VisiJet® material is safe, lawful and technically suitable to the customer's intended applications. The values presented here are for reference only and may vary. Customers should conduct their own testing to ensure suitability for their intended application.







ProJet® 3500 SD & HD

Professional 3D Printers



3DSYSTEMS

Extend Innovation. Extend Production. Extend Choices.

				
	ProJet 3510 SD	ProJet 3510 HD	ProJet 3510 HDPlus	ProJet 3500 HDMax
Printing Modes	HD - High Definition -	HD - High Definition UHD - Ultra High Definition -	HD - High Definition UHD - Ultra High Definition XHD - Xtreme High Definition	HD - High Definition HS - High Speed UHD - Ultra High Definition XHD - Xtreme High Definition
Net Build Volume (xyz)				
HD Mode	11.75 x 7.3 x 8" (298 x 185 x 203 mm)	11.75 x 7.3 x 8" (298 x 185 x 203 mm)	11.75 x 7.3 x 8" (298 x 185 x 203 mm)	11.75 x 7.3 x 8" (298 x 185 x 203 mm)
HS Mode	-	-	-	11.75 x 7.3 x 8" (298 x 185 x 203 mm)
UHD Mode	-	5 x 7 x 6" (127 x 178 x 152 mm)	8 x 7 x 6" (203 x 178 x 152 mm)	11.75 x 7.3 x 8" (298 x 185 x 203 mm)
XHD Mode	-	-	8 x 7 x 6" (203 x 178 x 152 mm)	11.75 x 7.3 x 8" (298 x 185 x 203 mm)
Resolution				
HD Mode	375 x 375 x 790 DPI (xyz); 32µ layers	375 x 375 x 790 DPI (xyz); 32µ layers	375 x 375 x 790 DPI (xyz); 32µ layers	375 x 375 x 790 DPI (xyz); 32µ layers
HS Mode	-	-	-	375 x 375 x 790 DPI (xyz); 32µ layers
UHD Mode	-	750 x 750 x 890 DPI (xyz); 29µ layers	750 x 750 x 890 DPI (xyz); 29µ layers	750 x 750 x 890 DPI (xyz); 29µ layers
XHD Mode	-	-	750 x 750 x 1600 DPI (xyz); 16µ layers	750 x 750 x 1600 DPI (xyz); 16µ layers
Accuracy (typical)	0.001-0.002 inch per inch (0.025-0.05 mm per 25.4 mm) of part dimension. Accuracy may vary depending on build parameters, part geometry and size, part orientation, and post-processing.			
E-mail Notice Capability	Yes	Yes	Yes	Yes
Tablet/Smartphone connectivity	Yes	Yes	Yes	Yes
5-Year Printhead Warranty	Optional	Standard	Standard	Standard
Build Materials	VisiJet M3-X VisiJet M3 Black VisiJet M3 Crystal VisiJet M3 Proplast VisiJet M3 Navy VisiJet M3 Techplast -	VisiJet M3-X VisiJet M3 Black VisiJet M3 Crystal VisiJet M3 Proplast VisiJet M3 Navy VisiJet M3 Techplast VisiJet M3 Procast	VisiJet M3-X VisiJet M3 Black VisiJet M3 Crystal VisiJet M3 Proplast VisiJet M3 Navy VisiJet M3 Techplast VisiJet M3 Procast	VisiJet M3-X VisiJet M3 Black VisiJet M3 Crystal VisiJet M3 Proplast VisiJet M3 Navy VisiJet M3 Techplast VisiJet M3 Procast
Support Material	VisiJet S300	VisiJet S300	VisiJet S300	VisiJet S300
Material Packaging	Build and support materials In clean 4.41 lbs (2 kg) bottles (machine holds up to 2 with auto-switching)			
Electrical	100-127 VAC, 50/60 Hz, single-phase, 15A; 200-240* VAC, 50 Hz, single-phase, 10A			
Dimensions (WxDxH)				
3D Printer Crated	32.5 x 56.25 x 68.5 in (826 x 1429 x 1740 mm)	32.5 x 56.25 x 68.5 in (826 x 1429 x 1740 mm)	32.5 x 56.25 x 68.5 in (826 x 1429 x 1740 mm)	32.5 x 56.25 x 68.5 in (826 x 1429 x 1740 mm)
3D Printer Uncrated	29.5 x 47 x 59.5 in (749 x 1194 x 1511 mm)	29.5 x 47 x 59.5 in (749 x 1194 x 1511 mm)	29.5 x 47 x 59.5 in (749 x 1194 x 1511 mm)	29.5 x 47 x 59.5 in (749 x 1194 x 1511 mm)
Weight				
3D Printer Crated	955 lbs, 434 kg	955 lbs, 434 kg	955 lbs, 434 kg	955 lbs, 434 kg
3D Printer Uncrated	711 lbs, 323 kg	711 lbs, 323 kg	711 lbs, 323 kg	711 lbs, 323 kg
ProJet® Accelerator Software	Easy build job set-up, submission and job queue management ; Automatic part placement and build optimization tools ; Part stacking and nesting capability ; Extensive part editing tools ; Automatic support generation ; Job statistics reporting tools			
Print3D App	Remote monitoring and control from tablet, computers and smartphones			
Network Compatibility	Network ready with 10/100 Ethernet interface			
Client Hardware Recommendation	1.8 GHz with 1GB RAM (OpenGL support 64 mb video RAM) or higher			
Client Operating System	Windows XP Professional, Windows Vista, Windows 7			
Input Data File Formats Supported	STL and SLC	STL and SLC	STL and SLC	STL and SLC
Operating Temperature Range	64-82 °F (18-28 °C)	64-82 °F (18-28 °C)	64-82 °F (18-28 °C)	64-82 °F (18-28 °C)
Noise	< 65 dBA estimated (at medium fan setting)			
Certifications	CE	CE	CE	CE



USA
Tel: +1 803.326.3900
moreinfo@3dsystems.com

UK
Tel: +44 1442 282 600
info@3dsystems-europe.com

**Germany, Scandinavia,
Eastern Europe, Middle East**
Tel: +49 8151 357 0
info@3dsystems-europe.com

Asia-Pacific
Melbourne Tel: +61 3 9819 4422
Sydney Tel: +61 2 9516 5571
3dprinters.asiapac@3dsystems.com

Warranty/Disclaimer: The performance characteristics of these products may vary according to product application, operating conditions, material combined with, or with end use. 3D Systems makes no warranties of any type, express or implied, including, but not limited to, the warranties of merchantability or fitness for a particular use.

© 2015 by 3D Systems Inc. All rights reserved. Specifications subject to change without notice. ProJet, VisiJet, 3D Systems and the 3D Systems logo are registered trademarks of 3D Systems, Inc. Windows is a registered trademark of Microsoft Corporation.

Appendix D

Magic Rubber

FILLERS
RUBBER

LV

Magic Rubber

Fast cross linking bicomponent rubber

Cross linking time:
15 minutes at 23°C
Volume resistivity:
>2 10¹⁵ Ω cm
Dielectric strength:
> 23 kV/mm
Specific weight:
1,22 approx
Degree of protection:
IP68 (in proper casings)

Bicomponent insulating liquid rubber, extremely conformable and fluid, flexible, elastic and re-enterable. In just a few minutes, transforms into a rubber with very high dielectric, thermal, mechanical and elastic characteristics.

- For installation up to 1kV
- Low smoke, toxic and corrosive gas emissions
- Ideal also for casts and moulds
- Non toxic and safe
- No shelf life



**Ray
Tech**



Magic Rubber & Rubber Fluid

Product	Colour	Package type	Total quantity
Magic Rubber 500	●	2 bicomponent bottles 1 measuring cup - 1 mixing palette	500 gr
Magic Rubber 10	●	2 bicomponent tanks 1 measuring cup - 1 mixing palette	10 kg
Rubber Fluid 200	●	Bicomponent single dose bags	200 gr
Rubber Fluid 350	●	Bicomponent single dose bags	350 gr



Mix the 2 components in a ratio of 1:1.



Mix for max 30".



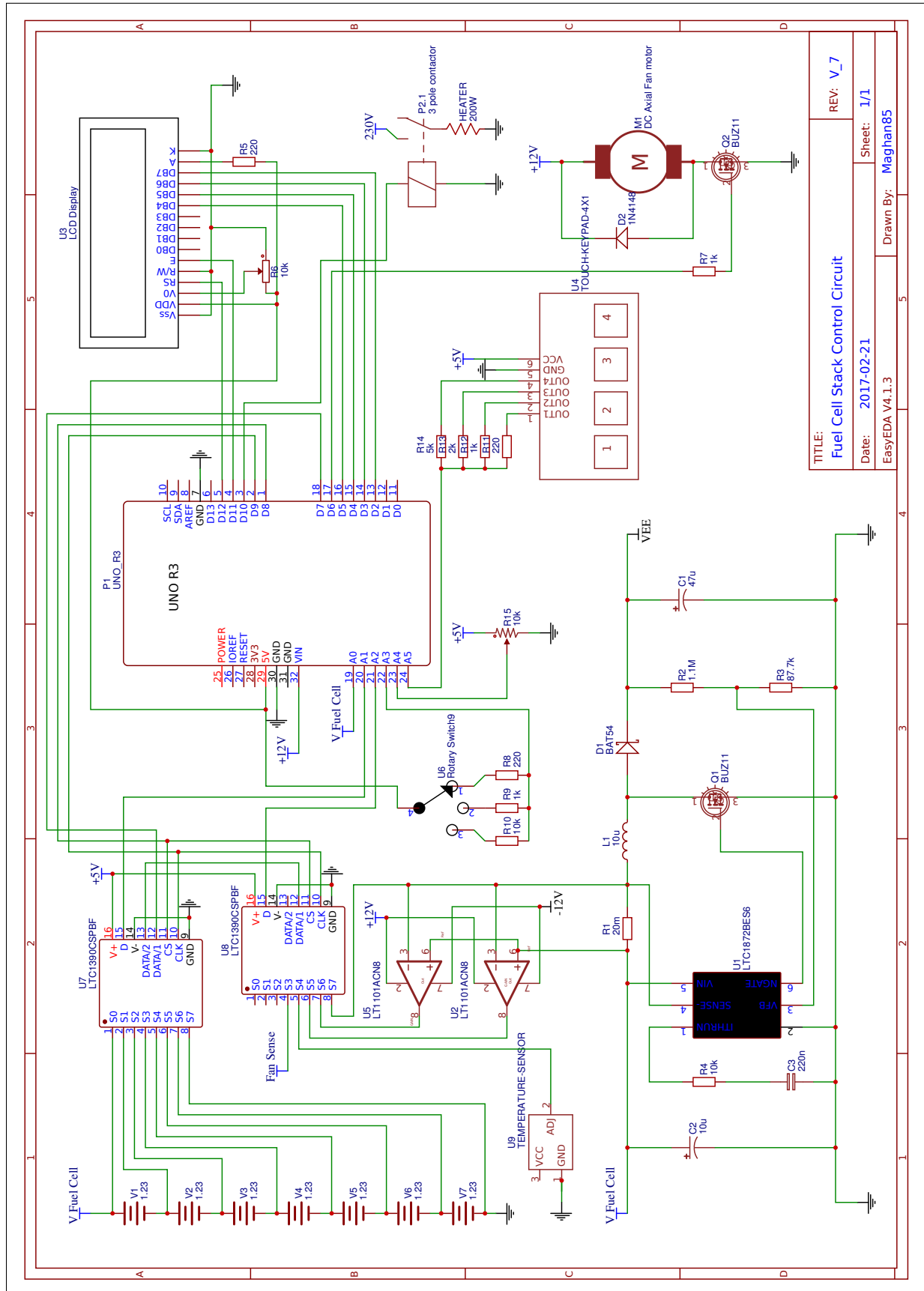
Pour the product into the casing to be filled.



In just a few minutes, the product transforms into rubber.

Appendix E

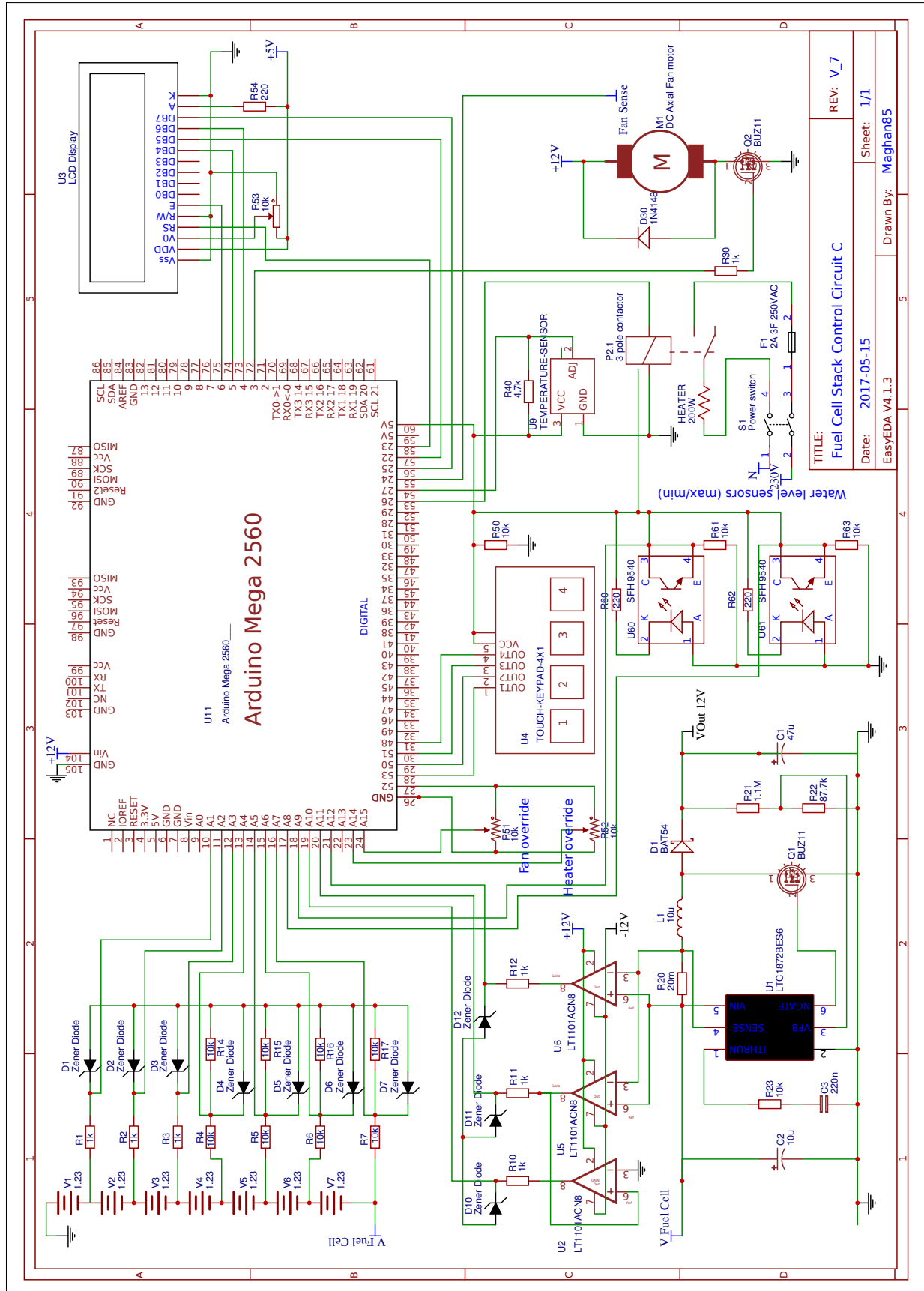
Fuel Cell Stack Control Circuit A



TITLE: Fuel Cell Stack Control Circuit
REV: V_7
Date: 2017-02-21
EasyEDA V4.1.3
Sheet: 1/1
Drawn By: Maghan85

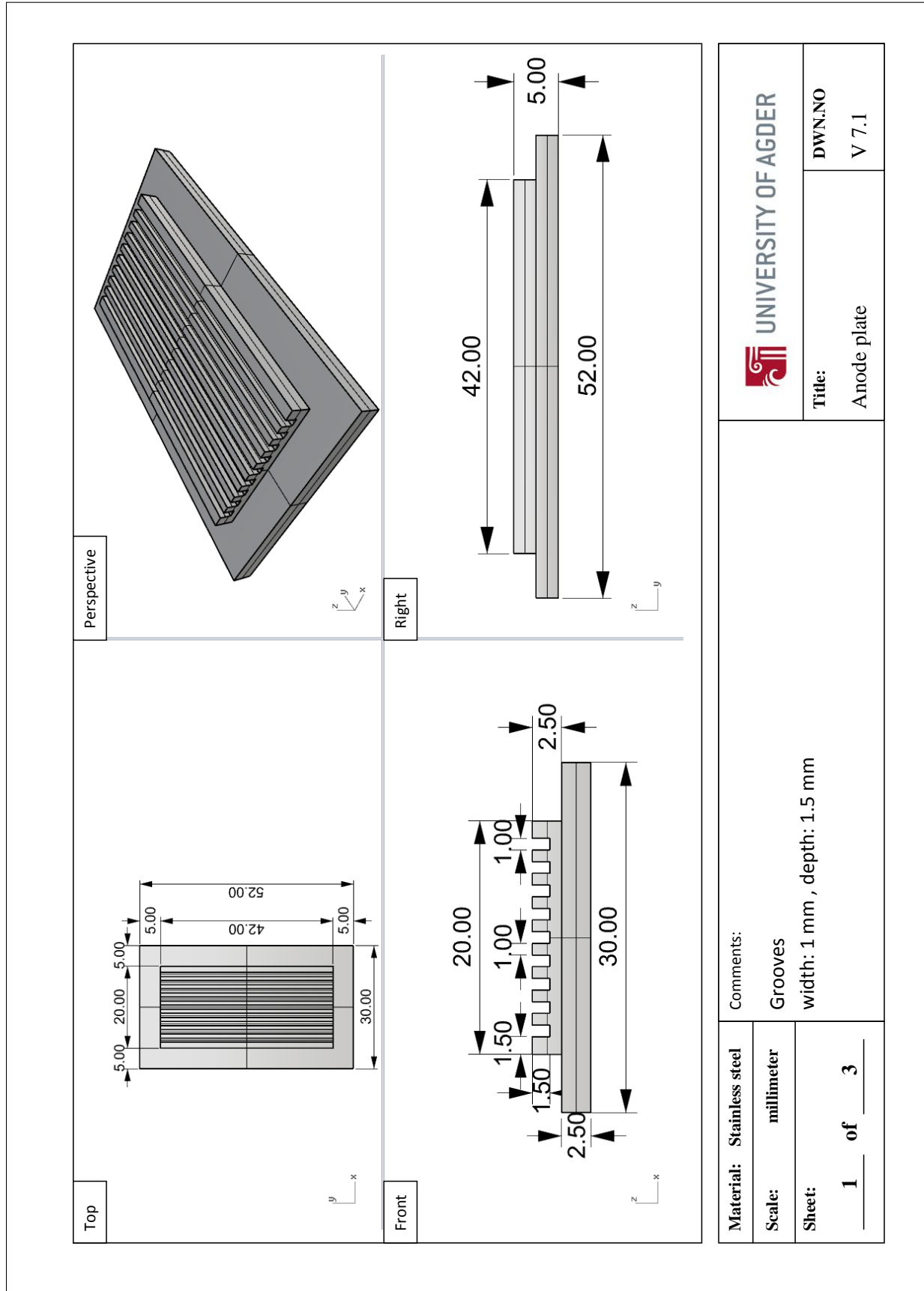
Appendix F

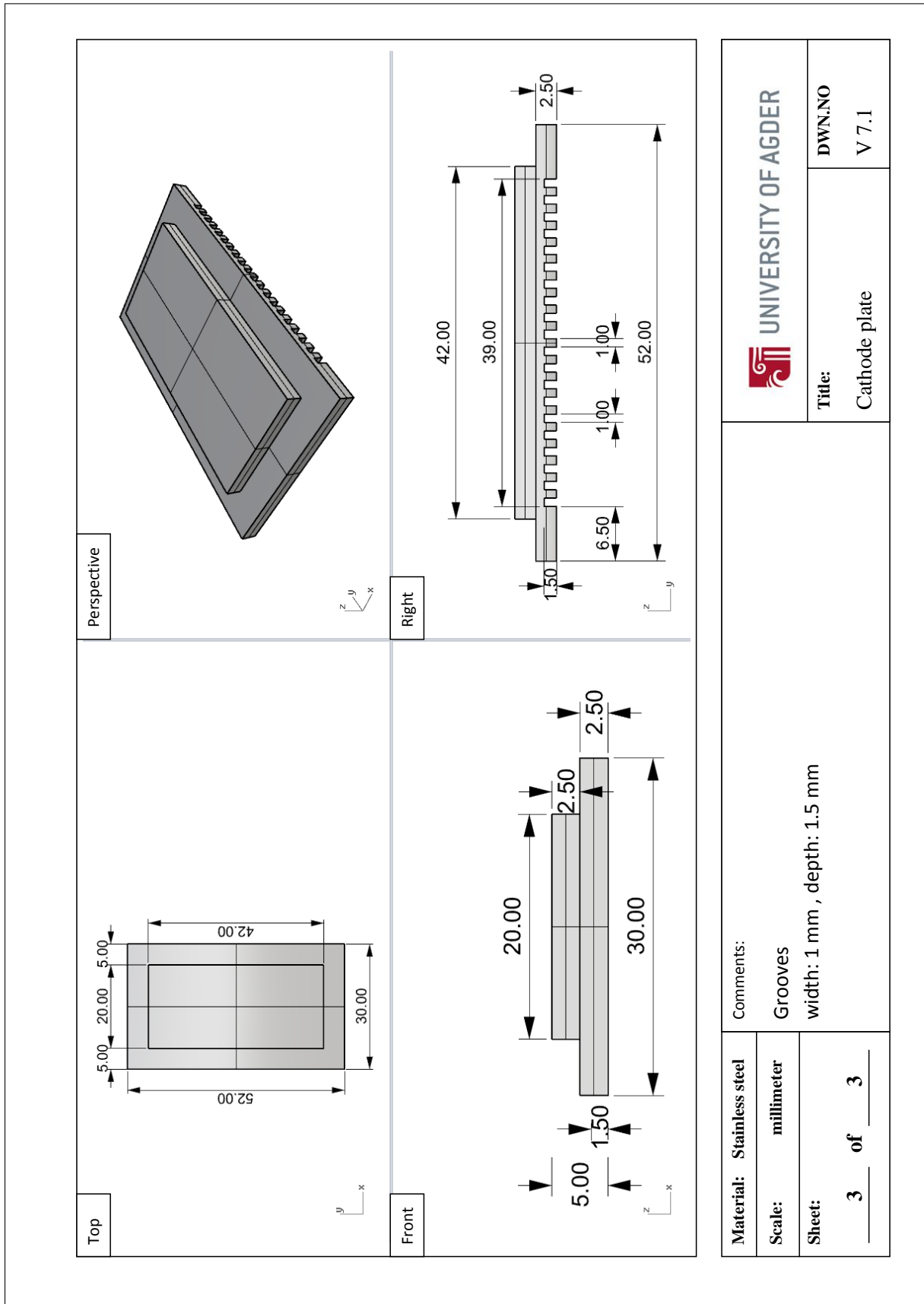
Fuel Cell Stack Control Circuit B



Appendix G

Technical drawing: Fuel Cell Plates

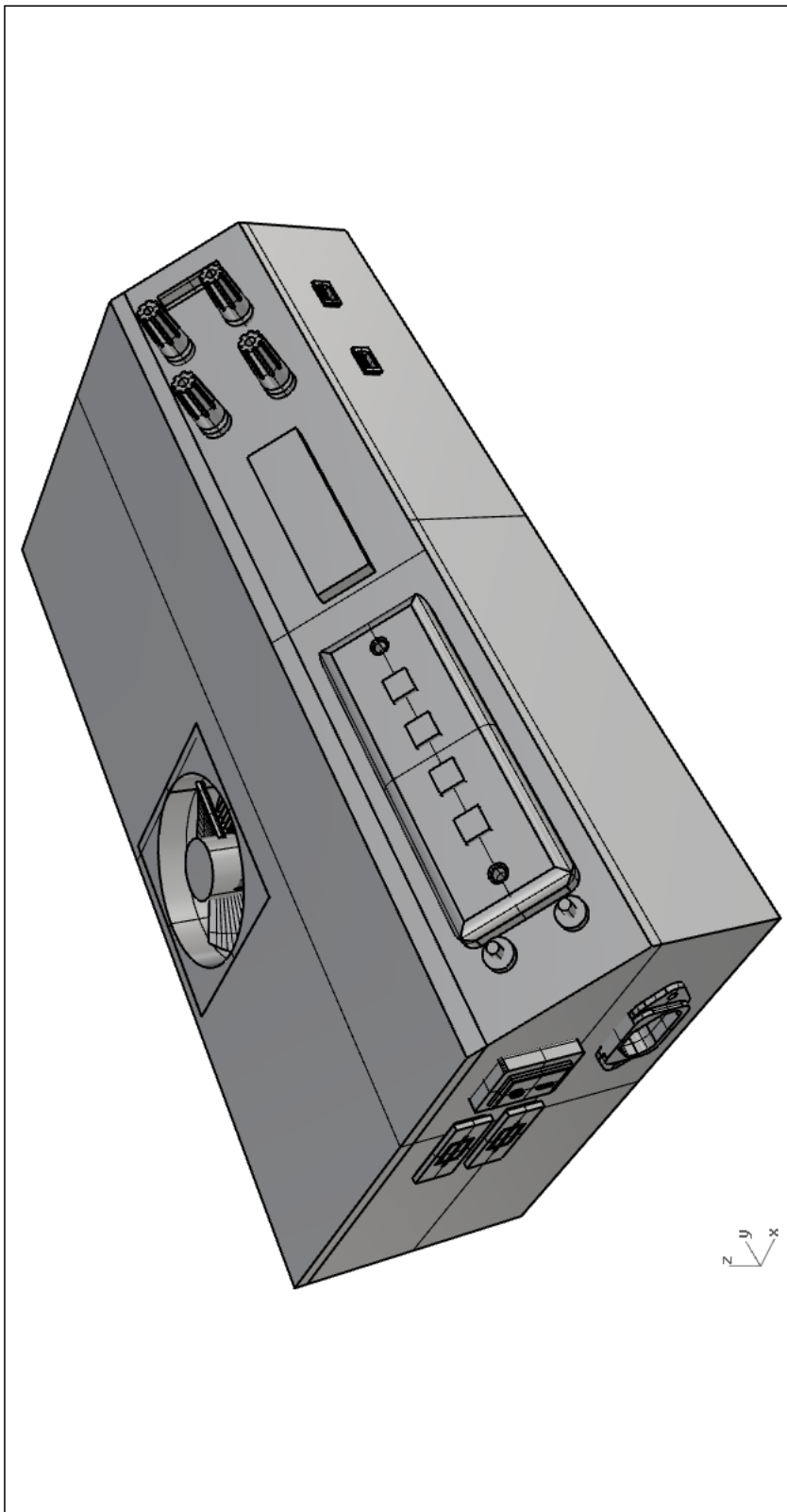





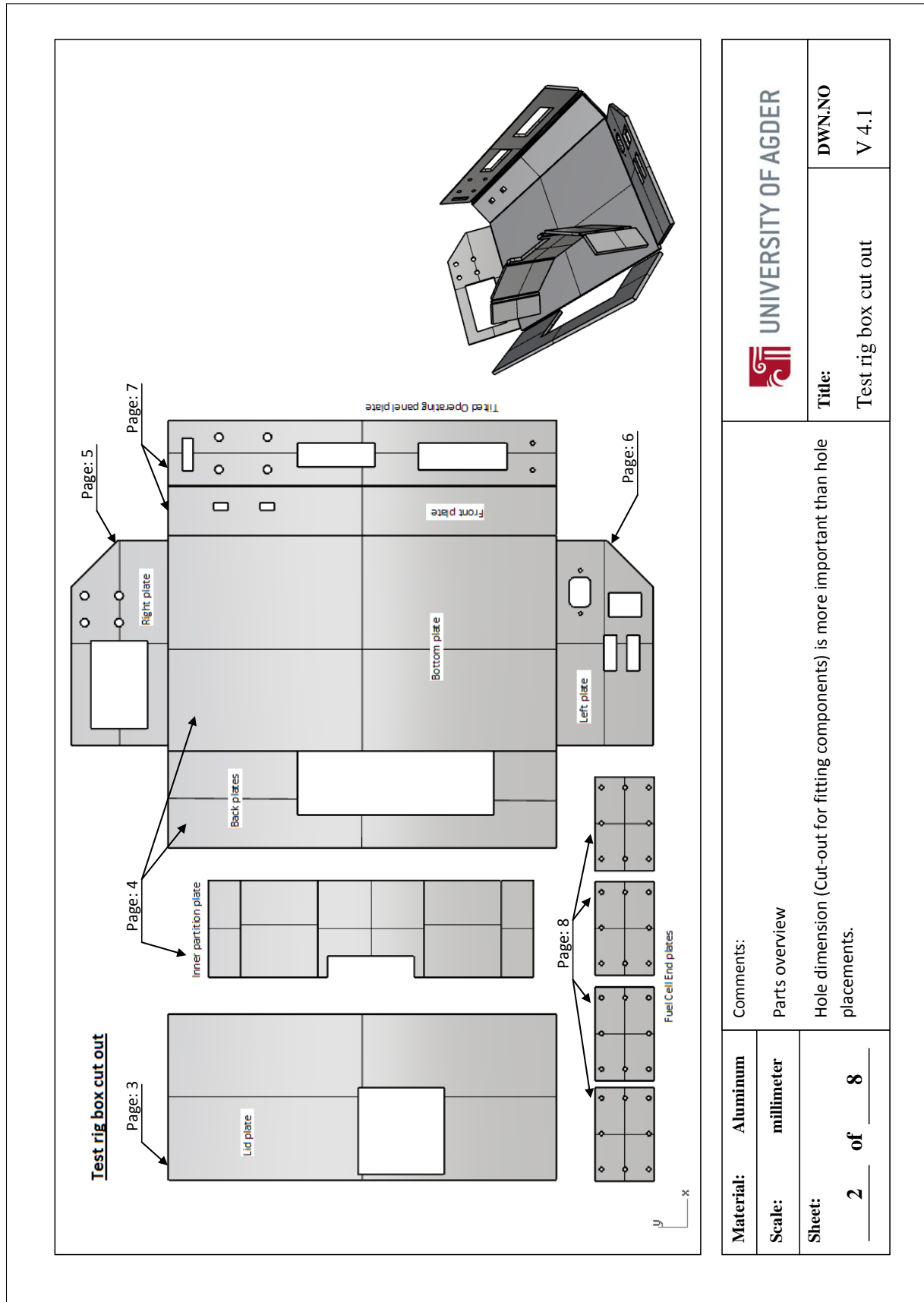
Material: Stainless steel Scale: millimeter Sheet: 3 of 3	Comments: Grooves width: 1 mm , depth: 1.5 mm	
	UNIVERSITY OF AGDER	DWN.NO V 7.1
Title: Cathode plate		

Appendix H

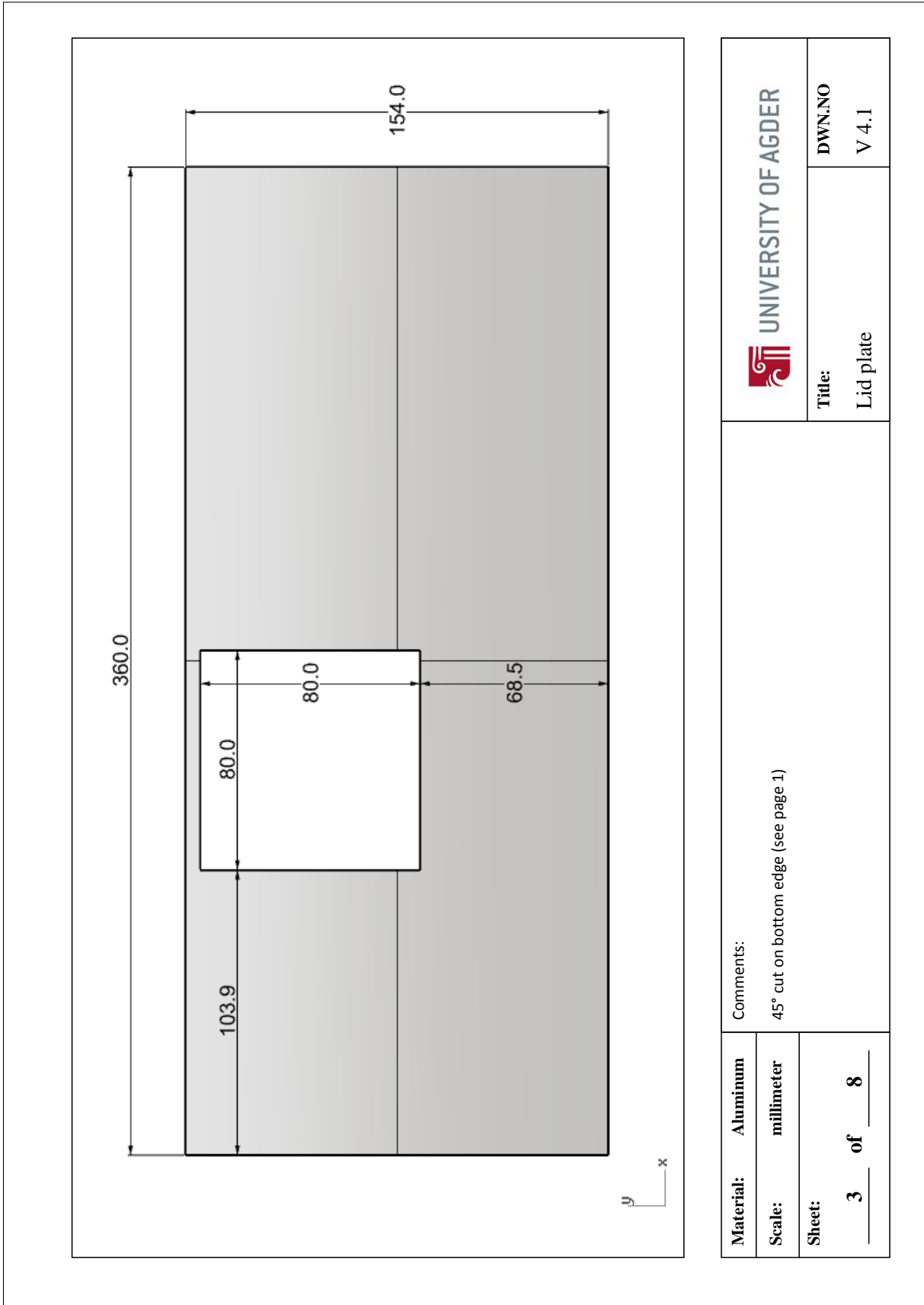
Technical drawing: Testing station

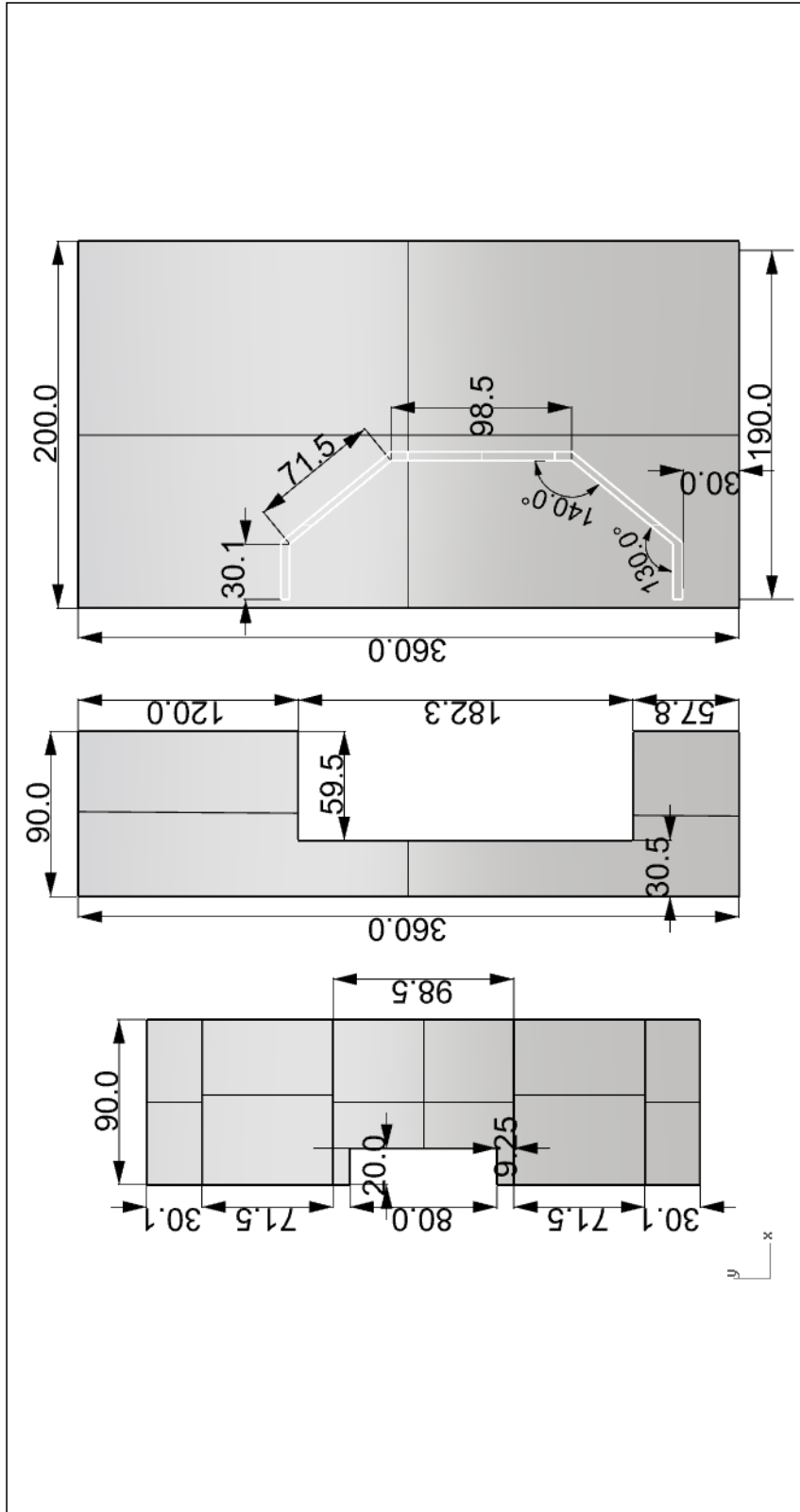


 UNIVERSITY OF AGDER		DWN.NO V 4.1	
		Title: Fuel Cell Test Rig	
Comments:			
Material:	Aluminum		
Scale:	millimeter		
Sheet:	1	of	8

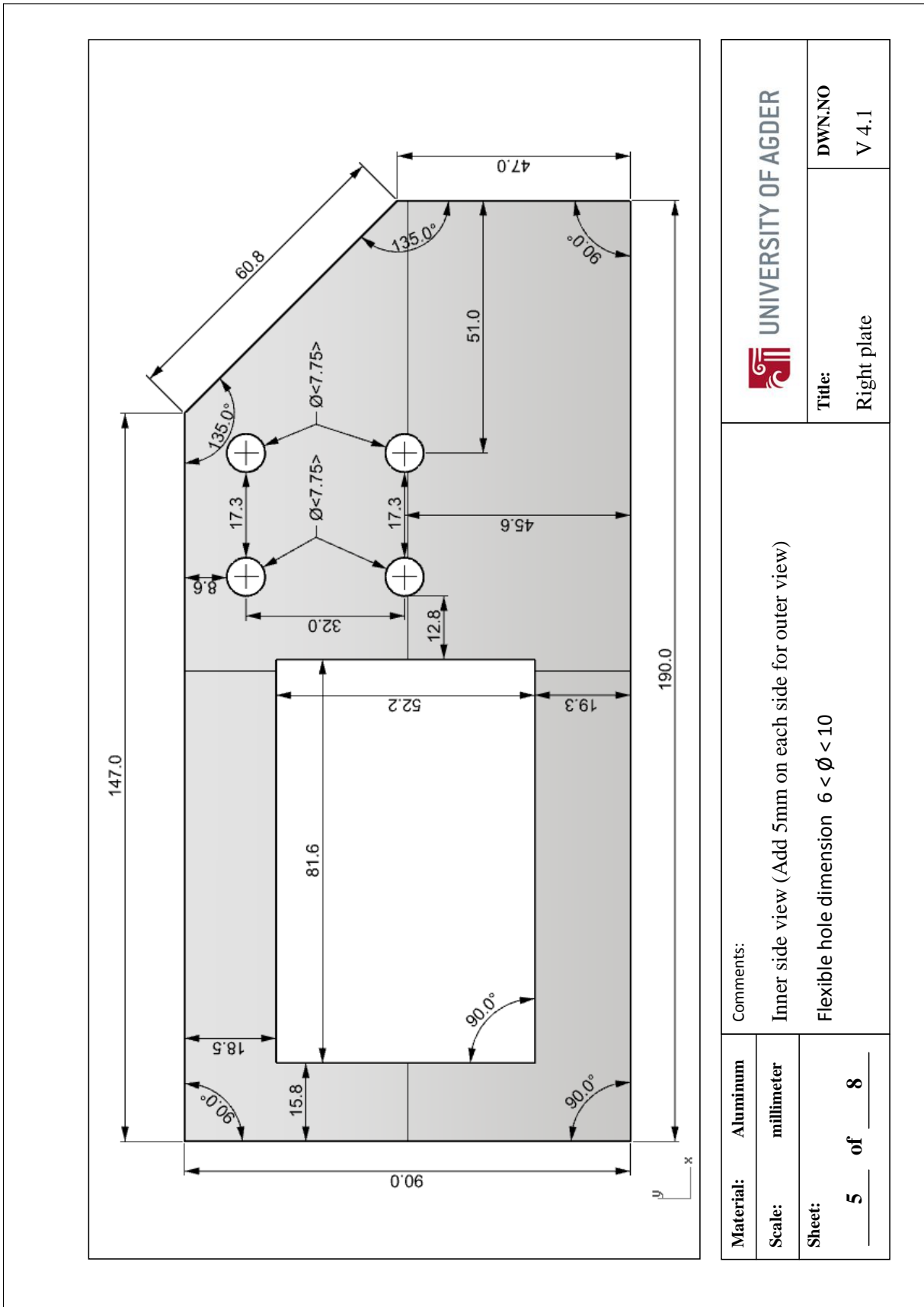


Material: Aluminum	Comments: Parts overview		UNIVERSITY OF AGDER	DWN.NO V 4.1
Scale: millimeter	Hole dimension (Cut-out for fitting components) is more important than hole placements.			
Sheet: 2 of 8				

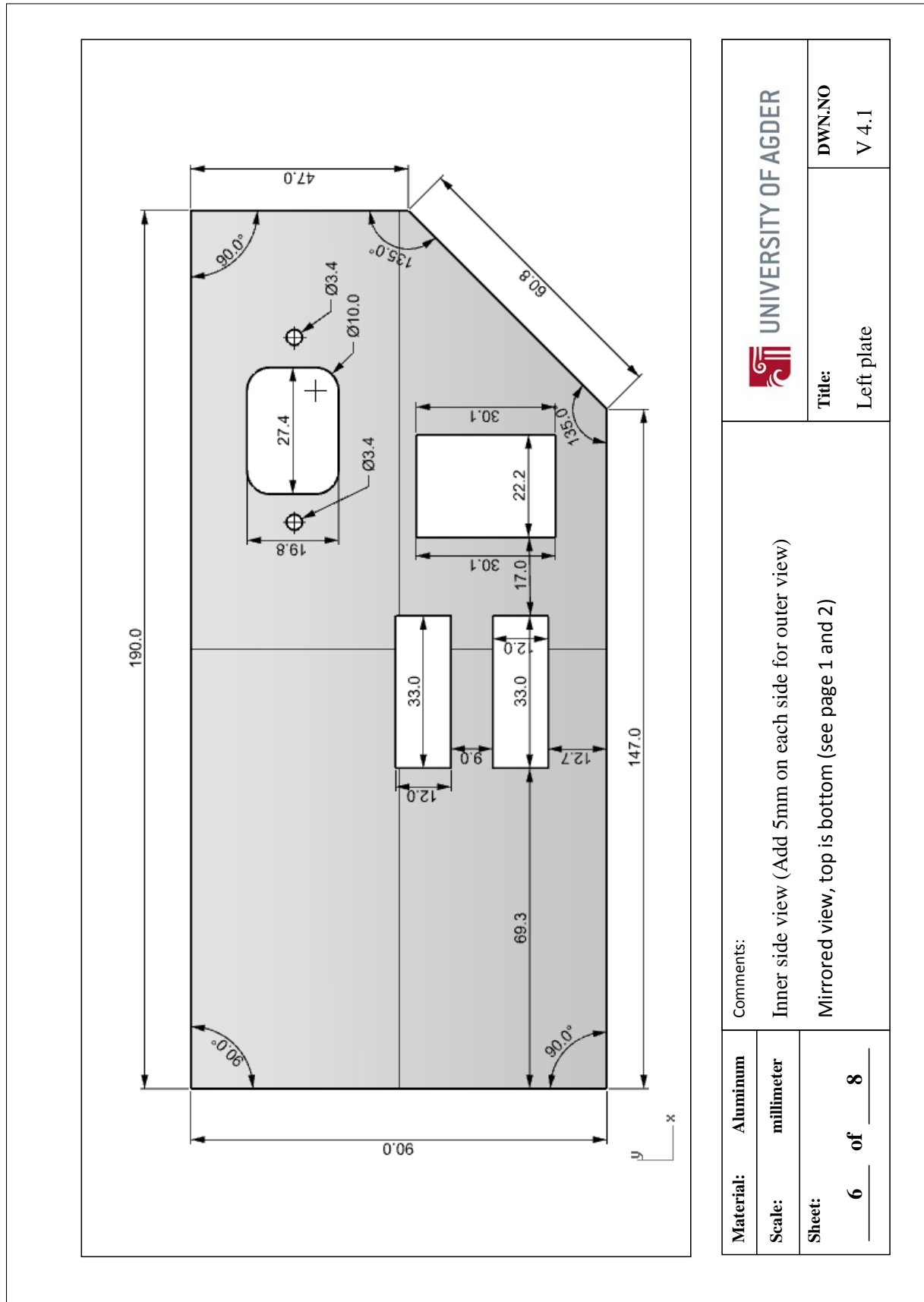




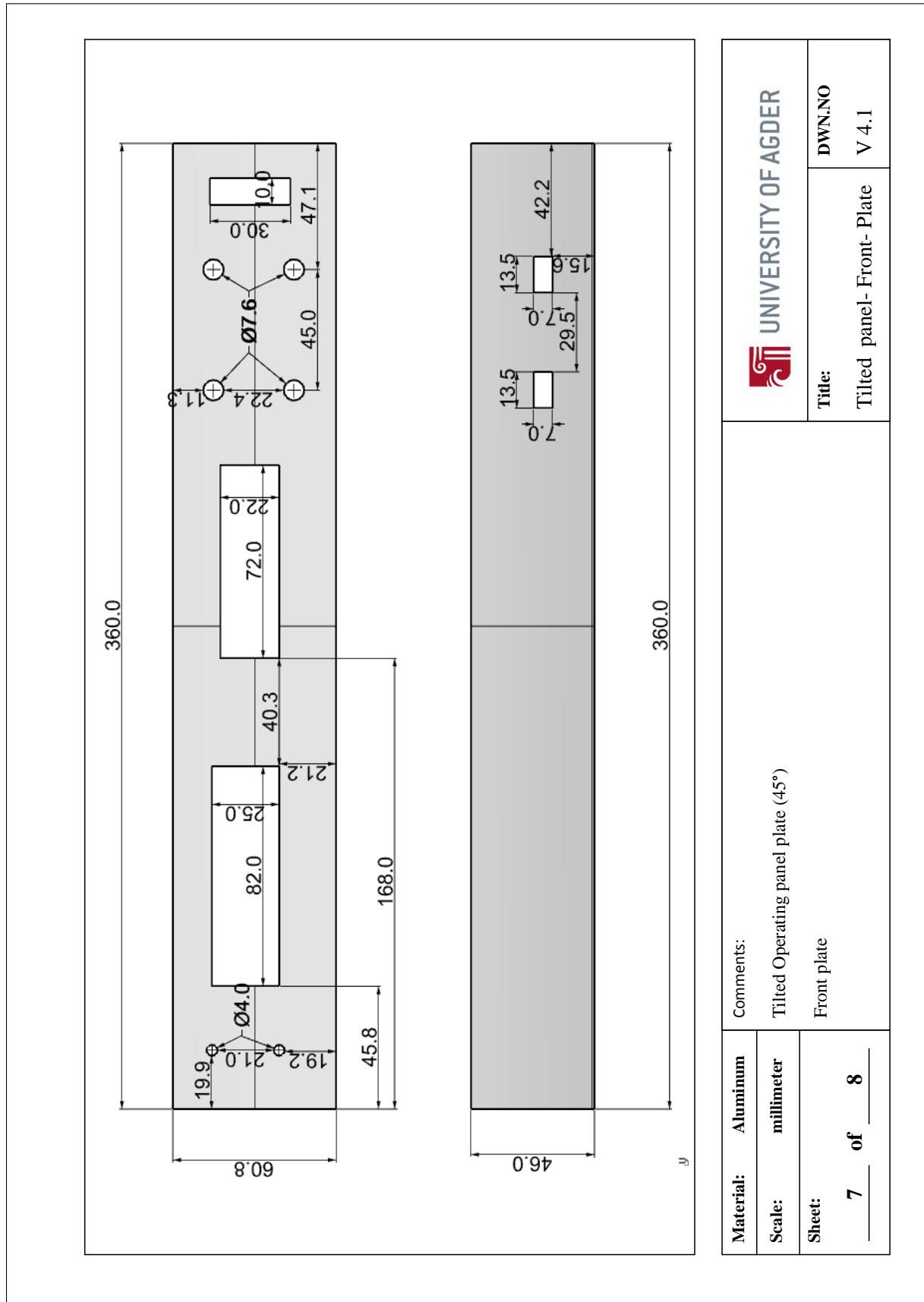
Material: Aluminum Scale: millimeter Sheet: 4 of 8	UNIVERSITY OF AGDER	
	Title: Inner- Back- Bottom- Plate	DWN.NO V 4.1
Comments: Inner partition plate Back plate Bottom plate (With Inner partition plate orientation)		



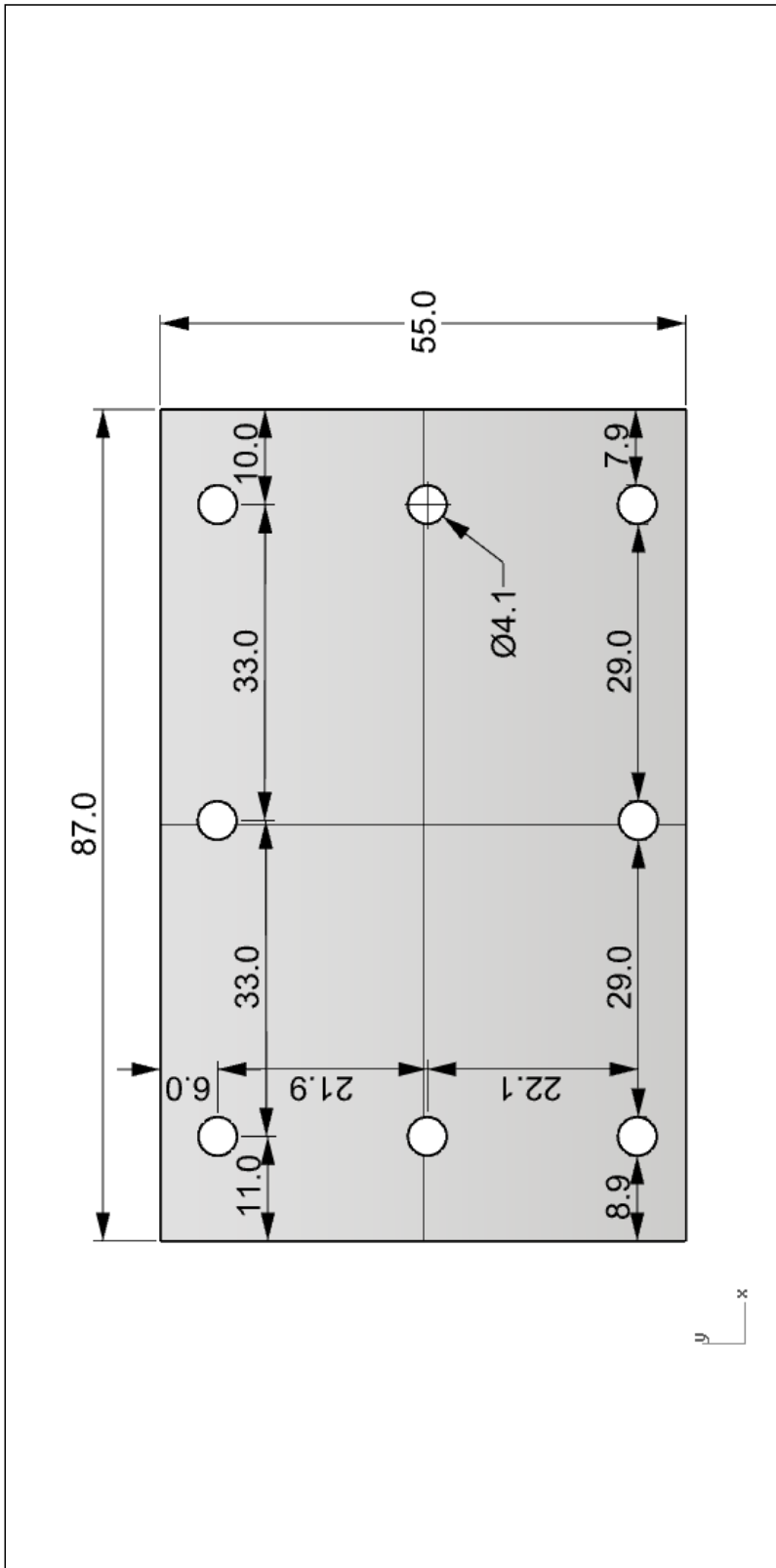
Material: Aluminum Scale: millimeter Sheet: 5 of 8	Comments: Inner side view (Add 5mm on each side for outer view) Flexible hole dimension $6 < \varnothing < 10$	
	UNIVERSITY OF AGDER	DWN.NO V 4.1
Title: Right plate		



Material: Aluminum Scale: millimeter Sheet: 6 of 8	Comments: Inner side view (Add 5mm on each side for outer view) Mirrored view, top is bottom (see page 1 and 2)	
	UNIVERSITY OF AGDER	DWN.NO V 4.1
Title: Left plate		



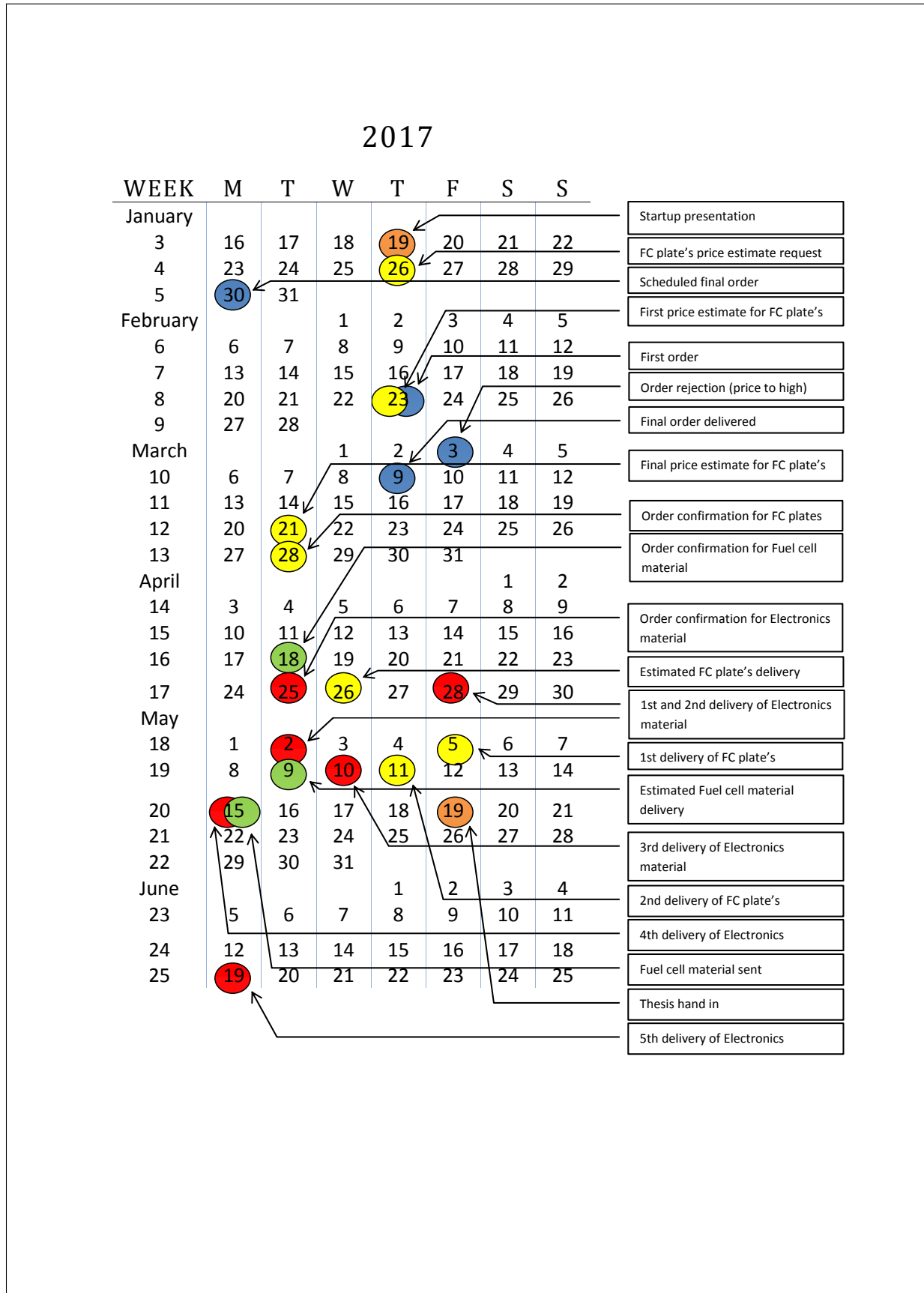
Material: Aluminum	Comments:	
	Tilted Operating panel plate (45°)	
Scale: millimeter	Front plate	
Sheet: 7 of 8	UNIVERSITY OF AGDER	DWN.NO V 4.1
	Title: Tilted panel- Front- Plate	



Material: Steel	Comments: New fuel cell stack end plates	
	Scale: millimeter	DWN.NO V 7.1
Sheet: 8 of 8	Title: Fuel Cell End plate	

Appendix I

Order schedule



Appendix J

Arduino script

```

#include <OneWire.h>
#include <DallasTemperature.h>
#define ONE_WIRE_BUS 27
OneWire oneWire(ONE_WIRE_BUS);
DallasTemperature sensors(&oneWire);

// include the library code:
#include <LiquidCrystal.h>

// initialize the library with the numbers of the interface pins
LiquidCrystal lcd(23, 6, 5, 22, 4, 25);

//initializing FanControl variables-----
int fanPot = A15;           //potmeter input
int mosfetControl = 3;     //Transistor control output
int sensorValue = 0;
int outputValue= 0;

//initializing HeaterControl variables-----
int baselineTemp = 25.0;
const int heater = 2;
int temperature = 0;
int tempPot = A14;

//initializing LCD variables-----
int digitalClicker1 = 53;
int digitalClicker2 = 50;
int digitalClicker3 = 51;
int digitalClicker4 = 48;
int voltage8 = A7;
int voltage7 = A6;
int voltage6= A5;
int voltage5 = A4;
int voltage4 = A3;
int voltage3 = A2;
int voltage2 = A1;
int currentLow = A10;
int currentHigh = A11;
int currentHigher = A12;
int const Vdiv = 2; //Voltage divider factor

int screenValue = 0;
int currentActual = 0;
int currentActualActual = 0;
int currentLowValue = 0;
int currentHighValue = 0;
int currentHigherValue = 0;
int fanControlCurrent = 0;

int cell1_ = 0;
int cell2_ = 0;
int cell3_ = 0;
int cell4_ = 0;
int cell5_ = 0;
int cell6_ = 0;
int cell7_ = 0;
int cell8_ = 0;

int cell1 = 0;
int cell2 = 0;
int cell3 = 0;

```

```

int cell4 = 0;
int cell5 = 0;
int cell6 = 0;
int cell7 = 0;
int cell8 = 0;

void setup()
{
  Serial.begin(9600);
  // FanControl setup-----

  pinMode(mosfetControl,OUTPUT);
  pinMode(fanPot,INPUT);

  // HeaterControl setup-----

  pinMode(heater,OUTPUT);
  sensors.begin();

  // LCD setup-----

  lcd.begin(16, 2);
  lcd.clear();

  pinMode(digitalClicker1, INPUT);
  pinMode(digitalClicker2, INPUT);
  pinMode(digitalClicker3, INPUT);
  pinMode(digitalClicker4, INPUT);
  pinMode(voltage8, INPUT);
  pinMode(voltage7, INPUT);
  pinMode(voltage6, INPUT);
  pinMode(voltage5, INPUT);
  pinMode(voltage4, INPUT);
  pinMode(voltage3, INPUT);
  pinMode(voltage2, INPUT);
  pinMode(currentLow, INPUT);
  pinMode(currentHigh, INPUT);
  pinMode(currentHigher, INPUT);
  screenValue = 2;
}

void loop() {
  currentLowValue = map(analogRead(currentLow), 0, 1023, 0, 5);
  currentHighValue = map(analogRead(currentHigh), 0, 1023, 0, 5);
  currentHigherValue = map(analogRead(currentHigher), 0, 1023, 0, 5);

  if (currentLowValue <= 4.65){
    currentActual = currentLowValue/1000;
  }

  else if (currentHighValue <=4.65 && currentLowValue >=4.65){
    currentActual = currentHighValue/100;
  }
  else if (currentHighValue > 4.65) {
    currentActual = currentHigherValue/10;
  }

  currentActualActual = currentActual/(20*10^-3);

  //FanControl loop-----

```

```

    sensorValue = analogRead(fanPot);
    outputValue = map(sensorValue, 0, 1023, 0, 255); //Dividing the
span of the potmeter into the PWM specter.
    fanControlCurrent = map(currentActualActual, 0, 2, 0, 255); //Dividing
the span of current into the PWM specter.

    if(sensorValue <= 50){ //If the potmeter is at a low value, the PWM is
controlled by the current of the system(fuel cell).
        analogWrite(mosfetControl, fanControlCurrent);
    }

else {
    analogWrite(mosfetControl, outputValue); //If the potmeter is at a
higher value the PWM is controlled by the potmeter.
}
    delay(1);

//HeaterControl loop-----

    sensors.requestTemperatures();
    temperature = sensors.getTempCByIndex(0);
    baselineTemp= map(tempPot, 0, 1023, 25.0, 60.0);
    if (temperature <baselineTemp) {
        digitalWrite(heater, LOW);
    }
    else {
        digitalWrite(heater, HIGH);
    }
    delay(1);

//LCD loop-----

    cell12 = map(cell12_, 0, 1023, 0, 5);
    cell13_ = analogRead(voltage3);
    cell13 = map(cell13_, 0, 1023, 0, 5);
    cell14_ = analogRead(voltage4);
    cell14 = map(cell14_, 0, 1023, 0, 5);
    cell15_ = analogRead(voltage5);
    cell15 = map(cell15_, 0, 1023, 0, 5);
    cell16_ = analogRead(voltage6);
    cell16 = map(cell16_, 0, 1023, 0, 5)*Vdiv;
    cell17_ = analogRead(voltage7);
    cell17 = map(cell17_, 0, 1023, 0, 5)*Vdiv;
    cell18_ = analogRead(voltage8);
    cell18 = map(cell18_, 0, 1023, 0, 5)*Vdiv;

    screenValue=1;
    if (digitalRead(digitalClicker1) == HIGH) {
        screenValue = screenValue+1;
    }
    delay(1);

    if (digitalRead(digitalClicker2) == HIGH) {
        screenValue = screenValue-1;
    }
    delay(1);
    if (screenValue>5) {
        screenValue=1;
    }
}

```

```
    if (screenValue == 1) {
      lcd.clear();
      lcd.setCursor(0,0);
      lcd.print("V: ");
      lcd.print(cell8);
      lcd.setCursor(10,0);
      lcd.print("I: ");
      lcd.print(currentActual);
      lcd.setCursor(0,1);
      lcd.print("P: ");
      lcd.print(cell8*currentActual);
    }

    if (screenValue == 2) {
      lcd.clear();
      lcd.setCursor(0,0);
      lcd.print("V1: ");
      lcd.print(cell2);
      lcd.setCursor(8,0);
      lcd.print("V2: ");
      lcd.print(cell3);
      lcd.setCursor(0,1);
      lcd.print("V3: ");
      lcd.print(cell4);
      lcd.setCursor(8,1);
      lcd.print("V4: ");
      lcd.print(cell5);
    }

    if (screenValue ==3) {
      lcd.clear();
      lcd.setCursor(0,0);
      lcd.print("V5: ");
      lcd.print(cell6);
      lcd.setCursor(8,0);
      lcd.print("V6: ");
      lcd.print(cell7);
      lcd.setCursor(0,1);
      lcd.print("V7: ");
      lcd.print(cell8);
    }

    if (screenValue == 4) {
      lcd.clear();
      lcd.setCursor(0,0);
      lcd.print("FanPot: ");
      lcd.print(analogRead(sensorValue));
      lcd.setCursor(0,1);
    }

    if (screenValue == 5) {
      lcd.clear();
      lcd.setCursor(0,0);
      lcd.print("SetTemp: ");
      lcd.print(analogRead(baselineTemp));
      lcd.setCursor(0,1);
      lcd.print("ActualTemp: ");
      lcd.print(analogRead(temperature));
    }
  }
}
```

Appendix K

Comsol DATA

Table K-1 Currents of different temperature for the entire cell.

Voltage	Temperatures[deg celcius]			
	35	45	55	65
0,9	0,034014	0,032977	0,032001	0,031081
0,85	0,106578	0,103521	0,100635	0,097904
0,8	0,298136	0,290728	0,283684	0,276976
0,75	0,69069	0,677138	0,664139	0,651657
0,7	1,305932	1,286497	1,26771	1,249537
0,65	2,102347	2,078681	2,055411	2,032749
0,6	3,02221	2,99573	2,969729	2,944207
0,55	4,010805	3,983741	3,956896	3,93029
0,5	5,024614	4,998085	4,971534	4,944993
0,45	6,040611	6,014883	5,988756	5,962321
0,4	7,032967	7,009908	6,985739	6,960635
0,35	7,953822	7,938788	7,91952	7,898333
0,3	8,741257	8,73446	8,723916	8,710055
0,25	9,358404	9,365868	9,364746	9,358922
0,2	9,825503	9,834122	9,840961	9,841968
0,15	10,16345	10,18284	10,19522	10,20095
0,1	10,41189	10,43572	10,44487	10,45365

Table K-2 Current density, with comparison from highest to lowest temperature

Voltage	Temperature [deg Celcius]				% diff 35-65
	35	45	55	65	
	Specific current A/cm2				
0,9	0,004049	0,003926	0,00381	0,0037	109,44 %
0,85	0,012688	0,012324	0,01198	0,011655	108,86 %
0,8	0,035492	0,034611	0,033772	0,032973	107,64 %
0,75	0,082225	0,080612	0,079064	0,077578	105,99 %
0,7	0,155468	0,153154	0,150918	0,148754	104,51 %
0,65	0,250279	0,247462	0,244692	0,241994	103,42 %
0,6	0,359787	0,356634	0,353539	0,350501	102,65 %
0,55	0,477477	0,474255	0,471059	0,467892	102,05 %
0,5	0,598168	0,59501	0,591849	0,58869	101,61 %
0,45	0,71912	0,716058	0,712947	0,7098	101,31 %

0,4	0,837258	0,834513	0,831636	0,828647	101,04 %
0,35	0,946884	0,945094	0,9428	0,940278	100,70 %
0,3	1,040626	1,039817	1,038561	1,036911	100,36 %
0,25	1,114096	1,114984	1,114851	1,114157	99,99 %
0,2	1,169703	1,170729	1,171543	1,171663	99,83 %
0,15	1,209935	1,212243	1,213717	1,214399	99,63 %
0,1	1,239511	1,242348	1,243437	1,244483	99,60 %

Table K-3 Power in a single cell at different temperatures

		Temperature [deg Celcius]			
		35	45	55	65
Voltage	Power single cell [W]				
0,9	0,030612	0,029679	0,028801	0,027973	
0,85	0,090592	0,087993	0,085539	0,083219	
0,8	0,238509	0,232583	0,226947	0,221581	
0,75	0,518018	0,507854	0,498104	0,488743	
0,7	0,914153	0,900548	0,887397	0,874676	
0,65	1,366525	1,351143	1,336017	1,321287	
0,6	1,813326	1,797438	1,781837	1,766524	
0,55	2,205943	2,191058	2,176293	2,16166	
0,5	2,512307	2,499042	2,485767	2,472497	
0,45	2,718275	2,706697	2,69494	2,683045	
0,4	2,813187	2,803963	2,794296	2,784254	
0,35	2,783838	2,778576	2,771832	2,764417	
0,3	2,622377	2,620338	2,617175	2,613017	
0,25	2,339601	2,341467	2,341186	2,33973	
0,2	1,965101	1,966824	1,968192	1,968394	
0,15	1,524518	1,527426	1,529283	1,530143	
0,1	1,041189	1,043572	1,044487	1,045365	

Table K-4 Power in a 7-cell stack at different temperatures

		Temperature [deg Celcius]			
		35	45	55	65
Voltage	Power entire stack[W]				
0,9	0,214287	0,207752	0,201604	0,195808	
0,85	0,634141	0,615952	0,598776	0,582531	
0,8	1,669561	1,628078	1,588629	1,551067	
0,75	3,626124	3,554976	3,486729	3,421201	
0,7	6,399068	6,303834	6,211777	6,122732	
0,65	9,565677	9,458001	9,352118	9,249007	

0,6	12,69328	12,58206	12,47286	12,36567
0,55	15,4416	15,3374	15,23405	15,13162
0,5	17,58615	17,4933	17,40037	17,30748
0,45	19,02792	18,94688	18,86458	18,78131
0,4	19,69231	19,62774	19,56007	19,48978
0,35	19,48686	19,45003	19,40282	19,35092
0,3	18,35664	18,34237	18,32022	18,29112
0,25	16,37721	16,39027	16,38831	16,37811
0,2	13,7557	13,76777	13,77734	13,77876
0,15	10,67163	10,69198	10,70498	10,711
0,1	7,288325	7,305005	7,311408	7,317557

Table K-5 Power density of the cell at different temperatures

		Temperatures[deg celcius]			
		35	45	55	65
Voltage	Power density[W/kg]				
0,9	0,317933	0,308237	0,299115	0,290517	
0,85	0,940863	0,913875	0,888391	0,864289	
0,8	2,477093	2,415546	2,357017	2,301286	
0,75	5,380006	5,274446	5,173188	5,075965	
0,7	9,494166	9,352869	9,216287	9,084172	
0,65	14,1924	14,03264	13,87555	13,72256	
0,6	18,83276	18,66775	18,50573	18,34669	
0,55	22,91039	22,75579	22,60245	22,45047	
0,5	26,09221	25,95445	25,81657	25,67875	
0,45	28,23134	28,1111	27,989	27,86545	
0,4	29,21708	29,12128	29,02087	28,91659	
0,35	28,91226	28,85761	28,78757	28,71056	
0,3	27,23537	27,21419	27,18134	27,13816	
0,25	24,29853	24,31791	24,31499	24,29987	
0,2	20,40906	20,42696	20,44116	20,44326	
0,15	15,83327	15,86348	15,88276	15,89169	
0,1	10,81354	10,83829	10,84779	10,85691	

Table K-6 Specific power of the cell at different temperatures

		Temperature [deg Celcius]			
		35	45	55	65
Voltage	Specific power [kW/m3]				
0,9	0,844963	0,819195	0,794951	0,7721	
0,85	2,500508	2,428784	2,361057	2,297001	
0,8	6,583312	6,419741	6,264188	6,116073	
0,75	14,29832	14,01777	13,74866	13,49027	
0,7	25,23242	24,8569	24,49391	24,14279	
0,65	37,7188	37,29422	36,87671	36,47013	

0,6	50,05139	49,61284	49,18224	48,75957
0,55	60,88839	60,47753	60,06998	59,66609
0,5	69,34464	68,97852	68,61209	68,2458
0,45	75,02977	74,71021	74,38569	74,05734
0,4	77,64953	77,39493	77,12809	76,85093
0,35	76,83943	76,69419	76,50805	76,30337
0,3	72,3828	72,32652	72,23921	72,12443
0,25	64,57762	64,62912	64,62138	64,58119
0,2	54,24067	54,28825	54,326	54,33156
0,15	42,07972	42,15999	42,21124	42,23496
0,1	28,73889	28,80466	28,82991	28,85415